500842
IN-18
176815
P- 107

NASA Contractor Report 4500

The Middeck 0-Gravity Dynamics Experiment

Summary Report

Edward F. Crawley, Marthinus C. Van Schoor,
and Edward B. Bokhour

CONTRACT NAS1-18690
MARCH 1993

(NASA-CR-4500) THE MIDDECK
0-GRAVITY DYNAMICS EXPERIMENT
Summary Report (MIT) 107 p

N93-30376

Unclas

H1/18 0176815

NASA

NASA Contractor Report 4500

The Middeck 0-Gravity Dynamics Experiment

Summary Report

Edward F. Crawley, Marthinus C. Van Schoor,
and Edward B. Bokhour
Massachusetts Institute of Technology
Cambridge, Massachusetts

Prepared for
Langley Research Center
under Contract NAS1-18690

National Aeronautics and
Space Administration
Office of Management
Scientific and Technical
Information Program
1993

Page intentionally left blank

Abstract

The overall experimental and analytical effort centered around the Middeck 0-gravity Dynamics Experiment is presented in this report. The results of the Structural Test Article (STA) experiments are given first. An analytic and experimental study of the changes in the modal parameters of space structural test articles from one- to zero-gravity is presented. Deployable, erectable, and rotary modules were assembled to form three one- and two-dimensional structures, in which variations in bracing wire and rotary joint preload could be introduced. The structures were modeled as if hanging from a suspension system in one-gravity, and unconstrained, as if free floating in zero-gravity. The analysis is compared with ground experimental measurements, made on a spring/wire suspension system with a nominal plunge frequency of one Hertz, and with measurements made on the Shuttle middeck. The degree of change in linear modal paramenters as well as the change in nonlinear nature of the response is examined. Trends in modal parameters are presented as a function of force amplitude, joint preload, and ambient gravity.

Next the results of the Fluid Test Article (FTA) experiments are given. An experimental study of the change in the lateral slosh behavoir of contained fluids betwen earth and space is presented. The experimental apparatus used to determine the slosh characteristics is described and a nonlinear analytical model of a coupled fluid/spacecraft is outlined. The forced response characteristics of silicone oil and distilled water in cylindrical tanks with either a flat or spherical bottom are reported and discussed. A comparison of the measured earth and space results identifies and highlights the effects of gravity on the linear and nonlinear slosh behavior of these fluids.

A technical description of the hardware and software systems used in the Middeck 0-gravity Dynamics Experiment (MODE) is presented last. MODE consists of three major elements: the Experiment Support Module, a dynamics test bed providing computer experiment control, analog signal conditioning, power conditioning, an operator interface consisting of a keypad and display, experiment electrical and thermal control, and archival data storage; the Fluid Test Article assembly, used to investigate the dynamics of fluid-structure

interaction in zero-gravity; and the Structural Test Article for investigating the open-loop dynamics of structures in zero-gravity.

Acknowledgments

This work was supported by the NASA Instep Flight Experiments Program, and the NASA Langley Research Center Reference No. NAS1-18690, with Dr. Sherwin Beck as monitor.

The ground and analytical studies were supported in part by the NASA Headquarters Grant No. ASGW-1335 to the MIT Space Engineering Research Center, with Dr. Robert Hayduk as technical monitor, and by NASA Headquarters Grant No. NAGW-2014 with Mr. Samuel Venneri as technical monitor.

The McDonnell Douglas Space Systems Company was intrumental in the supply of the structural test article, and the funding at McDonnell Douglas Space Systems Company of the experiments performed there.

The authors also acknowledge the contribution to the report writing and editing by Mark S. Barlow, Brett P. Masters of MIT, Andrew S. Bicos of McDonnell Douglas Space Systems Company, and R. Grimes, M. Hachkowski, C. Krebs, and J. Zapetis of Payload Systems, Inc.

Contents

Chapter 1: Introduction

In 1986 the Massachusetts Institute of Technology proposed to NASA the Middeck 0-gravity Dynamics Experiment (MODE), a cost effective experiment for the investigation of fluid-spacecraft interaction and structural dynamics in zero-gravity. The objective of MODE was to gather data on the dynamic interaction between fluid volumes stored in tanks and spacecraft dynamics, and on the dynamics of multi-element statically indeterminate space structures. The data derived were to be correlated with zero-gravity simulations in order to validate analytical models, which could then be applied to a broader class of problems.

MODE was funded by the NASA OAST In-Step program in 1988. The MIT Space Engineering Research Center was the prime contractor with cooperation from McDonnell Douglas Space Systems Company, who supplied the structural test articles. All other support hardware was manufactured by Payload Systems Inc. The NASA Langley Research Center was the technical and programmatic monitor of the program. The experiment was flown, and on orbit data were taken during the STS-48 mission in September of 1991. Mission specialists Mark Brown and James Buchli were assigned to the MODE team. With the assistance of Brown, Buchli performed the majority of the test protocols. From the day after launch, until July 1992, the approximately three billion measurements taken during the MODE flight and ground test program were reduced and examined. This report constitutes the summary data report on this experiment.

This report is divided into three subsequent chapters: one describing the research program which centers around the the Structural Test Article (STA), the next describing the investigation focused on the Fluid Test Article (FTA), and the final chapter describing the hardware and flight operations.

Chapter 2 is a summary of the analytic and experimental investigation of the changes from one- to zero-gravity in the modal parameters of the structural test article. Both on earth and on orbit, a set of deployable, erectable, and rotary modules were assembled to form three one- and two-dimensional configurations of the STA. In order to control the degree of nonlinearity, variations in bracing

wire and rotary joint preload were introduced. As a complement to the experimental program, the structures were modeled by linear finite element methods. The resulting analysis is compared with ground experimental measurements, and with measurements made on the Shuttle middeck. The degree of change in linear modal parameters as well as the change in nonlinear nature of the STA response is reported.

The experimental and analytical investigation of the influence of gravity on the lateral slosh behavior of contained fluids is presented in Chapter 3. The experimental apparatus used to determine the slosh characteristics, the FTA and associated equipment, is described. A nonlinear analytical model of a coupled fluid/spacecraft system is then outlined. The forced response characteristics of silicone oil and distilled water in cylindrical tanks with flat or spherical bottoms are reported and discussed. A comparison of the measured earth and on orbit results identifies and highlights the effects of gravity on the linear and nonlinear slosh behavior of these fluids.

Chapter 4 describes in more detail the hardware built for the MODE experiment, as well as the on orbit operations. The principal hardware elements were the Structural Test Article, the Fluid Test Article, and the Experimental Support Module, or ESM. The ESM contained, in the space of one middeck locker, all of the functionality of a small dynamics laboratory. Operated by the crew over the course of three days on orbit, the ESM controlled the experiment, and recorded the data for subsequent analysis.

Chapter 2: Structural Test Article Results

2.1 Introduction

This chapter will summarize the motivation, backround and planning of the structural dynamic segment of the MODE program. The key results of the ground testing will be presented, as will a comprehensive review of the flight data. The principal objectives of the structural dynamics segment of the research program are to study suspension and gravity influences on the structural dynamics of a modular truss system by comparing the measured response in ground and orbital tests, and to quantify the suspension and gravity induced perturbations using analytical models of the suspension and nonlinear effects. This report will focus on the first of these objectives, the comparison of the dynamics of a typical space structure as measured in ground and orbital testing.

In order to accurately predict the dynamic loads and open loop response of a structure, accurate numerical models must be created. If the structure is to be an element of the plant in a robust closed loop control system, an even higher premium is placed on the accuracy of the structural model. It is becoming apparent that it is now far easier to create a numerical structural dynamic model with great precision, than to assure its *a priori* accuracy within any stated bounds. Accuracy is degraded as a result of poor modeling due to inexact elements and boundary conditions, mismodeling by the analyst, and non-modeling of features such as damping and weak nonlinearities.

In the normal engineering evolution of a structural model, the inaccuracies are reduced by iterative comparison with experimental data. The poor modeling of stiffness inherent in a first generation or *a priori* model (one made from drawings and handbook properties before any hardware exists) is often noted by comparison with component or element testing. This information is then incorporated into a second generation model (one which includes updated component information based on measurements). Performing modal testing and identification then yields frequency, mode shape and damping data which can be used to further refine and update the model, producing what can be called a third generation model.

Such an orderly evolution of models is not always as straightforward for space structures, due to the complications introduced by the ground testing necessary as part of the prelaunch third generation model improvement. Gravity loads the structure, causing droop and local stiffness changes; gravity alters preload on potentially nonlinear joints; and gravity necessitates suspension, which alters the structure's dynamics while introducing its own. One of the remaining issues in open loop modeling is to understand the degree to which the presence or absence of gravity influences the dynamics of space structures. It was in part to address this issue that the MODE program was established at the MIT Space Engineering Research Center (SERC).

The experimental approach is to test three nominally identical shipsets of a model of a space structure, called the structural test article or STA, at two sites on the ground. In addition, testing of one shipset has and will be carried out in the micro-gravity of the Shuttle middeck.

The difficulty in directly comparing such on orbit structural dynamic test results with ground test results is due primarily to the complicating effects of gravity on the ground tests. Five classes of gravity influences can be identified: the need for a suspension and its complication of the dynamics; the direct effect of gravity loading on nonlinearities; the direct structural stiffening or destiffening due to gravity loading; the gravity deformation of the structure, which leads to dynamic perturbations about a deformed equilibrium; and the direct gravity influence on some inertial sensors and actuators. The degree of each influence depends on the stiffness of the test article, inherent nonlinearities, and the geometry of the suspension [Pinson, Hanks, 1983, Rey 1992]. The specific objective of the MODE program is to examine the first two gravity influences, those of suspension and nonlinearity.

In order to span several typical geometries and structural forms, the structural test article (STA) designed for MODE utilized a versatile set of modules, allowing several configurations to be assembled. These modules included deployable truss modules, erectable truss hardware, a rotary joint, rigid appendages, and a flexible appendage. By assembling various modules, straight and L-shaped trusses were formed and tested. A controlled degree of nonlinearity was introduced into the truss modules and the rotary joint. The preload on one deployable bay controlled the nonlinearity of the joints and bracing wires; similarly, the preload on the rotary joint controlled the friction and

propensity for axial rotation. The remainder of the chapter begins with a description of the test hardware and the experimental procedures used.

The next section of the chapter summarizes the ground test results, which were comprehensively reported in two earlier documents [Barlow, 1992 and Crawley et al., 1992]. Ground vibration testing was performed at MIT and McDonnell Douglas Space Systems Company (MDSSC) on two different shipsets, under highly controlled test conditions. For each of two shipsets, three configurations and several modes, variations were introduced by changing the stiffness of the suspension system, the force level, the joint preload, and by assembly/reassembly of the structure. The pertinent features and conclusions of this ground test program are summarized.

The on orbit structural dynamic test results will then be comprehensively presented. The orbital test results of three configurations are compared with the ground results for the same shipset, for variations in forcing level and preload. The ground data reported will be for the softest successfully tested suspension system, which most closely replicates the free free orbital test conditions.

The ground and orbital test results will be compared with linear analytical models which incorporate the presence (or absence, as appropriate) of the suspension and gravity stiffening. The nonlinearities of the test articles are also identified as a function of force amplitude and preload. The presence of the measured nonlinearities will be reported, but detailed nonlinear modeling and correlation with nonlinear experimental results await a future report.

2.2 Hardware and Test Procedure

2.2.1 Configurations

In order to examine the influence of gravity on the dynamics of space structures, a representative Structural Test Article (STA) was designed and fabricated. The STA was built up from erectable and deployable modules, which could be arranged to produce several configurations, as shown in Fig. 2.1. Each module was fashioned after a typical space structural form, and was included in the hardware set for a specific reason.

The simplest arrangement of the modules is called the baseline configuration. For this structure, two four-bay deployable modules (i.e.,

modules which are capable of being deployed and restowed by utilization of hinging joints and locking mechanisms) are connected in the center bay with erectable hardware components (i.e., hardware that can be assembled from individual components to form a truss section) to form a straight truss. The objectives of the tests of this configuration were to determine the impact of gravity and suspension influences on a straight truss composed of primarily deployable hardware, and to examine the influence of preload in the diagonal bracing wires of the deployable hardware on the measured ground and orbital modal parameters.

A slightly more complicated configuration, called the alpha configuration, is formed by replacing the erectable hardware of the center bay of the baseline with a rotary joint modeled after the Alpha Joint of the Space Station Freedom. Although this configuration still forms a straight truss, the additional mass and internal dynamics of the articulating joint substantially change the behavior of the system. The purpose of testing this configuration was to evaluate the influence of 1-g test methods on a truss with a rotary joint which contains a frictional interface with operating bearings.

A more complex configuration includes both deployable modules, erectable hardware, and the rotary joint to form a planar truss called the L configuration. Due to its shape and mass distribution, the L configuration was the most difficult to test in a 1-g field. Tests on this configuration were performed to provide the greatest challenge to the testing of a planar structure in a gravity field.

2.2.2 Modules

The three configurations of the structural test article are composed of several different modules. These modules include two deployable truss modules, erectable truss hardware, a rotary joint, and two rigid appendages. The modules are scaled models built by the AEC/Able Engineering Company for the McDonnell Douglas Space Systems Company, who supplied two shipsets to MIT (denoted STA 1 and STA 2). A third shipset, STA 3, was retained at MDSSC for their testing. All results reported in this article will be for STA 1.

Two deployable truss modules form the bulk of each configuration. The deployable truss resembles one of the designs proposed for the Space Station

Freedom solar array truss structure. Weighing approximately eight pounds, each section is four bays in length with a nominal bay comprised of an eight inch cubic section. Each Lexan longeron hinges at its midpoint (via a knee joint) and at its attachment points with the batten frames. The batten frames remain rigid when the truss is collapsed. The hinge arrangement allows the truss segment to fold like an accordion for stowage. All hardware that connects the Lexan rods is made of 6061 aluminum. Tension is maintained throughout the deployable module by the use of pretensioned cables which run diagonally between the batten stations. When the longerons lock in their over center deployed position, the tension in these cables reaches 25 lb. The cables are tensioned to prevent possible slop in the hinge and knee joints from entering the system dynamics. The preload maintains local longeron "string" modes above 40 Hz. Typical preload on the longerons is 28 lb. This loading is 50% of the estimated buckling load of the longerons and represents a compromise between sufficient preload to prevent slop at the joints and excessive preload which might destiffen a longeron.

A single bay of one of the two deployable modules includes a mechanism which allows for varying the preload level in the wires. The purpose of this feature is to permit the study of preload on the joints and its influence on the truss dynamics. Provisions for preloads of 24, 13, and 7 lb were incorporated into the truss design and were denoted as: the high preload, or preload 1 (PL1); the medium preload, or preload 2 (PL2); and the low preload, or preload 3 (PL3). Preload 1 corresponds to the same preload as in the wires of the non-adjustable bays. As the preload on this bay is reduced, it is possible for the joints to become unloaded as the cables begin to slacken. Both cable slackening and joint motion are expected to contribute to changes in the truss dynamic behavior. In summary, the deployable hardware consists of one module with four bays in which the wire pretension is fixed, and one module which contains one bay in which the preload is adjustable and three bays in which it is fixed.

Erectable truss hardware forms the next largest portion of the structure. Although scaled down in size, the erectable components are identical to hardware used by the NASA Langley Research Center for their Dynamic Scaled Model Technology structure [Gronet et al., 1989]. Erectable hardware consists of spherical nodes with 26 holes to which standoffs may be mounted. Longeron, diagonal, and batten members terminate in lugs which slip into these standoffs

and are secured by tightening a locking collar. Erectable segments are connected to the deployable hardware using standoffs incorporated into the two end batten frames of each of the deployable module. Erectable longerons and diagonals are connected to the standoffs on the deployable modules to form the baseline configuration, and are incorporated together with the alpha joint in the L configuration.

The alpha joint was intended to approximate the dynamics of the Rotary Alpha Joint proposed for Space Station Freedom. The 2.5 lb module is constructed around two aluminum disks which are connected at their centers by an axle, and at a radius of 2.75 in by 5.5 mm diameter stainless steel ball bearings. The two plates are free to rotate relative to each other on the bearings. The disk assembly has Lexan struts terminating in erectable-style lugs and locking sleeves to allow connection with erectable standoffs. The disk/strut module is sized as an eight inch cubic bay. Friction between the two plates is adjustable through the use of a cam mechanism set by a tensioning lever; the tight position is denoted as alpha joint tight (AT) and the loose position is alpha joint loose (AL). In the AT setting no relative rotation occurs, while in the AL setting the two plates can rotate relative to one another, constrained only by bearing friction. The alpha joint was used in the alpha and L configurations.

Rigid appendages have been added to the ends of each configuration to lower the system fundamentals below 10 Hz. These appendages are dumbbell-shaped and each weighs approximately 16 lb.

2.2.3 Sensors and Actuator

Several sensor types were utilized to measure the structural response to the force input created by a single proof-mass actuator. Accelerations were sensed by piezoresistive accelerometers, and the input force by a load cell. All electrical signals were routed off the STA through a single umbilical. Thirty-three pairs of 28 gauge stranded wire were loosely braided and wrapped in a fire resistant woven shell to form an 8 ft length of bundled wire. As in space flight hardware, cables connecting the sensor location to the umbilical attachment points were routed along the structure and tie-wrapped in place.

Excitation was provided by a proof-mass actuator. The shaker used a 1.0 lb throw-mass and interchangeable springs to permit both ground and orbital

testing. The mass and spring mounted to the support platform which in turn mounted to the load cell. Total weight of the actuator is approximately 1.8 pounds. For the spring selected for ground testing, the shaker's spring-mass resonance occurred at 2.3 Hz, while resonance occurred at 4.0 Hz with the space spring. Due to the change in springs from ground to orbit, the actual force differed slightly between ground and orbit for the same commanded voltage. The forcing amplitudes will be referred to as low, medium and high, but the actual value of measured forcing for any particular test can be found by referring to Table 1. The excitation acted in the vertical direction on the corner of the end batten frame of the deployable module which contained the bay with adjustable preload.

Eleven accelerometers were placed on the truss in such a manner as to make observable the modes of interest for each of the structural configurations. Three accelerometers were placed on the end batten frame which supported the proof-mass actuator, three at the batten frame four bays away at the far end of the same deployable module, three at the first batten frame of the second deployable module, and two at the far end of the second deployable module. Four strain gauges also instrumented the adjustable bay, for a total of sixteen channels of data.

Signal conditioning, data acquisition, and data storage were provided by an Experiment Support Module, or ESM. Sixteen channels of sensor signals were simultaneously sampled by 12 bit A/D's at 500 Hz and stored on a Write Once Read Many (WORM) disk. Sensor signals are amplified and low pass filtered using eight-pole tunable Bessel filters with a corner frequency of 250 Hz.

2.2.4 Test Procedures and Data Reduction

Testing on the ground and on orbit followed the same basic procedures. A structural configuration was assembled and suspended (on earth) or tethered (on orbit). The umbilical and actuator were attached, and the test protocol performed.

For the ground testing of the STA, a soft mechanical suspension system was selected to support the structure while approximating free-free boundary conditions. The suspension system consisted of steel wires hung from coil springs, attached to a rigid support frame. Three spring sets were used

providing nominal system plunge frequencies of 1, 2, and 5 Hz. All data reported in this chapter will be for the nominal one Hertz suspension. An overall spring-wire length of 120 in was maintained, which yielded a sway frequency of 0.28 Hz. Other suspension resonances (including transverse (violin string) wire modes, axial modes of the springs, and compound pendulum modes of the spring/wire) were sufficiently separated from the STA resonances to not complicate the identification of STA frequencies and damping ratios [Crawley et al., 1992].

On the middeck, tests were performed in a shirt sleeve, room temperature and pressure environment. Although a suspension system was not required, it was impossible for the STA to truly free float on the Shuttle. Residual velocity from the release by the crew, air circulation, and gravity gradient accelerations, as well as occasional firings of the vernier reaction control system, would cause contact of the STA with the cabin walls. To prevent such an impact, an elastic tether system was used, which consisted of four tethers of 0.0625 in square elastic surrounded by Nomex sheathing. The tethers were positioned to provide restoring forces in three orthogonal directions to prevent drift. After being attached to an STA longeron via a nomex and velcro cuff, each tether was attached to a prepositioned velcro pad mounted on the middeck interior. Based on video data, the frequency of the STA on this tether "suspension" was 0.025 Hz, about a factor of forty below the lowest ground suspension frequency, and three hundred below the STA fundamental.

The test procedure was the same for all configurations. Sine sweep testing was performed. As each protocol was conducted, signal time histories for each excitation frequency were stored. Post-test data reduction consisted of reducing the time history data to a single amplitude harmonic coefficient for each data channel at the tested excitation frequency by employing a harmonic balance technique. Next, estimates of natural frequency and damping ratio were determined using the circle fit method [Ewins, 1984]. Implicit in the use of this method is the assumption that the dynamic behavior is dominated by a linear resonance. For every forcing amplitude of each mode, channels with clean signals were selected for use in the determining modal parameters. Parametric data from each channel were then averaged to determine the modal values. In this manner, channels which had saturated or experienced small signals were removed from the parameter determination algorithm.

2.3 Modeling

2.3.1 Evaluation Models

ADINA (Automatic Dynamic Incremental Nonlinear Analysis) [Adina, 1987] was selected as the framework within which to develop analytical models of the structural test articles. Three ADINA models of the STA were constructed: a high order evaluation model which represents a free floating 0-g test article; an element level Guyan reduction of the high order model; and a 1-g model of the STA suspended on the suspension system in a gravity field, which is based on the Guyan reduced model.

Detailed evaluation models were made of each STA configuration. The models used 6 dof rod elements and 12 dof beam elements with lumped mass matrices, which were required for the subsequent 1-g modeling. In the detailed evaluation model construction, separate beam elements were used to model segments between every material or dimension change. For example, the deployable longeron was modeled with seven elements, representing the batten frame section, lug, Lexan rod, knee joint, Lexan rod, lug and batten frame section. Tensioning cables were modeled as a single rod element, and the alpha joint bay was modeled by 68 elements. The resulting model sizes were 2160, 2166, and 3150 dof for the baseline, alpha and L configurations respectively.

2.3.2 Development Models

Development models contained fewer dof than the evaluation models, and were obtained by reducing internal dof from the deployable longerons and erectable longerons and diagonals. For example, the seven element longeron was simplified to a single element. For models which contained the alpha joint, a small additional savings in dof was obtained by simplifying the model of the alpha joint support struts.

Guyan reduction was used to create equivalent beam elements for the longerons and diagonals [Guyan, 1965]. The system stiffness matrix for a given strut assembly was calculated and was then reduced using Guyan reduction. By equating elements of the single beam element stiffness matrix with the reduced matrix, values were determined for the equivalent beam section properties. Since each property enters the beam stiffness matrix in several places, an average can be made using each of the calculated values to arrive at an equivalent section

property estimate. Note that if only the entries on the diagonal of the Guyan reduced stiffness matrix were used to calculate the equivalent properties, the results would be identical to those obtained from a static equivalent analysis.

Because of the assumptions made in the condensation procedure, the reduced model will never reproduce the original eigenvalues exactly. However, as long as dof with significant mass contributions are included in the set of retained dof, the method produces satisfactory results.

2.3.3 1-g Models

ADINA was also used to model the suspended STA configurations in a 1-g field [Rey, 1992]. The suspension system models were based on the Guyan equivalent development models. For ground testing, the STA was suspended by coil springs and steel wires, which were modeled as nonlinear rod elements which incorporated axial stiffening and allowed large deflections. Thus, the stiffening of the suspension due to gravity loading was captured.

To determine the eigenvalues of the suspended system, a two step solution process was required. In the first step, a nonlinear static solution was performed. From an initial position in which the springs were unstretched, the model was allowed to descend under the influence of gravity until an equilibrium position was reached. Concentrated damping elements were added to the nodes of the structure and the suspension to prevent the structure from oscillating indefinitely. At each time step in this incremental scheme, the stiffness matrix of the system was recalculated to capture the stiffening effects of gravity on the structure and the suspension. ADINA could not begin the solution algorithm unless the stiffness matrix was initially nonsingular. In the first steps of the time integration of the equations, initial strain was added to the axial elements to remove the singularity.

In the second of the two steps, an eigensolution was performed using the reformed stiffness matrix of the static calculation. Concentrated nodal dampers were removed and infinitesimal displacements were assumed. Among the phenomena included in the model were: pendulum modes of the structure; plunge, pitch, and roll modes; axial modes of the springs; violin string modes; and spring/wire transverse modes. Although gravity stiffening was included on

the "flexible" elements (longerons, battens, etc.), no influence of gravity on the potentially nonlinear behavior of the joints was captured.

2.4 Test Results

2.4.1 Test Matrix Selection

This section will briefly review the parameter matrix explored in ground and orbital testing, then go on to summarize the principal ground test results, before presenting the orbital test results.

As described above, combinations of the hardware modules allowed for variation in configuration, deployable bay joint preload, and alpha joint preload. Any number of modes could be tested at multiple force levels. Three different shipsets were available to test on various suspension systems on the ground and in zero-gravity on orbit. Assemble and reassemble repeatability tests could also be conducted. Considering all of these parameters, the resulting test matrix has seven dimensions: configurations, preloads, modes, force level, shipsets, suspension/gravity, and assembly/reassembly. Because of the limited nature of on-orbit test time, a specific subset of the multidimensional test matrix was completed on orbit.

The on orbit test matrix data are represented in Tables 2.2, 2.3, and 2.4, which contain analytically predicted and experimentally measured modal parameters. As indicated in Table 2.2, the baseline configuration was tested in its first torsion, bending and shearing modes, with high, medium and low bay preload. The alpha configuration was tested in its first torsion and bending modes, and the L in a torsion and two bending modes, as indicated in Tables 2.3 and 2.4. The alpha and L configurations were always tested with the high deployable bay preload, and with the alpha joint in either the tight or loose settings. In general the test articles were driven at low, medium and high force amplitudes, which were approximately linearly spaced over one decade (Table 2.1). In some cases selected amplitudes were omitted to conserve test time. Only one shipset (STA 1) was tested on orbit and no assembly/reassembly testing was performed.

Prior to and following the orbital testing, the hardware was the subject of extensive ground testing. The ground test matrix included tests on STA 1 at MIT

for the same submatrix of configurations, modes, forcing levels, and deployable bay and alpha joint preloads as were tested on orbit. In addition, the ground testing filled out the overall matrix by testing two different shipsets at two different sites: STA 1 at MIT and STA 3 at MDSSC. For both shipsets, assembly/reassembly testing was performed, and in the MIT tests, three different suspension systems were employed.

2.4.2 Ground Test Results

Four levels of analysis were performed on the ground test data. First the frequency transfer functions from measured force input to acceleration output were calculated and examined for indications of linearity or nonlinearity. Then the linear modal parameters were extracted from the frequency transfer function by a circle fit in the complex plane. Thirdly, these modal parameters were examined for trends as a function of force level, suspension stiffness, reassembly, etc. Finally, statistical information was obtained on the variance in the modal parameter as a function of force level, reassembly etc. The results of the ground testing are documented in Barlow, 1992.

The overall results of the ground testing were that the STA had well separated modes which were lightly damped and exhibited weak to moderate nonlinear behavior. The various STA configurations had three to five modes below 30 Hz, with little modal overlap, allowing easy identification of modal parameters. The damping ratio averaged 0.7%, and ranged from modal averages of 0.2 to 1.6%. Except for the alpha joint loose tests, the modal transfer functions were weakly nonlinear, in that the modal parameters shifted with force amplitude and joint preload. The general, but not universal trend was softening and increased damping with increased force excitation and decreased joint preload. In this context, weakly nonlinear is used to connote the case when the frequency transfer function is more or less symmetric about its resonance within several half power band widths, and the shifts in modal parameters are small. In the case of alpha joint loose, the behavior is termed moderately nonlinear, in that the frequency domain transfer function begins to become nonsymmetric and the resonant frequency shifts are more pronounced. Strongly nonlinear behavior such as jumps, multiple solutions and chaos were not evident in the ground measurements.

Of the seven dimensions of the test matrix discussed above, three could be predicted by the finite element models developed. The frequencies of the two or three modes tested of the three configurations were predicted as well as can be reasonably expected by a first generation finite element model; that is, a model which does not incorporate any test data. The mean error between the Guyan reduced Adina model and the experimental data was 1.4% in frequency, and the standard deviation from the mean was 4.6%. Of course the Adina model had no prediction of damping. The ability of the Adina model to predict shifts in frequency due to suspension was surprisingly good. In all cases the qualitative prediction of the shift in modal frequency from the 1 Hz to the 2 Hz to the 5 Hz suspension was good, in most cases quantitatively accurate.

Of the remaining four dimensions of the test matrix, the variations in two (forcing level and preload) are in principle deterministic, and the remaining two (assembly/reassembly and shipset) are inherently statistical. Variation in the modal parameters with forcing level and preload could be modeled by an appropriate nonlinear model, if it existed. In the absence of such a model, the variations with force level and preload can be treated as being statistical as well.

The statistics of variations in modal parameters as a function forcing level, preload, reassembly and shipset were determined for the ground test results. The standard deviations were 1.25% in frequency (normalized by the mean) and 0.45% in damping ratio ζ (not normalized by the mean, but reported in units of ζ) when all variations were combined. The standard deviations were slightly lower for the baseline configuration, which did not contain the alpha joint, and slightly higher for the alpha and L configurations which did contain the alpha joint. Of the four variations, the statistics of the variation in shipset are not relevant to the comparison of ground and orbital results, since results from the same test article, STA 1, will be compared in both environments. The statistics on variation in force level and preload are useful background, but the variations will be examined for deterministic trends in the discussion below.

However, the statistics on modal parameter variation with assembly/reassembly are extremely relevant. While it is true that the data presented below will purport to show the difference between tests on the ground and on orbit, it will also have embedded in it the differences between data taken from several assembly/reassembly tests on the ground and one assembly on orbit. Only if the difference in modal parameters obtained on ground and on

orbit is greater than the standard deviation obtained in ground reassembly tests can it be asserted that the modal parameter changes from the ground to orbit are statistically significant, and then the difference can be attributed to a change from one- to zero-gravity. The relevant standard deviations for reassembling the structure are 0.54% in frequency and 0.22% in damping ratio.

2.4.3 Orbital Test Results

Baseline Configuration. The first torsion, bending and shearing modes of the baseline configuration were excited on orbit. Representative transfer functions for the baseline configuration with high preload (PL1) are shown in Figure 2.2. The three symbols indicate the transfer function for low medium and high excitation force levels (Table 2.1). For all plots shown in this and subsequent figures, the transfer functions for the torsion, bending and shearing modes are from the measured force input to an accelerometer at the actuator end, center and far end of the truss respectively. Identified modal parameters for the baseline configuration are listed in Table 2.2.

Low forcing of the torsion mode displays a clear and nearly linear resonance (Fig. 2.2). As the force level is increased, the resonance quickly begins to appear nonlinear. Due to the structural nonlinearity, the mode softens and becomes more damped with increased forcing amplitudes. For these and subsequent nonlinear transfer functions, the linear parameters reported in Tables 2.2, 2.3 and 2.4 can be interpreted as best linear approximations of the modal parameters. For the bending mode, distinct resonances remain for all force levels. The apparent resonance changes only slightly as the excitation force is increased. Damping, on the other hand, more than doubles between low and medium forcing levels, and continues to increase for the third amplitude. The third or shearing mode appears to possess a relatively linear resonance, with a slight softening and increase in damping. The response of this first configuration with a tight preload can be characterized as weakly nonlinear in bending and shearing, and moderately nonlinear in torsion.

A comparison of the low and high amplitude excitation of torsion modes for high bay preload for ground and orbital tests can be found in the first of the three transfer functions of Figure 2.3. From the figure and Table 2.2, it is obvious that the modes of the space data occurred at lower frequencies and, where

calculable, larger damping ratios. Upon comparison, it is evident that the nonlinearities manifest themselves much more strongly in the orbital data.

Similar comparisons can be made for the bending and shearing mode. For the bending mode (see Figure 2.3), the space frequencies are again lower than those of the ground data but by a much smaller percentage. Even though they are similar at low force levels, the space damping levels become almost double the levels seen in ground testing at the highest force level. The ground and orbital modes seem to exhibit the same characteristics with the exception that the orbital data are generally more damped. Figure 2.3 also contains a comparison of the shearing modes of ground and orbital tests. Although the space data were softer, only very slight changes in damping were present.

On orbit data were obtained for the one deployable bay with medium and low preload. The results for the medium (PL2) preload are generally intermediate to the high and low cases, and are listed in Table 2.2. Figure 2.4 contains transfer function plots of the low preload (PL3) for medium and high forcing levels for space and ground; estimated modal frequency and damping are listed in Table 2.2.

As can be seen in the first transfer function in Figure 2.4, the two tested amplitudes for the first mode have resonances that are barely within the left boundary of the test window. It is significant to note that although certain test windows did partially or completely miss the intended modes, all windows were based on pre-flight ground test data. Each orbital test window was selected by referring to several ground tests and estimating the amount of expected shifting. Therefore, a missed orbital test mode indicates a significant and unexpected shift in frequency.

The influence of reduced bay preload can be observed by comparing the space traces for medium and high excitation for low preload in Figure 2.4 with the traces for medium and high excitation for high preload in Figure 2.2. The magnitude curves for the torsion mode indicate a continued softening and dampening, as well as increasing structural nonlinearity. The behavior of the bending mode was remarkably unchanged with preload in orbit, still with notable increase in damping but little change in frequency with increased force amplitude. Shearing is slightly softer but no more damped at low preload, and

again softened slightly and experienced a small increase in damping with increased force.

Comparative plots of ground vs. orbital data can also be found in Figure 2.4 for torsion, bending, and shearing modes, respectively. For the torsion mode, the space data are softer and more damped than the ground data. With low preload, even the ground response is moderately nonlinear, with a distinct nonsymmetric resonance. For the bending mode, the frequency increased slightly in space, but the damping was greater. Only small differences exist for the shearing mode. The space data are softer and slightly less damped than the ground test equivalents.

Two physical mechanisms are likely to cause the nonlinear behavior observed in the baseline configuration: slackening of the tensioning cables and accumulated microfriction. Stranded cables such as those used in the bay possess highly nonlinear stiffness as they become slack, and are noticeably nonlinear when preloaded up to significant fractions of their yield stress, well above the stress at which they were preloaded, even at the high preload settings. Microfriction is an alternate explanation. With increasing amplitude, there is increasing friction breakage, resulting in softening and increased dissipation. A more thorough analysis of the nonlinear response awaits a detailed set of measurements on the nonlinear behavior of the truss components.

In order to more easily visualize the influences of gravity, preload and force level, the trends in the three modes of the baseline configuration are shown in Figures 2.5a, 2.5b and 2.5c. The damping ratio (in percent) is plotted versus the change in frequency normalized by a reference frequency (in percent). The first test of STA 1 at MIT with high preload and low excitation level was considered the reference. The lines connect tests of constant bay preload, and the symbols indicate tests of different force amplitudes. For the case of the torsion mode in Figure 2.5a, the trends are quite clear. Both on earth and in space, increasing force amplitude softens and damps the system. The rate at which damping increases in space is greater. Decreasing bay preload softens the system, but does not strongly affect damping. Finally, the absence of gravity softens and damps the response.

The bending mode trends are displayed in Figure 2.5b. The ground data show only a weak trend of decrease in frequency with force level, and no

organized sensitivity to damping ratio. On the other hand, the space data show a strong increase in damping with force level for all preloads, a trend not seen on the ground. The trends for shearing, shown in Figure 2.5c, are like those for torsion, but more subtle. Increasing force and decreasing preload slightly soften and dampen the mode. On orbit the mode softens, but does not show a significant change in damping.

It is now appropriate to apply the tests of statistical significance to the changes observed between earth and orbit. Based on extensive ground assembly/reassembly testing, it was determined that the standard deviation due to reassembly was about one half percent in frequency and one quarter percent in damping ratio. Examining Figures 2.5a, 2.5b and 2.5c, and comparing the shifts in frequency and damping ratio for equivalent test conditions, it can be concluded that: for torsion, both the shift in frequency and damping is significant; for bending, only the change in damping is significant; and for shearing, the change in frequency is marginally significant.

Alpha Configuration. The additional feature of the alpha configuration was the relatively massive articulated rotary joint which replaced the center bay of erectable hardware. This configuration was tested in the torsion and bending modes, with the alpha joint tight and loose. Testing of the alpha configuration was performed with the preload in the adjustable bay of the deployable module in the high preload setting, so that it was closest to that of the other, nonadjustable bays.

The alpha configuration was first tested in the alpha tight setting. Representative transfer functions may be found in Figure 2.6. For the second mode, the low force data is unreliable due to a saturation of the accelerometer. Estimates of natural frequencies and damping ratios for the tested modes are contained in Table 2.3. The first plot of Figure 2.6, for the torsion mode, bears remarkable resemblance to the torsion mode of the baseline, Figure 2.2. Softening, dampening and increasing nonlinearity are present with increased force amplitude. Comparison of the modal parameters in Tables 2.2 and 2.3 for the space data of the baseline high preload and the alpha tight show only a slight drop in frequency and the same range of damping. Obviously the presence of the tight alpha joint in the middle of the truss, at a node of the torsion mode, has only a slight impact on the parameters of that mode.

By way of contrast, the bending mode has dropped almost a factor of two in frequency, due to the large mass of the alpha joint at an antinode of bending mode. For fixed damping and a drop in frequency by factor of two, one would expect an increase by factor of two in damping ratio. The data reveal more or less the expected factor of two in damping ratio. Thus, other than the addition of mass, the alpha joint in its tight preload has a small effect on the dynamics of the STA.

Ground and orbital test data are overplotted for the torsion mode in Figure 2.7. Although similar at lower force levels, the relative appearance of the two curve sets changes with increased forcing amplitude; the ground data display smooth transitions while the orbital curves exhibit more irregular behavior. Generally, however, the space data are softer and more damped than the ground data. For the bending mode, the parameters in Table 2.3 show that the space data are slightly softer and more damped than the ground data. Again these are the same trends as seen in the baseline high preload case.

The alpha configuration with loose preload was tested next. For this test, transfer function data are plotted in Figure 2.8, while parametric estimates are given in Table 2.3. The torsion mode appears to exhibit jump phenomena for the two upper amplitudes. For low forces, the static friction within the alpha joint is thought to be sufficient to keep the joint locked, producing essentially linear behavior and the familiar modal peak. However, as the forcing level is increased, the joint may begin to slip causing the discontinuities in the plot. For these jumps, no damping estimate can be calculated. For the force amplitudes where jump occurred, the parameter table will contain the jump frequencies. It is worth noting that no indications of jumping occurred for the alpha tight tests of this configuration. Unlike the torsion mode, the bending mode appears only weakly nonlinear, with evidence of slight softening with increasing excitation. The low force trace is again unreliable due to saturation.

The orbit and ground results can be compared by examining Figures 2.8 and 2.9. Upon comparison with ground results, the orbital torsion data appear markedly different except for the low amplitude. The ground data softened and became much more damped but saw no jump phenomena. On the other hand, the orbital data had a clear peak for the low force level but displayed jumps for higher amplitudes. During ground testing, gravity may have preloaded the

alpha joint enough to prevent rotations and jumps from occurring. As a result, damping increased but jumps were not in evidence.

The trend plots for the alpha configuration are shown in Figures 2.10a and 2.10b. For the torsion mode in Figure 2.10a, only the on orbit data which did not show a jump are presented. The statistically significant softening and dampening influence of zero-gravity on the torsion mode is quite apparent. Likewise, statistically valid decrease in stiffness and damping are present in the bending modes, as can be seen in Figure 2.10b.

L Configuration. Finally, the most challenging configuration, the L configuration, was tested with the alpha joint tight and loose in a torsion and two bending modes. The narrow test windows specified prior to flight did not manage to catch a single mode well enough to produce modal estimates, due to unexpectedly large frequency shifts. A low force sine sweep was performed up to 30 Hz via a manual protocol. Coarse location of the torsion mode was identified, and is compared with the ground results in Table 2.3. Since this mode dropped 7%, and the other modes dropped enough to be outside the test windows, it can be concluded that qualitatively significant softening of the two dimensional configuration occurred in 0-g.

2.4.4 Comparison of Finite Element and Experimental Results

With the experimental results discussed above, it is possible to evaluate the performance of the finite element models described earlier. Two comparisons will be given: unsuspended models with orbital data, and suspended models with ground data. For the unsuspended model results, both evaluation (or full) and development (or Guyan) reduced model will be compared to the orbital results. Since the Guyan reduced model formed the basis of the suspended model, it is the only one appropriate to compare with the one-gravity results. The models are compared to orbital data in Figures 2.5 and 2.10 by the symbols on the zero damping axis (since the model had no damping prediction) and in Tables 2.2 through 2.4. Because the models included no nonlinearities, there was no way to reflect the effect of a change in preload. The predicted frequencies of the linear model are listed in the tables next to all of the cases for which they are appropriate.

For the baseline configuration, both the evaluation model and the development model did a reasonable job of predicting the frequencies since all errors were near to or less than 5% (Fig. 2.5). In some modes the evaluation or full model was more accurate, and in others the reduced model more closely matched the data. As the structural complexity increased, the models became less accurate as can be seen in the trend plots for the alpha configuration in Figure 2.10. The evaluation model of the alpha configuration had larger errors than the development model (in an average sense) but both did a fair job of matching frequencies. The first mode of the L configuration had frequency errors of approximately 10%, indicating that this mode was not very well modeled. The higher modes were missed on orbit resulting in no comparison data.

On average, the evaluation model was only slightly better than the development model. For the baseline and alpha configurations, where some degree of confidence exists in the frequency data, the frequencies of the evaluation models averaged 1.4% high with a 4.6% standard deviation; the development models were 1.8% high with a 4.8% standard deviation. The fact that the differences are small reinforces the validity of the development models.

The finite element model of the suspended STA did a poor job of predicting the shift in frequency from one-gravity on a one Hertz suspension to zero-gravity. This is in marked contrast to the success of the suspended model in predicting the change in frequency from a one, to two, to five Hertz suspension in the ground tests [Crawley et al., 1992]. The inference is that the changes in modal parameters from one suspension to another in one-gravity were dominated by linear effects, while the changes due to the shift to zero-gravity were dominated by nonlinear influences.

It should be noted that the finite element models are first generation; that is, models which were constructed with dimensional data from blueprints and material properties from standard references. No attempts were made to "adjust" the nodal locations, dimensions or material properties based on either component tests or ground vibration tests in order to better match the experimental frequencies.

2.5 Conclusions

The shuttle middeck has proven to be an excellent environment in which to perform 0-g experiments of scaled structural models. The pressurized atmosphere of the middeck allowed experimental determination of gravity influences in an earth-like pressure and temperature environment. Scaled models serve as the preferred means by which to utilize the middeck as a laboratory, due to the limited size of the facility.

Significant differences between 1-g and 0-g identified modal parameters were measured for the MODE structural test article. Generally, data taken on orbit showed lower resonant frequencies and higher damping ratios. Gravity preload of the structure and the presence of a suspension resulted in higher frequencies and lower damping ratios for ground test data.

The STA exhibited weakly, moderately and strongly nonlinear structural behavior. Deployable joints, tensioning cables, and the alpha joint all contributed to the overall nonlinear behavior of the truss. As a result, modes generally softened and experienced increased damping levels as the excitation force was increased. In both test environments, as the adjustable bay preload was decreased, the nonlinear behavior became stronger. A dramatic difference was seen between tests where the alpha joint was tight and loose; strongly nonlinear behavior occurred with the alpha joint loose in the torsion mode, while the STA displayed only moderately nonlinear behavior with the joint tight. The jump phenomenon witnessed for the orbital test of the alpha configuration with loose preload was not seen in ground data; no indication of this behavior could be deduced based on ground tests.

A trend was seen in the data that indicated that the differences between one- and zero-gravity are stronger at lower frequencies and diminish at higher frequencies. For first or torsion modes, the change in transfer function magnitude with increasing force was often abrupt, causing a resonant peak to be indiscernible. In the alpha loose tests, jumps occurred on orbit for which no indication could be found in the ground data. Although higher modes were also different in orbital tests, these differences were largely due to smaller shifts in frequency and changes in damping ratio. Unfortunately, it is often the first few modes of a structure that are most important for loads, dynamics and control analysis.

With few exceptions, the orbital test data produced modes which were softer than those of the applicable ground tests. Two mechanisms for this destiffening are elimination of suspension stiffening of the boundaries and gravity preload of the structure. To evaluate the influence of the first mechanism on the ground test results, several variants in suspension stiffness were used in an earlier set of experiments. It was found that the finite element model correctly predicted the linear stiffening of the STA due to 1, 2 and 5 Hz suspensions. However, the linear model underpredicted the destiffening due to the removal of the suspension altogether. Therefore, it can be concluded that the absence of gravity loading directly on the structural elements was the cause of the destiffening. However, the finite element model also captured the "linear" gravity geometric stiffening, such as that which leads to buckling. The inference is that the softening in space must be due to gravity loading on the nonlinear elements of the structure.

In general, the space data were also more damped than the 1-g suspended data. Again, two mechanisms exist to explain the change in damping between the ground and orbital tests. Measured damping can be due to transmission of energy out of the structure or true dissipation. Comparing the transmission paths present in the middeck and ground tests, one finds the same umbilical, same atmosphere, and a much less intrusive suspension on the middeck; thus, the transmission losses must be the same or less on orbit. This is substantiated by the relatively similar damping measured at high preloads and low excitation amplitudes. Therefore, the increase in damping is once again due to internal mechanisms, probably dominated by the nonlinear elements. When testing in 0-g, no gravity field exists to preload the joints and wires of the deployable structure. With the gravity induced bias removed, the joints would be able to participate more freely and increase the effective damping of the structure. Also, with the gravity induced preload on the alpha joint removed, the joint would be freer to introduce damping, especially when in the alpha joint loose setting. Thus, the potentially nonlinear elements (the joints, wires and alpha joint) are the likely sources of the softening and dampening which occurs on orbit.

The first generation models (those derived from drawings and handbook data) clearly did a poor job of modeling all the structural configurations. In fact, the differences between the models and the actual structures were typically larger than the differences between the ground and orbital test results. Further,

the modeling of suspension influences was only partially successful, due to the fact that the influence of gravity on the nonlinear elements was not modeled. Since the development models retained less information than the evaluation models from which they were developed, the evaluation models outperformed the development models, but only by a fraction of a percent in mean error, and with no noticeable difference in standard deviation. The bias error in frequency was about 1.5%, and the standard deviation was about 5%, typical of first generation finite element model.

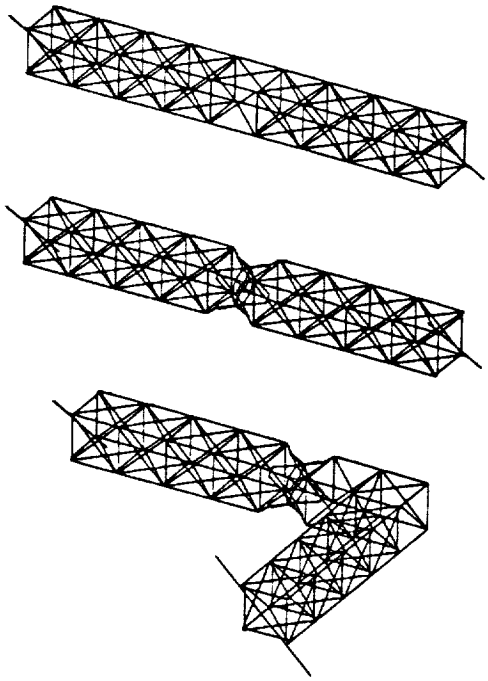

Figure 2.1 STA baseline, alpha joint and L configurations.

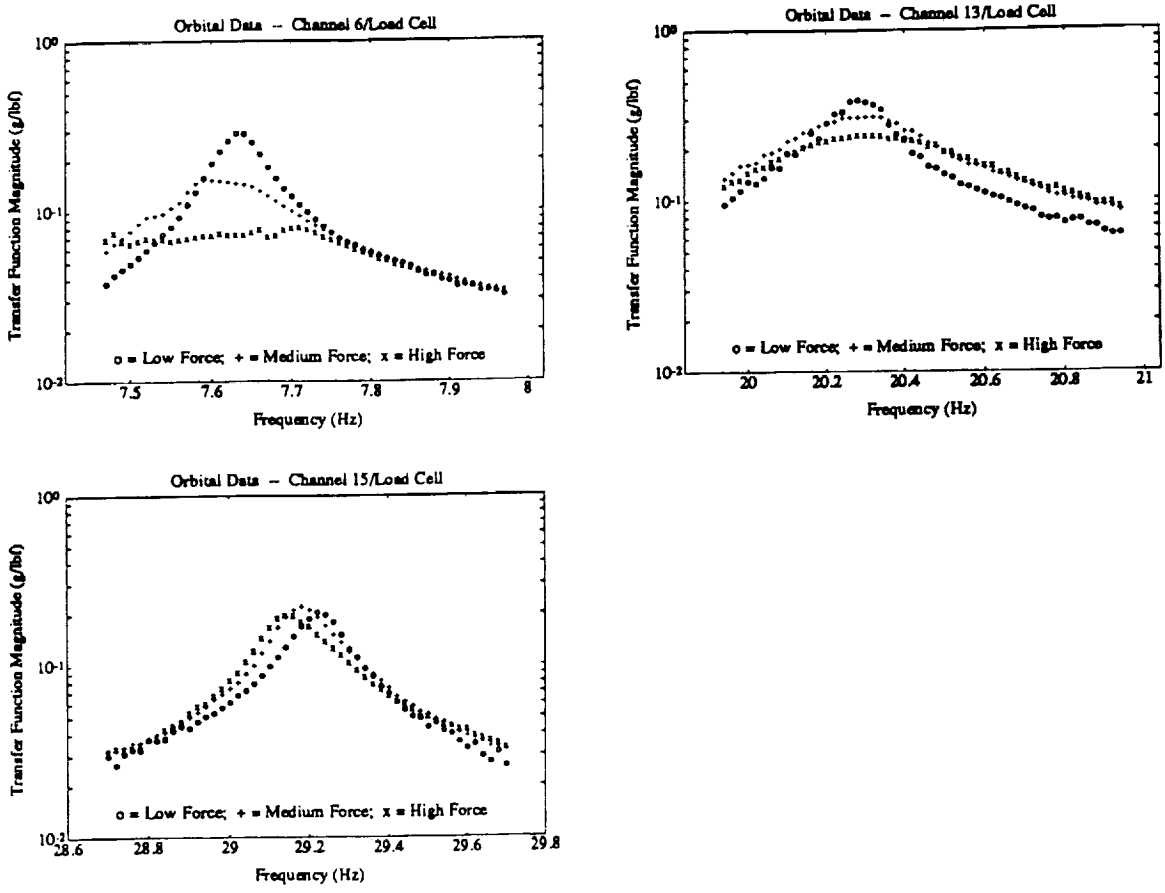

Figure 2.2 Transfer functions of the torsion, bending and shearing modes for baseline configuration, on orbit data.

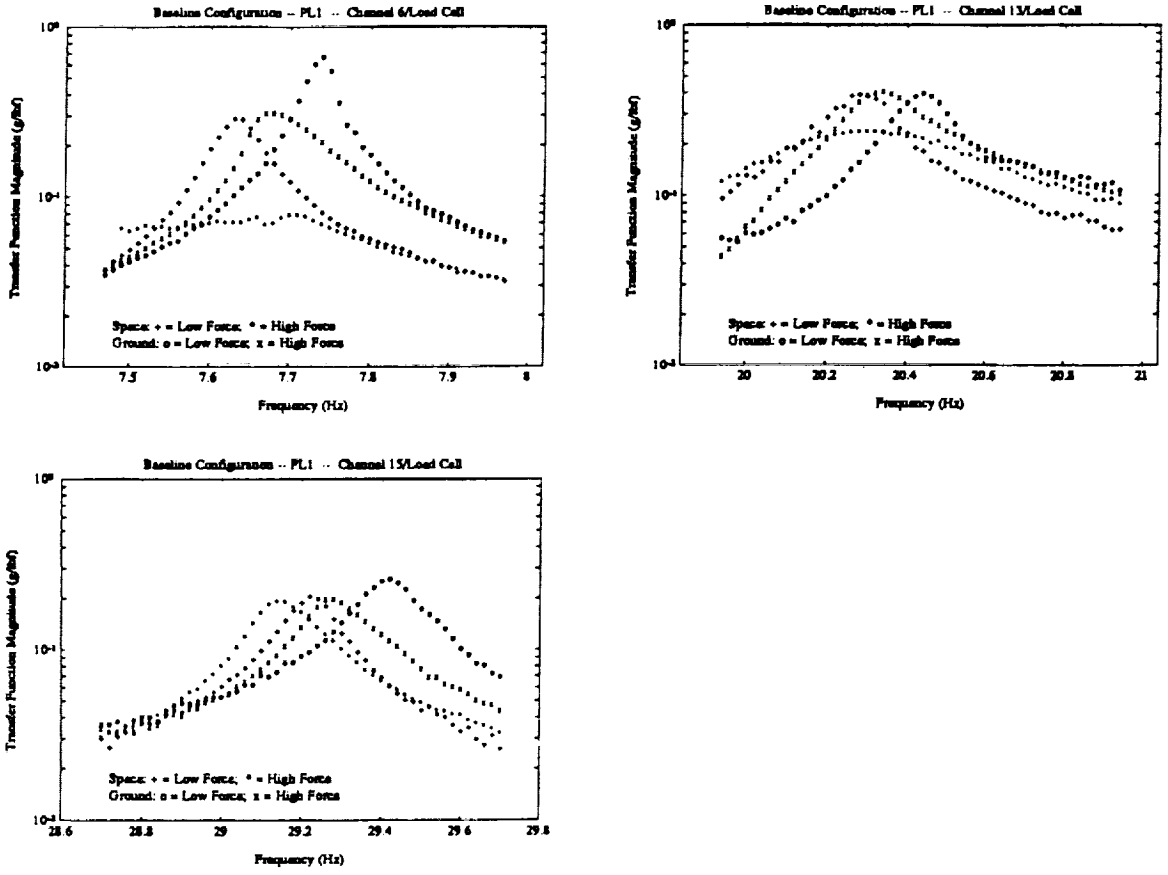

Figure 2.3 Transfer functions of the torsion, bending and shearing modes for baseline configuration, high preload (PL1), on orbit vs ground data.

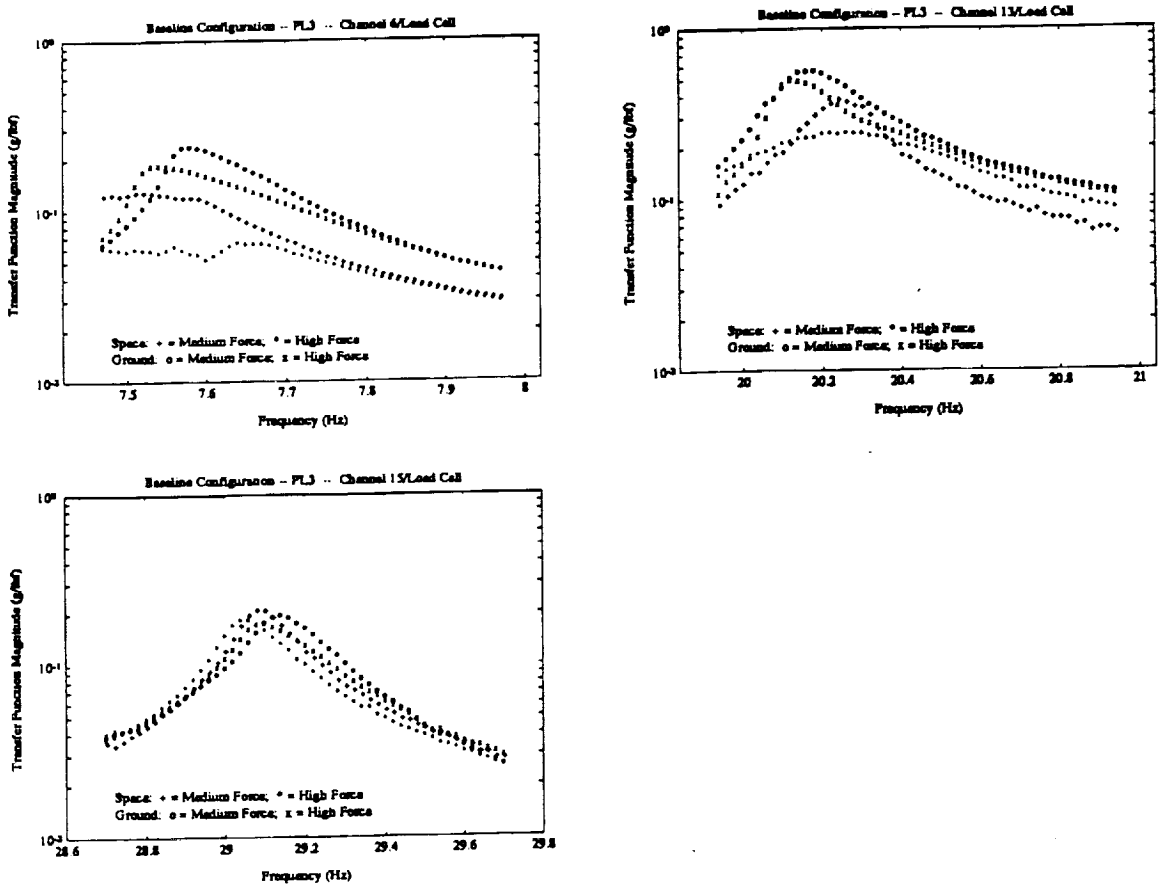

Figure 2.4 Transfer functions of the torsion, bending and shearing modes for baseline configuration, low preload (PL3), on orbit vs ground (1 Hz suspension) data.

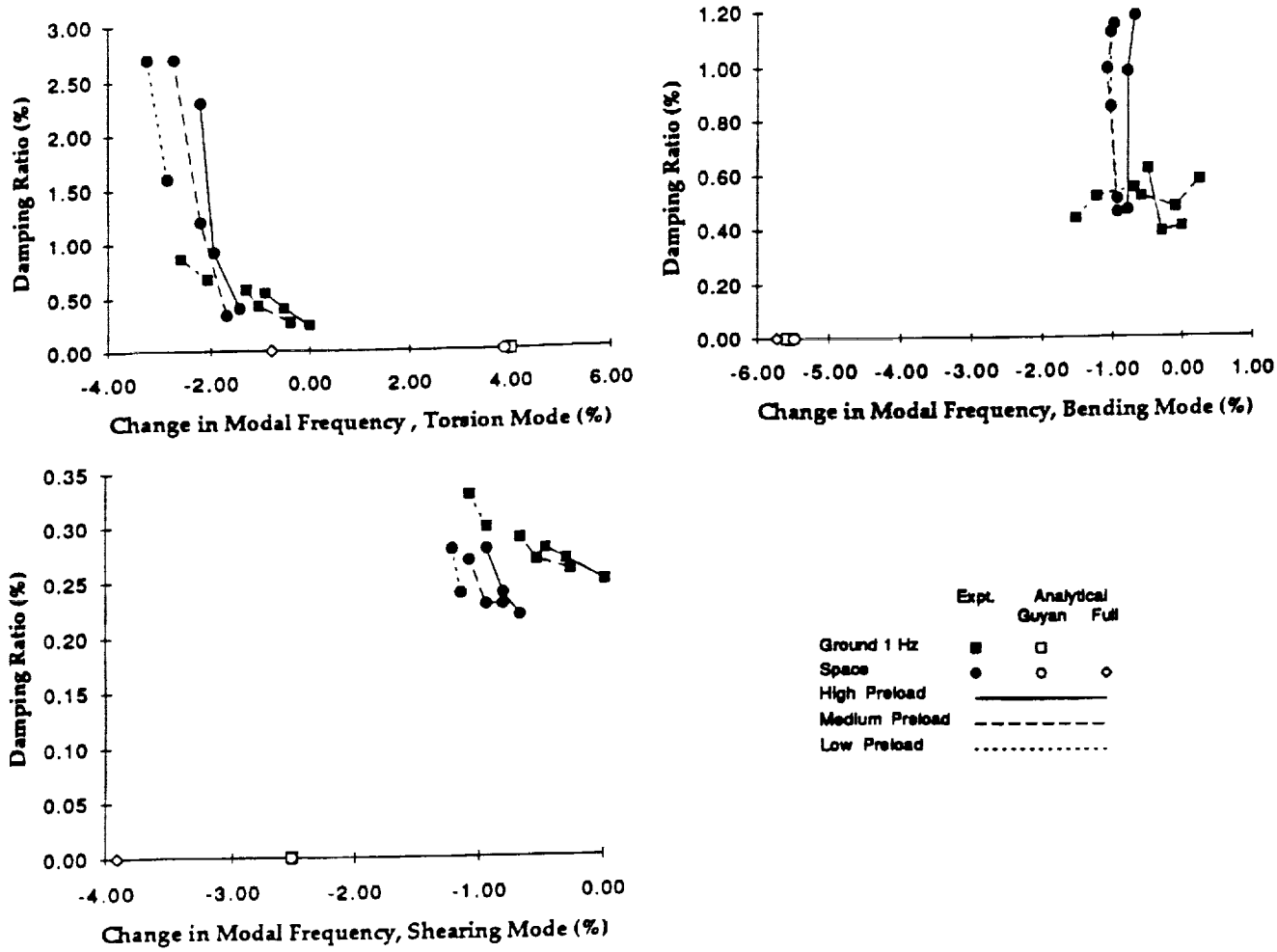

Figure 2.5 Trends in modal parameters, baseline configuration, torsion, bending and shearing modes, on orbit and ground (1 Hz suspension) data.

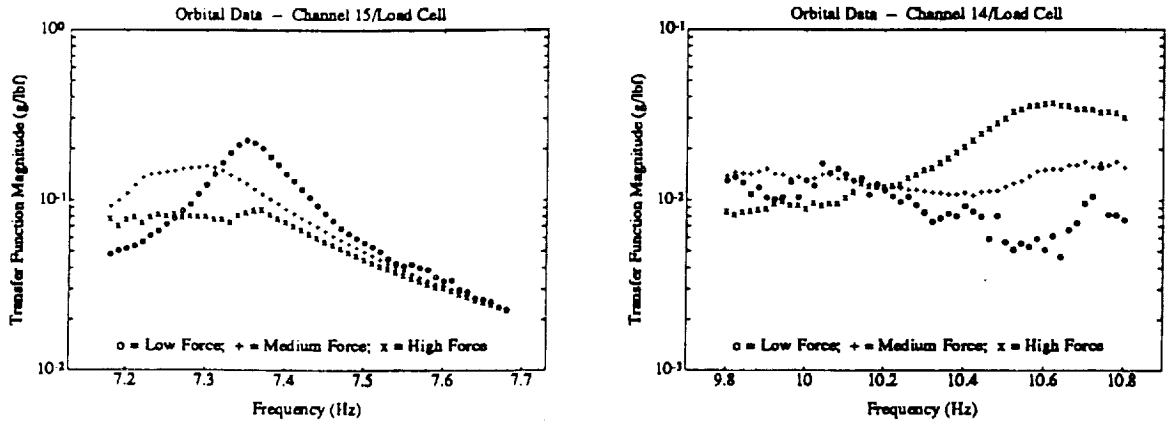

Figure 2.6 Transfer functions of torsion and bending modes, alpha configuration, alpha tight, on orbit data.

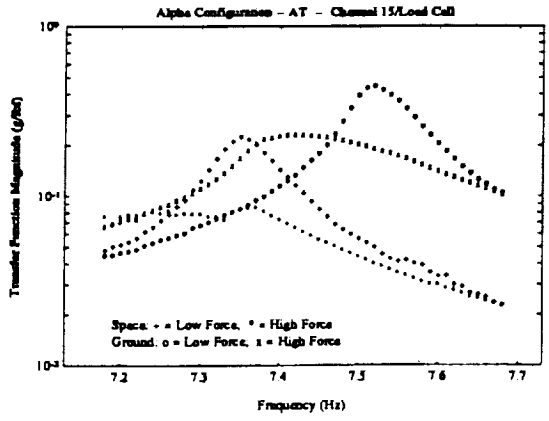

Figure 2.7 Transfer functions of torsion mode, alpha configuration, alpha tight, on orbit vs ground (1 Hz suspension) data.

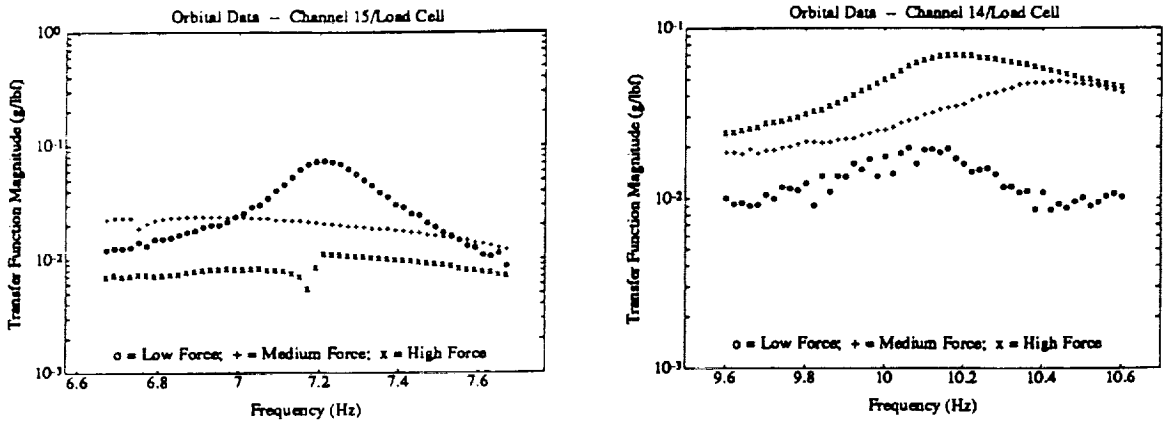

Figure 2.8 Transfer functions for torsion and bending modes, alpha configuration, alpha loose, on orbit data.

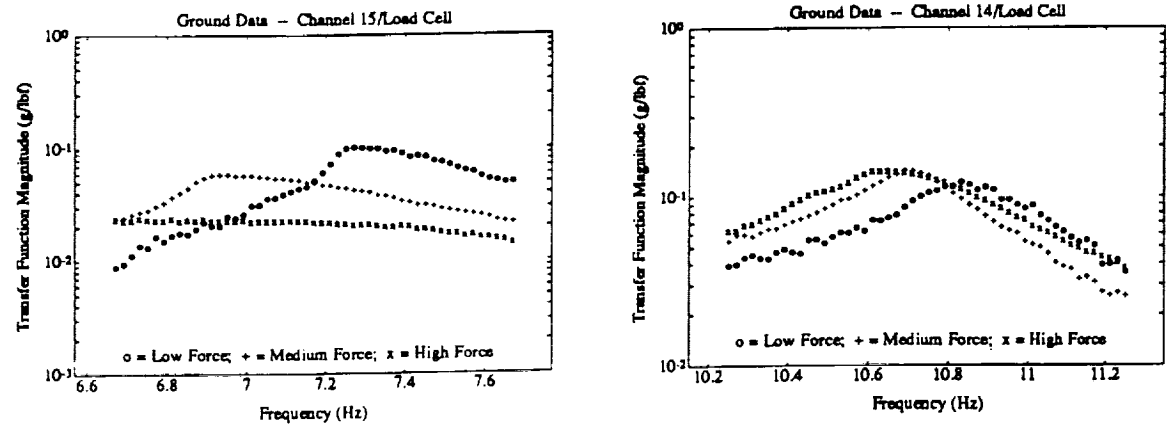

Figure 2.9 Transfer functions for torsion and bending modes, alpha configuration, alpha loose, ground data.

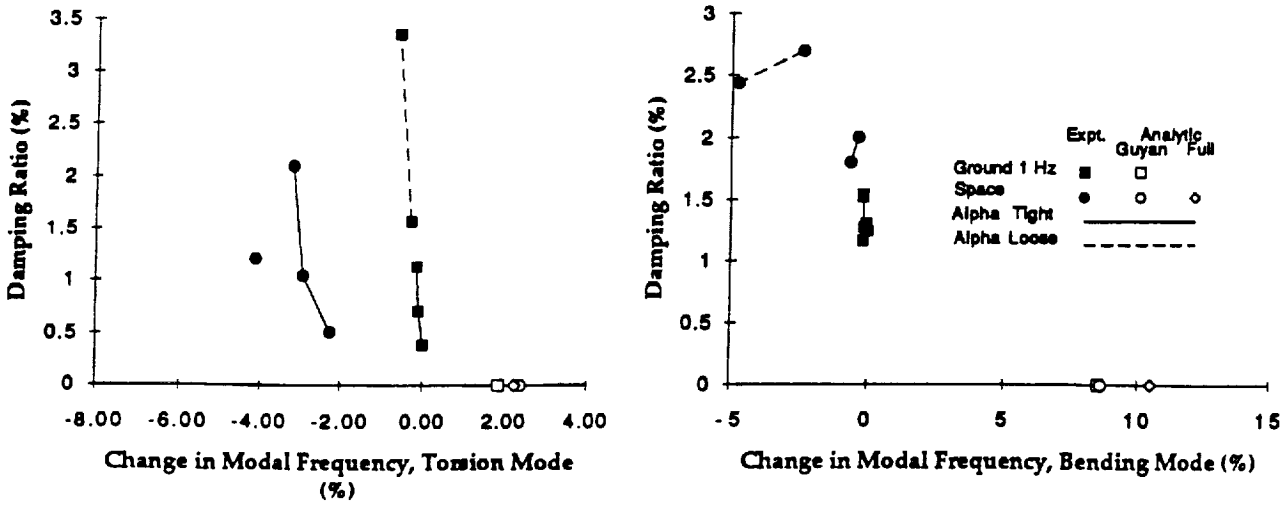

Figure 2.10 Trends in modal parameters, alpha configuration, torsion and bending modes, on orbit and ground (1 Hz suspension) data.

Table 2.1 Force amplitude used in STA excitation.

Config.	Mode	Type	Approx. Freq. (Hz)	Amplitude 1 Ground (lbf)	Amplitude 1 Space (lbf)	Amplitude 2 Ground (lbf)	Amplitude 2 Space (lbf)	Amplitude 3 Ground (lbf)	Amplitude 3 Space (lbf)
Baseline	1	Torsion	7.75	0.046	0.052	0.224	0.296	0.396	0.530
	2	Bending	20.0	0.044	0.046	0.208	0.228	0.368	0.407
	3	Shearing	29.0	0.043	0.046	0.204	0.223	0.362	0.397
Alpha	1	Torsion	7.25	0.046	0.051	0.227	0.303	0.276	0.547
	2	Bending	10.5	0.043	0.048	0.130	0.257	0.380	0.462
L	1	Torsion	7.75	0.047	0.048	0.263	0.292	0.471	0.526
	2	Bending	25.5	0.039	-	0.226	0.224	0.404	-
	3	Bending	30.5	0.030	-	0.223	0.221	0.399	-

Table 2.2 Predicted and measured modal parameters of the baseline configuration.

		Pred. Freq. (Hz)		Frequency (Hz)			Damping Ratio (%)		
	Suspension	Full	Guyan	Low Force	Medium Force	High Force	Low Force	Medium Force	High Force
Torsion									
High	1 Hz		8.05	7.74	7.70	7.67	0.24	0.40	0.54
Preload	0-g	7.68	8.04	7.63	7.59	7.57	0.40	0.92	2.3
Med.	1 Hz		NA	7.71	7.66	7.64	0.27	0.42	0.57
Preload	0-g		NA	7.61	7.57	7.53	0.34	1.2	2.7
Low	1 Hz		NA	-	7.58	7.54	-	0.67	0.86
Preload	0-g		NA	-	7.52	7.50	-	1.6	2.7
Bending									
High	1 Hz		19.29	20.43	20.37	20.33	0.41	0.39	0.62
Preload	0-g	19.26	19.31	20.27	20.27	20.29	0.47	0.98	1.18
Med.	1 Hz		NA	20.48	20.41	20.31	0.58	0.48	0.52
Preload	0-g		NA	20.24	20.21	20.23	0.46	0.99	1.15
Low	1 Hz		NA	20.29	20.18	20.12	0.55	0.52	0.44
Preload	0-g		NA	20.24	20.22	20.22	0.51	0.85	1.12
Shearing									
High	1 Hz		28.68	29.42	29.33	29.28	0.25	0.27	0.28
Preload	0-g	28.27	28.68	29.22	29.18	29.14	0.22	0.24	0.28
Med.	1 Hz		NA	29.34	29.26	29.22	0.26	0.27	0.29
Preload	0-g		NA	29.18	29.14	28.10	0.23	0.23	0.27
Low	1 Hz		NA	-	29.14	29.10	-	0.30	0.33
Preload	0-g		NA	-	29.08	29.06	-	0.24	0.28

Table 2.3 Predicted and measured nodal parameters of the alpha configuration tested with high deployable bay preload.

		Pred.Freq. (Hz)		Frequency (Hz)			Damping Ratio (%)		
	Suspension	Full	Guyan	Low Force	Medium Force	High Force	Low Force	Medium Force	High Force
Torsion									
Tight	1 Hz		7.66	7.52	7.44	7.41	0.39	0.71	1.14
	0-g	7.69	7.70	7.35	7.30	7.28	0.51	1.05	2.1
Loose	1 Hz	NA		7.31	7.08	-	1.58	3.36	-
	0-g	NA		7.21	6.74	7.19	1.21	NDR	NDR
Bending									
Tight	1 Hz		11.57	10.85	10.68	10.69	1.24	1.16	1.54
	0-g	11.78	11.58	-	10.62	10.59	-	2	1.8
Loose	1 Hz	NA		10.79	10.72	10.68	1.31	1.91	1.52
	0-g	NA		-	10.40	10.15	-	2.7	2.44

Table 2.4 Predicted and measured modal parameters of the L configuration tested with high deployable bay preload.

		Prediction		Frequency			Damping Ratio		
	Suspension	Full	Guyan	Low Force	Medium Force	High Force	Low Force	Medium Force	High Force
Torsion									
Tight	1 Hz		7.90	7.87	7.77	7.73	0.42	0.78	0.92
	0-g	8.12	8.00	7.34	-	-	-	-	-
Loose	1 Hz		NA	7.76	7.63	7.57	0.51	0.77	0.71
	0-g		NA	-	-		-	-	-
Bending									
Tight	1 Hz		25.16	25.84	25.74	25.70	0.4	0.34	0.33
	0-g	25.29	25.28	-	-	-	-	-	-
Loose	1 Hz		NA	25.83	25.76	25.73	0.37	0.32	0.37
	0-g		NA	-	-	-	-	-	-
Bending									
Tight	1 Hz		30.78	31.69	31.47	31.46	0.55	0.73	1.32
	0-g	31.30	31.15	-	-	-	-	-	-
Loose	1 Hz		NA	31.77	31.58	31.59	0.45	0.84	1.27
	0-g		NA	-	-	-	-	-	-

2.6 References for Chapter 2

ADINA User's Manual, ADINA R&D, Watertown, MA, 1987

Barlow, Mark S., "Modeling and Ground Modal Identification of Space Structures," S.M. Thesis, MIT Cambridge, MA., January 1992

Crawley, E.F., Barlow, M.S., van Schoor, M.C., Bicos, A.S., "Variation in the Modal Parameters of Space Structures," Proceedings of the 33rd AIAA/ASME/ASCE/AHS Structures, Structural Dynamics and Materials Conference, Dallas, TX, April 1992.

Ewins, D.J., "Modal Testing: Theory and Practice," Research Studies Press, 1984, pp. 158-168.

Gronet, M.J., Crawley, E.F., Dienhols, D., "Design, Analysis, and Testing of a Hybrid-Scale Structural Dynamic Model of the Space Station."AIAA Paper N. 89-1340, 1989

Guyan, R.J., "Reduction of Stiffness and Mass Matrices," AIAA Journal, Vol. 3, 1965, p. 380.

Kienholz, D.A., Crawley, E.F. and Harvey, I.J., "Very Low Frequency Suspension Systems for Dynamic Testing," AIAA Paper No. 89-1194, 1989.

Pinson, L.D. and Hanks, B.R. "Large Space Structures Raise Testing Challenges," Astronautics and Aeronautics, Vol. 21, No. 10, 1983, p. 34.

Rey, D.A., "The Effects of Suspension Systems and Gravity on Ground Based Tests of Controlled Space Structures," S.M. Thesis, MIT Cambridge, MA, August 1992.

Chapter 3: Fluid Test Article Results

3.1 Introduction

The on orbit results of the fluid slosh dynamics segment of the MODE program, as well as backround and key ground results, will be presented in this chapter. The prime objectives of the MODE fluid slosh experiments were: to provide a fundamental insight into the lateral oscillatory behavior in micro-gravity of contained fluids typical of those found in on orbit fluid tanks; to provide data for calibrating and verifying a well-posed model of such phenomena; and in doing so to provide the basic scientific and practical engineering knowledge needed to design space-based systems such as fuel depots and other fluid storage systems. This report will focus on the presentation of the on orbit and ground results, highlighting their differences and comparing them where possible to linear theory.

The precise operating requirements of modern spacecraft demand a detailed model of all of the dynamic components of the system, including the dynamics of onboard contained fluids. This modeling requirement becomes more important as spacecraft increasingly rely on higher efficiency liquid propellants. Since the nonlinear fluid/spacecraft motion caused by finite amplitude fluid slosh departs significantly from motion predicted by linear theory, the standard approach of using linearized models of the contained fluid dynamics for structural and control analyses is inadequate for addressing this problem [van Schoor, 1990].

The theory of nonlinear fluid slosh, despite the contributions of many researchers and experimenters, is still one of the areas of classical fluid dynamics that is not well understood. Contained fluids on board spacecraft exhibit nonlinear dynamic characteristics that were, in the past, routinely avoided by conservative spacecraft designs. These nonlinear dynamic characteristics, if unmodeled, can adversely affect the performance and stability of the spacecraft and lead spacecraft designers to conservative designs, with associated mass and cost penalties.

The importance of the slosh characteristics of contained fluids is reflected by the research efforts of the engineering and science communities [Abramson, 1966, Agrawal, 1984, Dodge and Garza, 1967 and 1970, Komatsu, 1987, Kutler and Sigillito, 1984, Martin 1986, Miles 1984a and 1984b, Salzman and Masica, 1969, Satterlee and Reynolds, 1964, Yeh, 1967]. The importance is also stressed by the research in the former Soviet Union [Ganiev, 1977 and Limarchenko, 1981 and 1983]. Since 1985, researchers at MIT have developed a non-linear, non-planar contained fluid/spacecraft model. This model was verified for one-gravity conditions by comparing predicted slosh forces with those measured for an extensive test matrix on fluids contained in cylindrical, spherical and rectangular tanks [van Schoor et al, 1989]. However, given that gravity has a significant influence on the modal characteristics of contained fluids, a shuttle experiment was proposed as part of the MODE program.

The first part of this chapter describes the MODE hardware and the fluid test articles. As a motivation for investigating nonlinear slosh, the hardware description is followed by a summary of the major sources of non-linearity in the slosh dynamics and their variation with apparent gravity. The chapter then presents the ground and on orbit experimental results, and concludes with a discussion of the trends in these results.

3.2 Hardware and Test Procedure

3.2.1 Hardware Description

The MODE hardware as used in the fluid slosh experiments consisted of the Experiments Support Module (ESM), shaker and force balance assembly, and the Fluid Test Articles (FTA's). The functional objective for the MODE hardware was to establish on the shuttle middeck a small dynamics laboratory with which the forced response of various systems could be determined. The core of this laboratory is the MODE experimental support module (ESM). The ESM has a computer, a 16-key keyboard, an alphanumeric display, a 200 MB WORM disk for storage, 64 Digital Input and Output (DIO) lines, and 16 Analog to Digital (A/D) channels. The ESM has excitation, data storage, signal conditioning and experiment control functions, and can be used with various types of dynamic test articles.

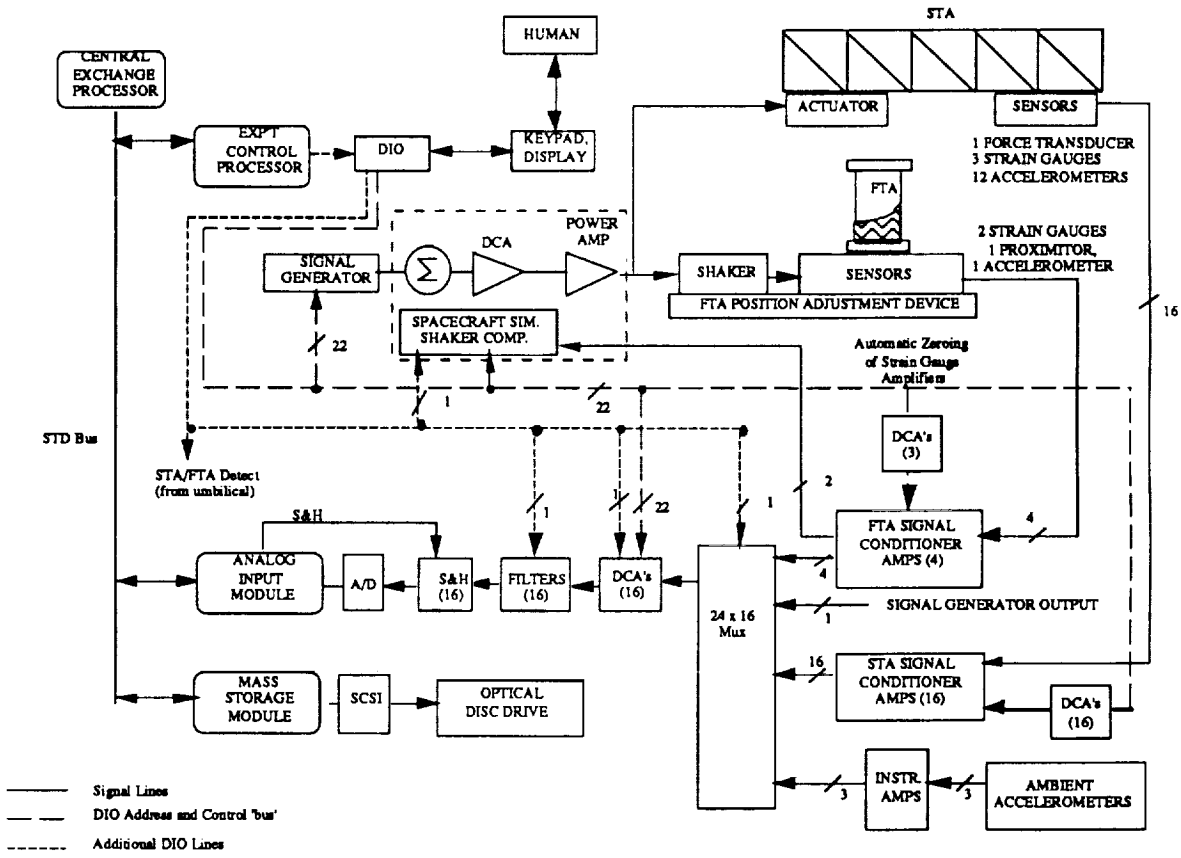

Figure 3.1 Schematic of MODE hardware

Figure 3.1 is a schematic of the MODE hardware. Both the fluids and structural experiments are controlled by the ESM. Upon power-up the astronaut can select a pre-stored protocol, which contains the desired forcing amplitude, duration and frequency information for each specific experiment. Given a forcing amplitude and frequency, the ESM generates the appropriate sinusoidal excitation signal. For fluid slosh experiments, this signal is fed via a power amplifier to an electro-mechanical shaker to which a very sensitive force balance is attached (Table 3.1 and Figure 3.2). This force balance can measure slosh forces in both the planar (x) and non-planar (y) directions. The frequency response of the fluid is determined by sinusoidal dwell testing. The experimental control function allows for the sinusoidal excitation frequency to be smoothly increased or decreased; i.e., changed without loss of phase continuity. In addition to the measurement of the slosh forces, the displacement and acceleration of the tank in the x-direction is also measured, as are the ambient accelerations. The fluid slosh behavior was also recorded by a video camcorder.

Table 3.1 FTA sensor and balancing sensitivities.

Measurement	Symbol	Sensitivity
Planar Slosh Force	K_{Fx}	20.90 V/N
Non-planar Slosh Force	K_{Fy}	21.51 V/N
Displacement	K_x	0.327 V/mm
Acceleration	K_{ax}	0.78 V/ms^{-2}

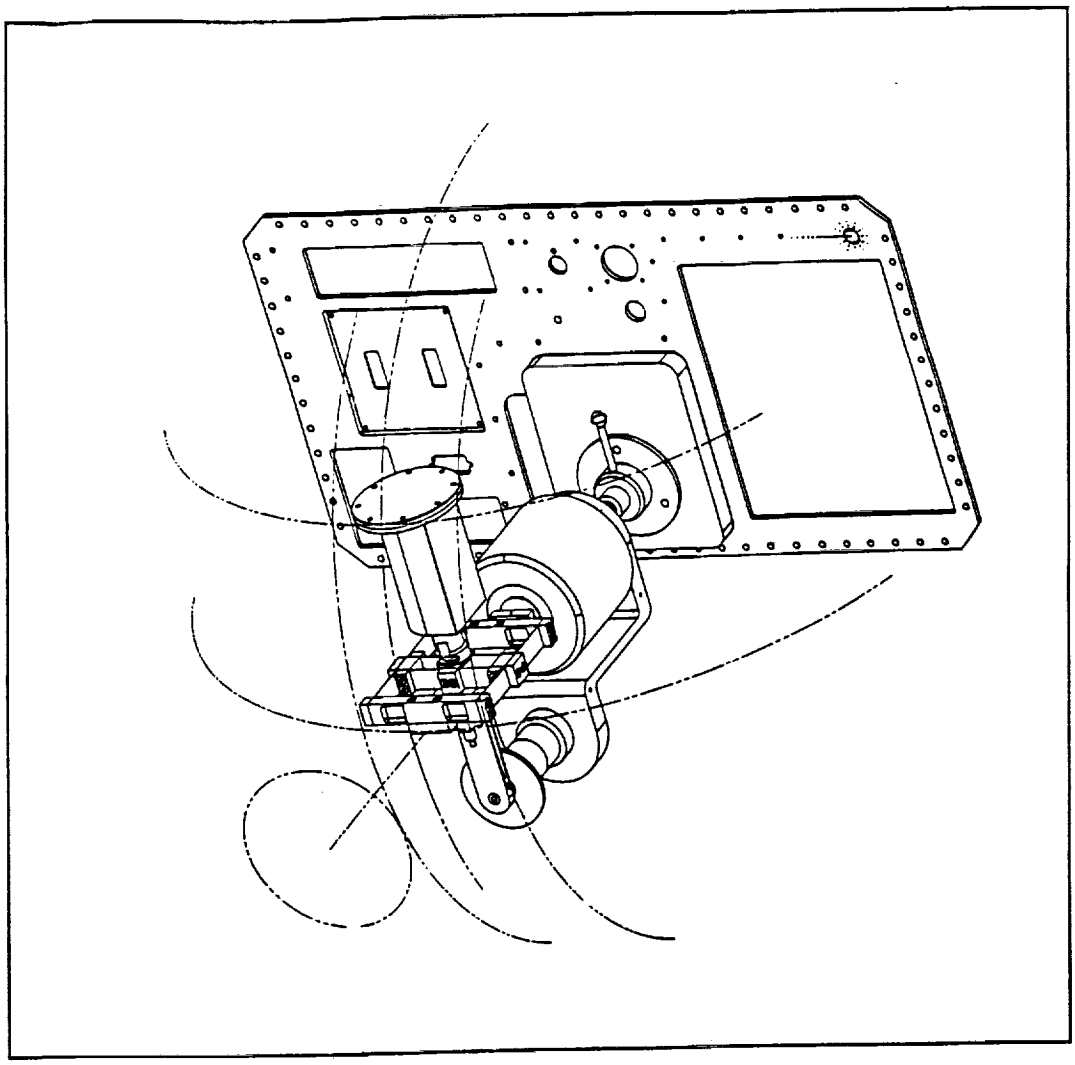

Figure 3.2 Line drawing of the MODE FTA force balance.

The FTAs containing the fluids under investigation are attached to the force balance via a quick release coupling. Since the experiment design calls for the fluid to be aligned in the bottom of the tank, this quick release coupling enables the astronauts, after having aligned the fluid, to attach the tank to the force balance without disturbing the fluid alignment. Alignment of the fluid is required at the start of a new experiment or when unanticipated re-alignment occurs.

A unique feature of the MODE hardware is that the force balance and accelerometer signals are automatically zeroed by the ESM. This avoids signal saturation due to thermal drifts. The digitally controlled amplifiers (DCA) in the signal paths also enable researchers to select optimal signal gains to ensure the best possible signal-to-noise ratios and to avoid channel saturation. The sensitivities of the measured signals at an amplifier gain of unity are summarized in Table 3.1. By using the DCAs, each of these sensitivities can be amplified by as much as 16 times.

The MODE hardware allows the investigation of both the uncoupled behavior of a fluid, and the coupled behavior of a fluid/spacecraft system. In the uncoupled configuration, a commanded displacement signal directly drives the motion of the electro-mechanical shaker. In the coupled configuration, the force excitation signal is fed to a analog simulation of a spacecraft lateral mode (Figure 3.3). The analog simulation is also fed a signal which is the measured slosh force; i.e., the total force measured by the reaction balance minus the dry force component. The calculated spacecraft displacement is then commanded of the shaker. In both the uncoupled and coupled configurations, a shaker servo loop ensures that the commanded displacement is tracked within 2% in amplitude and 5° in phase. The parameters of the simulated spacecraft mode (i.e., frequency (G_ω), damping ratio (G_ζ), mass (G_{SM}) and the dry mass component ($\omega^2 G_{DM}$)) are stored in the protocols and are digitally set with the ESM's DIO lines.

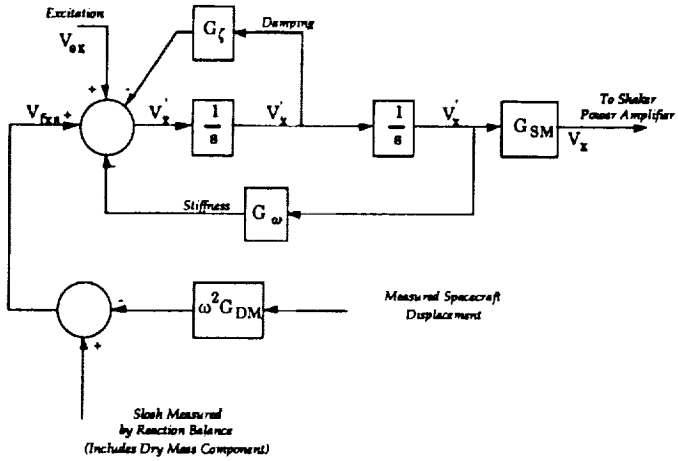

Figure 3.3 Analog simulation of a spacecraft lateral mode.

3.2.2 Fluids and Tank Geometries

The selection of the test fluids was driven by the following criteria: for safety reasons the fluids had to be safe; and for engineering relevance the fluids properties had to match the properties of typical spacecraft propellants (Table 3.2). Given these criteria, silicone oil with a 5 centistoke viscosity was selected as the primary test fluid. This silicone oil is non-toxic and non-flammable and it approximately matches the properties of Liquid Oxygen. However, the free surface stability of the silicone oil was a concern. Given the proven free surface stability of water, triply distilled water was selected as the secondary test fluid. The properties of the silicone oil and of water are also presented in Table 3.2.

Table 3.2 Fluid properties.

Fluid	Density (ρ) (kg/m^3)	Kinematic Viscosity (ν) (cm^2/sec^2)	Surface Tension (σ) (dyne/cm)
Liquid H_2	70.0	0.002	1.9
Liquid O_2	1140.0	0.002	13.2
Hydrazine	1010.0	0.010	63.2
Silicone oil	920.0	0.005	19.7
Distilled Water	998.0	0.010	72.75

The geometry of the fluid test article was selected such that the results could be extrapolated to typical space storage tanks. A cylindrical tank with a flat bottom and a cylindrical tank with a spherical bottom were chosen. A variety of existing ground experimental results were available on these tank shapes to support design and analysis.

In sizing the tanks, an important criterion was that the equilibrium free surface of the fluid must be retained during all space shuttle maneuvers except primary RCS firings. Eq. 3.1 gives the critical negative acceleration at which the free surface will loose stability and re-orient.

$$g^{\text{Critical}}_{\text{Re-orientation}} = \frac{(-3.4 + 2.6\cos\alpha)\sigma}{\rho a^2} \tag{3.1}$$

where α is the contact angle and a is the tank radius.

An evaluation of the ambient and operational accelerations on board the space shuttle resulted in a requirement that the contained fluid must withstand at least 7 mg's of negative acceleration before realignment.

A second criterion that governed the selection of the tank size was a minimum slosh frequency of 0.5 Hz. A slosh frequency much below this would require extremely long testing times and place severe requirements on the sensitivity of the acceleration and forcing/sensing elements. A 3.1 cm diameter tank satisfied both the free surface stability and minimum slosh frequency requirements. The decision to use 3.1 cm diameter tanks was further justified by the fact that a multitude of ground experimental results were already available

for this diameter tank. The two cylindrical model tanks, one with a flat bottom and one with a spherical bottom, are depicted in Figure 3.4.

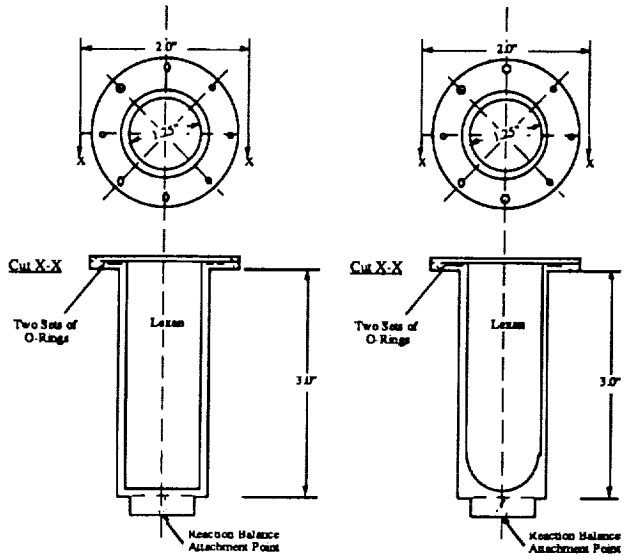

Figure 3.4 MODE FTA cylindrical flat and spherical bottom model tanks.

3.2.3 Test Procedures and Data Reduction

The fluid response data were obtained by sine dwell over a range of frequencies, and for the different force levels. Typical frequency sweeps contained 65 frequency points and dwell times of 6 to 40 seconds. The excitation window ranged from 50% below the first natural slosh frequency to 2 times this frequency. The signal sampling rate for both the ground and on orbit experiments was 50 Hz, with the anti-aliasing filters set at 18 Hz.

In post-processing the results, the time traces of force, displacement and acceleration were read from the WORM disks and the harmonic frequency information was extracted from these signals. This retrieval process was repeated for each forcing frequency and amplitude test point. The linear modal characteristics of the contained fluids were determined by fitting a two-complex pole approximation to the "linear" (lowest forcing amplitude) uncoupled displacement to planar-force transfer function. Eq. 3.2 is a linearized model of the fluid's first slosh mode.

$$F_{xs} = -\ddot{x}m_f - \ddot{q}_1\lambda m_f$$
$$\ddot{q}_1 + 2\zeta_{q_1}\omega_s\dot{q}_1 + \omega_s^2 q_1 = -\ddot{x} \qquad (3.2)$$

where m_f is the fluid mass, x is the displacement of the tank, q_1 is the first fluid slosh mode degree-of-freedom, λ is the fraction of the fluid mass participating in the resonant motion, ζ_{q_1} is the damping ratio of the first mode and ω_s is the natural frequency of the first mode. The modal parameters λ, ζ_{q_1} and ω_s are obtained from the fit.

The frequency domain transfer functions of displacement to planar slosh force and displacement to non planar slosh force were also obtained for the uncoupled tests. In the coupled tests, the transfer functions of excitation force to tank displacement were also obtained for the different excitation amplitudes.

3.3 Modeling

3.3.1 Nonlinear Fluid Phenomena

Because the MODE scientific objective is to understand the coupled nonlinear slosh of fluids in microgravity, an appropriate nonlinear model was developed at MIT to compliment the experimental program [van Schoor, 1989]. A complete description of the model and its correlation with ground and flight data is beyond the scope of this report, but a summary of the major sources of non-linearities in contained fluids and the major differences between the one-gravity (earth) and micro-gravity (space) dynamic behavior of fluids is outlined, as is the model derivation. The section concludes with a summary of linearized fluid slosh models with which the linear, low slosh amplitude, modal behavior of contained fluids can be predicted, and which will be used for experimental correlation.

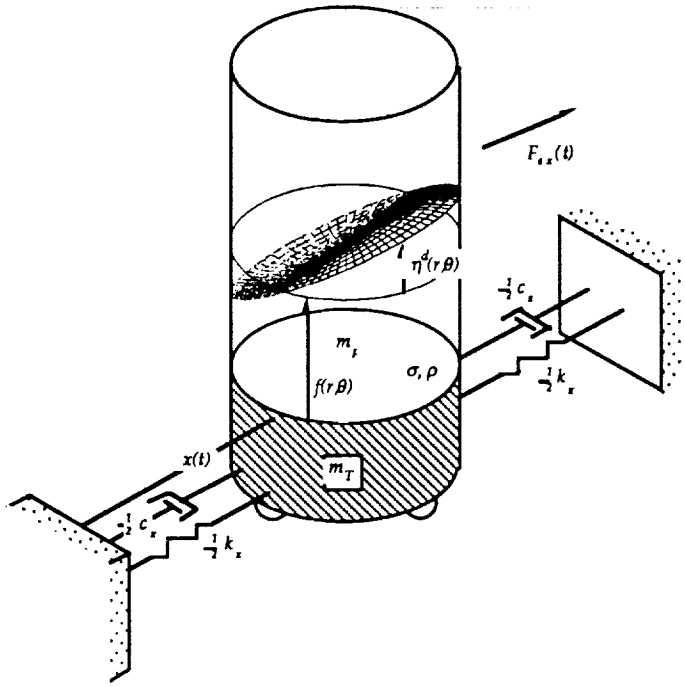

Figure 3.5 Fluid/spacecraft study model of a contained fluid.

Figure 3.5 is a schematic representation of a contained fluid in a flat bottom cylindrical tank. The springs and dash pots are a mechanical representation of a spacecraft attitude control mode or a flexible mode. In this model, the free surface is described by the sum of two two-dimensional functions, $f(r,q)$, the equilibrium free surface height, and the dynamic perturbation from this equilibrium, $\eta^d(r,q)$. The internal flow can be described by a three dimensional potential function (ϕ). The two major contributions to the nonlinear dynamic behavior of the contained fluid and the gravity influence on these contributions are outlined in the next two subsections.

Time Dependent Free Surface Boundary Condition. The relationship between the fluid flow potential function and the free surface function is one of the major sources of non-linearities in the fluid slosh behavior for finite motion [Abramson, 1966 and Miles, 1984b]. Consider the action of the convection forces at the free surface of the fluid. The potential flow (ϕ) and the free surface motion (η) must satisfy the kinematic boundary condition:

$$\frac{\partial \eta}{\partial t} + \nabla\phi \bullet \nabla\eta\Big|_{z=\eta} = \frac{\partial \phi}{\partial z}\Big|_{z=\eta} \tag{3.3}$$

This equation is an analytical expression of the Dirichlet and Neumann problems and constitutes a nonlinear relation between the fluid flow potential (ϕ) and the free surface motion (η). The effects of a change in the ambient acceleration (gravity) can be better revealed when free surface motion is expressed in terms of the equilibrium free surface (f) and the dynamic motion of the free surface (η^d), that is:

$$\eta = f + \eta^d \tag{3.4}$$

Using Eq. 3.4, Eq. 3.3 can be written as:

$$\frac{\partial \eta^d}{\partial t} + \nabla\phi \bullet \nabla\left(f + \eta^d\right)\Big|_{z=\eta} = \frac{\partial \phi}{\partial z}\Big|_{z=\eta} \tag{3.5}$$

From this equation it is clear that the nonlinear free surface boundary condition is a function of the equilibrium free surface. The equilibrium free surface is strongly dependent on gravity, as can be seen by examining Figure 3.6, an analytical prediction of the equilibrium free surface under one- and zero-gravity conditions. One can conclude that the nonlinear effects of the free surface boundary condition will change between one-gravity and micro-gravity conditions.

Capillary Potential Energy. Another source of non-linearities is the potential energy associated with the capillary forces [Limarchenko, 1981 and 1983].

$$U_\sigma = \sigma \iint_S \sqrt{1 + \nabla\eta \bullet \nabla\eta}\, dS \tag{3.6}$$

The potential energy of the free surface is a function of the total dynamic free surface area, which is a complex nonlinear function of the free surface shape (η). Using Eq. 3.4, it can be shown that the capillary energy is also a function of the equilibrium free surface, that is:

$$U_\sigma = \sigma \iint_S \sqrt{1 + \nabla\left(f + \eta^d\right) \bullet \nabla\left(f + \eta^d\right)}\, dS \tag{3.7}$$

The shape of the equilibrium free surface is a function of the Bond number, a non-dimensional measure of the relative importance of gravity versus capillary forces:

$$Bo = \frac{\rho g a^2}{\sigma} \tag{3.8}$$

where (ρ) is the fluid density, (g) is the mean apparent gravity level, ($a = d/2$) is the tank radius and (σ) is the surface tension. On earth, gravity forces dominate while in space the equilibrium free surface is determined largely by the surface tension forces. Gravity tends to minimize the free surface height, and the capillary forces (given the required contact angle) tend to minimize the free surface area. Note that, due to gravity gradients, moderate Bond numbers can exist in space, especially for larger tanks and spacecraft.

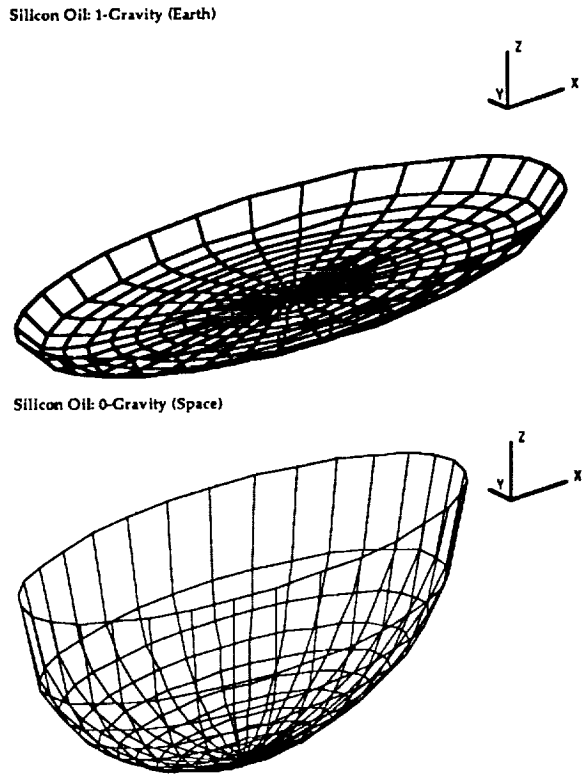

Figure 3.6 Predicted equilibrium fluid free surface for silicon oil on earth and in space. (Cylindrical tank, diameter = 3.1 cm, contact angle $\alpha = 1°$)

3.3.2 Nonlinear Fluid/Spacecraft Model

These nonlinear effects can be included in a low order nonlinear, nonplanar model [van Schoor, 1989]. If the fluid viscous effects are restricted in a

Stokes layer near the wall of the tank, the fluid flow velocity **u** relative to the tank reference frame can be completely described by an irrotational, three dimensional potential field ϕ:

$$\mathbf{u} = \nabla\phi \tag{3.9}$$

Since the fluid is incompressible, the divergence of the velocity field must vanish throughout the fluid volume:

$$\nabla \bullet \mathbf{u} = 0 \tag{3.10}$$

The partial differential equation describing the flow potential is the Laplace equation:

$$\nabla^2\phi = 0 \tag{3.11}$$

The Neumann surface boundary problem of Eq. 3.9 can be satisfied [Luke, 1967] by requiring that the integral of Eq. 3.12 remains stationary with respect to arbitrary variations of the function ϕ:

$$I = \frac{1}{2}\iiint_V (\nabla\phi \bullet \nabla\phi)dV - \iint_{S_F} \phi\Big|_{z=\eta} dS_F \tag{3.12}$$

This integral is minimized by the exact nonlinear solution to the kinematic problem. In the absence of a known exact solution, an approximate solution to the kinematic problem can be found using assumed potential flow behavior and assumed free surface motion. The assumed potential and free surface motions are not independent and their relationship can be found by substituting the assumed motions into Eq. 3.12 and requiring the result to be stationary with respect to arbitrary fluid motions.

Ignoring geometric nonlinearities, it is assumed that the free surface motion η is described in terms of the departure from the equilibrium free surface shape f (Fig. 3.5) by the superposition of a finite modal set:

$$\eta = f + \sum_{n=1}^{N} \xi_n q_n(t) \tag{3.13}$$

where q_n are the generalized coordinates of the free surface motion. The fluid potential field ϕ is assumed to be of the form:

$$\phi = \sum_{m=1}^{N} \chi_m p_m(t) \tag{3.14}$$

in which the p_m are the generalized coordinates for the flow potential.

The relationship between the two dependent sets of generalized coordinates q_n and p_m is found by requiring that the variational integral (Eq. 3.12) remains stationary for arbitrary variations of p_m. Eq. 3.12 can be expressed in a power series of p_m using a Taylor series expansion. The terms in the Taylor series are truncated to yield a fluid flow description valid to cubic order in the amplitude of the motion.

Given a relationship between the two sets of assumed modal series, the kinetic and potential energy can be expressed in terms of a single modal set. Using the fluid free surface coordinate (q_n) as the independent generalized coordinate, the kinetic energy of the fluid system shown in Fig. 3.5 is given by Eq. 3.15.

$$T_F = \frac{1}{2} m_F \left(\dot{x}^2 + \dot{y}^2\right) +$$

$$\frac{\rho}{2} \sum_{m=1}^{N} \sum_{n=1}^{N} \left[\left\{ \begin{array}{l} \alpha_{mn}^{(0)} + \sum_{r=1}^{N} \alpha_{mnr}^{(1)} q_r + \\ \sum_{r=1}^{N} \sum_{s=1}^{N} \alpha_{mnrs}^{(2)} q_r q_s \end{array} \right\} \dot{q}_m \dot{q}_n \right] +$$

$$\rho \dot{x} \left[\sum_{n=1}^{N} \dot{q}_n \iint_S \xi_n x dS \right] + \rho \dot{y} \left[\sum_{n=1}^{N} \dot{q}_n \iint_S \xi_n y dS \right] \qquad (3.15)$$

where the α's are elements from the slosh depth matrix, which represent the depth of fluid having a mass equal to the associated free surface modal inertia.

The fluid potential energy (the sum of the acceleration and capillary potential energies) is:

$$U = \rho \iiint_V g \vec{e} dV + \sigma \iint_S \sqrt{1 + \nabla\eta \bullet \nabla\eta} \, dS \qquad (3.16)$$

where $\vec{e}$ is the displacement of the fluid in the direction of the mean acceleration field (g). This equation can also be expressed as a power series of q_n by binomial expansion of the square root term and a Taylor expansion of the terms in the volume integral. Again truncation can be performed to yield a model valid to cubic order in the amplitude of the motion. The coefficients of the nonlinear

terms depend on both the free surface mode shapes and the shape of the equilibrium fluid free surface, and therefore on the Bond number. The relative influence of the capillary potential energy on the fluid dynamics will thus be a function of the Bond number.

The governing nonlinear differential equations describing the fluid and spacecraft motion are obtained by applying Lagrange's principle to the system Lagrangian which is obtained by adding the kinetic and potential energy of the spacecraft's mode to that of the fluid. Note that the effects of capillary viscous forces are not included in this model. A viscous damping term, equal to the measured linear slosh damping ratio, is added to the governing differential equations.

3.3.3 Linearized Models

For very small slosh amplitudes, linearized models [Abramson, 1966, Salzman and Masica, 1969] can be used to describe the fluid slosh dynamics. This section summarizes the linear models with which the natural frequency and damping ratio of the fluid can be predicted. The MODE ground and on orbit experimental results will be used to determine the accuracy of these models for one- and micro-gravity conditions.

For an inviscid fluid in a flat bottom cylindrical tank, with its contact angle free to move, Eq. 3.17 is an approximate equation for the first slosh frequency (ω_{S_1}).

$$\omega_s = \left(\frac{\sigma}{\rho a^3} \tanh\left(1.84 \frac{h}{a} \right) \{ 6.26 + 1.84 Bo - 4.76 \cos\alpha \} \right)^{\frac{1}{2}} \tag{3.17}$$

where h is the average fluid depth and α is the contact angle. Note that Eq. 3.17 is not valid for fluids that exhibit contact angle hysteresis and that, in general, contact angle hysteresis tends to increase the slosh natural frequency. A more complex model, which includes the first order effects of contact angle hysteresis, is presented in Abramson [1966] but requires numerical solution.

The major effect of capillary viscous forces is on the amount of energy dissipated (damping) by the fluid motion. These dissipative effects are important since the orbital lives of most satellites are determined by the fuel expenditure required to control the nutational stability of the spacecraft. The fuel

expenditure is proportional to the energy dissipated by the capillary viscous forces and other non-conservative forces.

Although some analytical scaling analysis and estimation are possible [Miles 1984], the prediction of fluid damping relies heavily on the results of previous experiments. At high Bond numbers (Bo > 10), the damping of the free surface waves scales with gravity and viscosity in a non-dimensional parameter similar to the Reynolds number:

$$N_{\nu_1} = \frac{\nu}{\sqrt{ga^3}} \tag{3.18}$$

where ν is the kinematic viscosity of the fluid. When gravity approaches zero, this parameter is not the proper scaling, for it would imply that the fluid becomes infinitely damped under micro-gravity conditions. When Eq. 3.18 is multiplied by the square root of the Bond number (Eq. 3.8) an alternative scaling parameter is obtained:

$$N_{\nu_2} = \nu\sqrt{\frac{\rho}{\sigma a}} \tag{3.19}$$

The multiplication of Eq. 3.18 by $\sqrt{Bo}$ is equivalent to scaling the Navier-Stokes equations using surface tension instead of gravity forces as a reference. Salzman and Masica [1969] experimentally obtained slosh damping ratios for fluids in a bare-wall cylindrical tank using drop tower tests. These experiments predict the slosh damping ratio as a function of the Bond number as shown in Fig. 3.7.

3.4 Test Results

3.4.1 Test Matrix Selection

The potential matrix of test cases includes two tanks, with two fluids, uncoupled and coupled for any number of fluid modes, amplitudes and fill heights, and for the coupled tests any number of spacecraft mass, frequency and damping ratios. The matrix of the test actually conducted on orbit is shown in Table 3.3, with a far more extensive test matrix completed on the ground. Since the MODE pre-cursor flight indicated that silicone oil presented a possible free surface equilibrium stability problem, this fluid was only tested in the uncoupled

configuration. For the coupled tests, the spacecraft model parameters were the first slosh frequency normalized by the spacecraft frequency ratio (ν = 1.04) and the fluid mass normalized by the spacecraft's mass (μ = 0.15); they were selected to yield the highest possible fluid/spacecraft dynamic coupling. The damping ratio (ζ) of the spacecraft's mode was set to 5% of critical. Table 3.3 also summarizes the tank fill levels and fluid masses associated with each of the different tests in the orbital test matrix.

Table 3.3 Space test matrix

Fluid	Tank Bottom	Test Type	Fluid Mass m_f (g)	Fluid Depth h (mm)
Sil. Oil	Flat	Uncoupled	19.10	27.51
Sil. Oil	Sph.	Uncoupled	16.02	28.24
Water	Flat	Uncoupled	23.42	31.00
Water	Sph.	Uncoupled	19.51	31.00
Water	Flat	Coupled	23.42	31.00
Water	Sph.	Coupled	19.51	31.00

The forced response characteristics for all the fluids and tanks were determined by using three logarithmically spaced forcing amplitudes. Increasing excitation frequency sweeps were used at all the forcing amplitudes. An additional sweep, with the excitation frequency decreasing from one test point to the next, was also performed at the highest forcing amplitude. The excitation displacement amplitudes for the uncoupled tests were x_{ex}/d = 0.32%, 1.02% and 3.22%. The forcing excitation amplitudes for all the coupled tests were chosen so that below resonance the displacement response would be comparable to the uncoupled tests. For the ground tests, the forcing amplitudes were F_{ex} = 1.35, 4.27 and 13.51 mN. The excitation amplitudes for all the space coupled tests were F_{ex} = 0.346, 1.095 and 3.46 mN.

Figures 3.8 to 3.27 present the ground and orbital results for all the cases in the test matrix (Table 3.3). In these figures, each symbol represents the harmonic component as measured for that forcing amplitude and frequency. Table 3.4 presents a legend for the symbols used in these graphs. In order to facilitate the comparison of the ground and orbital results, the ground transfer

functions are followed by the results of the equivalent on orbit test. In the next two sections, the ground and on orbit results are discussed separately and then compared.

Table 3.4 Symbols used in Figures 3.8 to 3.27.

Forcing amplitude	Direction of Change in Forcing Frequency	Symbol
Low	Increasing	+
Medium	Increasing	*
High	Increasing	x
High	Decreasing	o

3.4.2 Ground Test Results

Silicone Oil Uncoupled Results. The measured linear modal parameters of the uncoupled silicone oil tests, as obtained from the complex two-pole fit (Eq. 3.1), are summarized in Table 3.5. The ground Bond number for both of the tank geometries is 116. The predicted slosh frequencies and damping ratios presented in Table 3.5 are obtained from Eq. 3.17 and Figure 3.7, respectively. Note that it is assumed for both the silicone and water cases that the predicted parameters which are nominally only valid for a flat bottom cylindrical tank can be used as estimates of the modal characteristics of the fluids in the spherical bottom tanks.

Table 3.5 Silicone Oil: measured and predicted linear modal parameters.

		1st Slosh Frequency		Damping Ratio		Mass Fraction
Tank	**Test**	**Pred.** ω (Hz)	**Meas.** ω (Hz)	**Pred.** ζ (%)	**Meas.** ζ (%)	**Meas.** λ
Flat	Earth	5.19	5.24	1.4	4.0	0.24
Flat	Space	0.49	0.68	11.6	36.3	0.24
Spherical	Earth	5.19	5.26	1.4	4.2	0.22
Spherical	Space	0.49	0.65	11.6	39.1	0.33

For silicone oil, the measured linear modal frequencies are within 1% of the predicted values but the measured damping ratios are roughly three times higher than those predicted. The experimental results (Figs. 3.8, 3.10 and 3.12) show strong amplitude dependent nonlinear slosh behavior. For the flat bottom tank, Figure 3.8 shows that the first slosh frequency shifts from 5.24 Hz, at the lowest forcing amplitude (x_{ex}/d = 0.32%), to 4.6 Hz at the highest forcing amplitude (x_{ex}/d = 3.2%). This is a shift of 12% in frequency. For the spherical bottom tank, this shift from 5.26 Hz to 4.6 Hz (Fig. 12) is also 12%.

When the planar and non-planar slosh force responses of the fluid in the flat bottom tank are studied, it is clear that the fluid swirls at the highest forcing amplitude. This swirl motion manifests itself in a second resonance peak, which appears close to the linear slosh frequency (5.26 Hz). Not only does the fluid swirl at this forcing amplitude, but the slosh also has multiple response states. The slosh response is different for up- and down-frequency sweeps between 5.6 and 6 Hz (Figs. 3.8, 3.10 and 3.12). Depending on in which direction the forcing frequency is changed, the fluid motion is either a planar slosh or a non-planar swirl. This behavior is also observed for the silicone oil in the spherical bottom tank (Fig. 3.12).

When the slosh behavior of silicone oil in the flat bottom tank (Fig. 3.8) and in the spherical bottom tank (Fig. 3.12) is studied, one finds no observable difference in the behavior of the fluid slosh in these tanks. From theory it is known that the flow potential (f) decays exponentially with depth and it must be concluded that the flow potential near the bottom of the tank is too weak to change the slosh behavior of the fluid.

Water Uncoupled Results. The measured linear modal parameters of the uncoupled water tests are summarized in Table 3.6. The ground Bond number for both the tank geometries is 34. The predicted slosh frequencies and damping ratios, also presented in Table 3.6, were obtained from the linear model (with a correction for contact angle hysteresis [Abramson, 1966]) and Figure 3.7, respectively. Once the linear model was corrected to include the linear effects of contact angle hysteresis, the predicted and measured frequencies were within 2.5%. However, the measured damping ratios are roughly 60% higher than the predicted values.

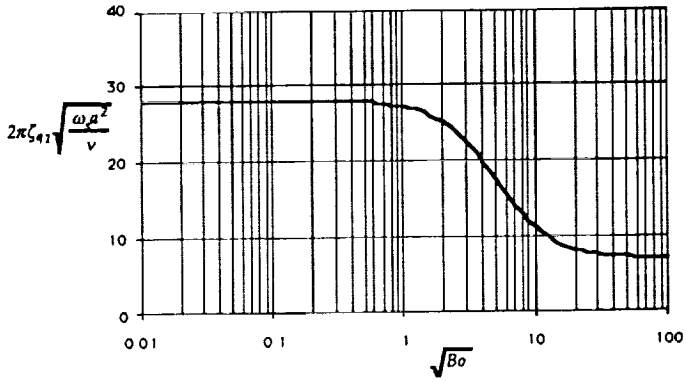

Figure 3.7 Predicted slosh damping ratios as a function of the Bond number for fluids in a cylindrical tank.

Table 3.6 Water: measured and predicted linear modal parameters.

		1st Slosh Frequency		Damping Ratio		Mass Fraction
Tank	**Test**	**Pred.** ω (Hz)	**Meas.** ω (Hz)	**Pred.** ζ (%)	**Meas.** ζ (%)	**Meas.** λ
Flat	Earth	6.26	6.30	2.6	4.0	0.26
Flat	Space	3.18	3.31	6.5	4.4	0.17
Spherical	Earth	6.26	6.40	2.6	4.2	0.24
Spherical	Space	3.18	3.37*	6.5	6.5*	0.28

The ground results (Figs. 3.14, 3.16, 3.18 and 3.20) show strong amplitude dependent nonlinear slosh behavior. In Fig. 3.14 the first slosh resonance shifts from 6.3 Hz at the lowest forcing amplitude (x_{ex}/d = 0.32%) to 4.95 Hz at the

highest forcing amplitude (x_{ex}/d = 3 .2%), a shift of 21%. For the spherical bottom tank, this shift from 6.5 Hz to 5.15 Hz (Fig. 18) is 22%.

Examining the planar and non-planar slosh force-response, it is clear that the fluid swirls at the higher forcing amplitudes. When the water results (Figs. 3.14 and 3.16) are compared with the silicone oil results (Figs. 3.8 and 3.10), it is also evident that this amplitude dependent behavior manifests itself at lower forcing amplitudes in the water experiments. In the water experiments (Figs. 3.14, 3.16, 3.18 and 3.20) it can be seen that between 5.9 and 6.7 Hz for the intermediate forcing amplitude, and between 5.2 and 7.2 Hz for the highest forcing amplitude, the fluid response is a non-planar swirl. This swirl motion manifests itself in a second resonance peak, which appears close to the linear planar slosh frequency (6.3 Hz). Not only does the fluid swirl at this forcing amplitude, but the slosh also has multiple response states. The slosh response is different for up- and down-frequency sweeps between 6.3 and 7.2 Hz (Figs. 3.14, 3.16, 3.18 and 3.20). Depending on the direction in which the forcing frequency is changed, the fluid motion is either a planar slosh or a non-planar swirl. Similar behavior was also observed for the water in the spherical bottom tank.

As with the silicone oil, the results from the flat bottom tank (Fig. 3.14) and in the spherical bottom tank (Fig. 3.16) show no significant difference, reinforcing a weak dependence on tank bottom geometry for this fill ratio.

Water Coupled Results. The water coupled ground experimental results are depicted in Figures. 3.22, 3.24 and 3.26. In Figures. 3.22 and 3.26, the lower frequency resonance peak is the coupled spacecraft mode and the higher frequency resonance peak is that of the first fluid slosh mode. The frequencies at which these resonances occur decrease as the forcing amplitude is increased. The spacecraft mode frequency decreases from 5.9 (lowest forcing amplitude, x_{ex}/d = 0.32%) to 5.3 Hz (highest forcing amplitude, x_{ex}/d = 3.2%), a 10% shift. The frequency of the slosh mode changes from 7.15 to 6.35 Hz, an 11% shift. From Figure 3.24 it is clear that the slosh is not only nonlinear but that it also exhibits non-planar swirl similar to the non-planar motion observed in the uncoupled tests. The frequency range over which this non-planar swirl occurs is roughly from 5.5 to 6.7 Hz. Multiple response states can also be observed between 5.3 and 5.7 Hz (Fig. 3.22 and 3.26).

When the uncoupled and coupled results are compared, one can conclude that the filtering effect of the spacecraft mode tends to reduce the nonlinear behavior of the system. Yet, even with this "filtering" it is clear from the results (Figs. 3.22 to 3.26) that a linear model would fail to accurately model the dynamic behavior of a coupled fluid/spacecraft system.

3.4.3 Orbital Test Results

Silicone Oil Uncoupled Results. When the results for the linear parameters of the microgravity fluid tests in Table 3.5 are studied, it can be seen that the measured linear modal frequencies (0.68 and 0.65 Hz) are approximately 35% higher than the frequencies predicted by the linear model. As with the ground experiments, the measured damping ratios are roughly three times higher than the predicted values.

Studying Figures 3.9, 3.11 and 3.13, it can be concluded that the silicone oil slosh dynamics are essentially linear and planar in space. The high energy dissipation in the on orbit tests reduces the slosh modal amplitudes and thus the amplitude associated non-linear behavior. One may expect that higher forcing amplitudes could result in nonlinear slosh behavior, but from the MODE video observations it is indicated that higher forcing amplitudes may actually cause the fluid to slosh "around" the top of the tank.

When the slosh behavior of the silicone oil in the flat bottom tank (Fig. 3.9) and in the spherical bottom tank (Fig. 3.13) is studied, one finds, as with the ground experiments, no observable difference in the behavior.

Water Uncoupled Results. The linear parameters of the on orbit water tests are listed in Table 3.6, and the frequency responses are shown in Figures 3.15, 3.17, 3.19 and 3.21. Unfortunately, the frequency excitation window for the spherical bottom tests (Figs. 3.19 and 3.21) was not centered around the first planar slosh natural frequency. The on orbit experiments failed to completely capture the linear (low amplitude) slosh characteristics, but valuable data were still obtained for the higher forcing amplitudes. The modal characteristics for this case (marked with an asterisk in Table 3.6) are of lower accuracy than the other measured parameters. Considering both the flat and spherical bottom tanks, the agreement between the predicted and measured natural frequencies (within 6%) and the damping ratios (within 48%) must be considered acceptable.

Recall that the model used for the frequency prediction included the linear effects of contact angle hysteresis.

For the flat bottom tank, the natural frequency changes from 3.3 Hz at the lowest forcing amplitude, to 2.4 Hz at the highest forcing frequency, a 27% shift. The planar slosh force results (Fig. 3.15) show the same "double" resonance observed in the ground experiments: the first, around 2.4 Hz, is interpreted as the shifted non-linear planar slosh frequency; and the second is associated with the swirl motion that occurs close to the linear planar slosh frequency (3.3 Hz). Swirl is clearly evident when the non-planar slosh force results are studied (Fig. 3.17). The transition into the swirl motion is smooth. Multiple response states, dependent on the direction in which the forcing frequency is changed, are observed between 2.6 and 3.15 Hz (Figs. 3.15 and 3.17).

Despite the less than optimal spherical bottom tank frequency window, one can conclude from Figures 3.15 and 3.19, as well as 3.17 and 3.21, that the fluid behavior in the flat and spherical bottom tanks is qualitatively similar, but more quantitative differences are present than in the silicone oil and water ground results.

Water Coupled Results. The water coupled on orbit experimental results for the flat bottom tank are depicted in Fig. 3.23, 3.25 and 3.27. The frequency window used for the coupled tests on the spherical bottom tank (not shown) again failed to capture the fluid resonance for the lowest forcing amplitude.

In Figures 3.23 and 3.27, the lower frequency resonance peak is the coupled spacecraft mode and the higher frequency resonance peak is that of the first fluid slosh mode. The frequencies at which these resonances occur decrease as the forcing amplitude is increased. The spacecraft mode's frequency decreases from 2.82 (lowest forcing amplitude, x_{ex}/d = 0.32%) to 2.6 Hz (highest forcing amplitude, x_{ex}/d = 3.2%), a 8% shift. The frequency of the slosh mode changes from 3.6 to 3.13 Hz, a 13% shift in frequency. At the highest forcing amplitude, multiple response states can also be observed between 2.55 and 3.0 Hz (Figs. 3.23 and 3.27). From Figure 3.25 it is also clear that the slosh exhibits swirl similar to the non-planar motion observed in the ground tests. The frequency range over which this non-planar swirl occurs is roughly from 2.5 to 3.6 Hz.

Similar to ground tests, it was observed that the nonlinear behavior has been moderated by the linear spacecraft mode.

3.4.4 Comparison of Ground and Orbital Results

Silicone Oil Uncoupled Tests. The overwhelming difference between the ground and on orbit results for the silicone oil tests is the sharp increase in the modal damping ratio on orbit. While a frequency shift of 12% between the lowest and highest forcing amplitude was observed in the ground tests (Figs. 3.8 and 3.12), almost no shift was observed in the orbital results (Figs. 3.9 and 3.13). Multiple solutions and swirl behavior are also absent in space. The linearizing influence is due to the high slosh damping ratio in space, which effectively limits the amplitude of response and suppresses amplitude dependent nonlinearities.

The very high space damping ratio, as predicted by Figure 3.7, can be explained in terms of the fluid slosh force mechanisms. In space, the dominant restoring force (stiffness) is the weak capillary surface tension, while on earth it is gravity. The sharp drop in restoring force results in a drop in the slosh natural frequency from 5.24 Hz on earth to 0.68 Hz in space. However, the fluid slosh damping mechanism (the non-conservative action of the capillary viscous forces in the Stoke's layer) is not significantly altered by the presence or absence of gravity. Keeping these mechanisms in mind and studying the equation of a second order system,

$$m\ddot{q} + d\dot{q} + kq = F$$
$$\ddot{q} + 2\zeta\omega\dot{q} + \omega^2 q = \frac{F}{m} \tag{20}$$

one can conclude that if the damping coefficient (d) remains constant as the frequency (ω) decreases, the damping ratio (ζ) must increase, as was observed in the data; i.e., if the changes in the non-conservative action of the capillary viscous forces are minor, the product of the frequency and damping ratio should be invariant to the change from earth to orbit. The earth and space products differ by only 15% (Table 3.5), confirming that the change in restoring force does not fundamentally alter the loss mechanism.

Water Uncoupled Tests. Both the ground and on orbit results exhibit strong nonlinear and non-planar slosh characteristics. Some aspects of the response are slightly more nonlinear in space, and some more nonlinear on the ground. In space, when the forcing amplitude is changed from the lowest amplitude to the highest, the shift in resonant frequency (Fig. 3.15) is 27%; in the ground experiments, for the same change in forcing amplitude the shift is 22%.

In contrast, when Figures 3.16 and 3.17 are compared it is evident that the onset of the swirl is more gradual in space than on earth, and multiple solutions and jumps are less evident. By comparison with the silicone oil ground results, the qualitative nature of the nonlinearity is retained in the on orbit results.

The decrease in the first slosh frequency, between ground and space (Table 3.6), is much smaller for water than the decrease observed in the silicone oil experiments (Table 3.5). The explanation for this trend is the influence of contact angle hysteresis. The first order effect of contact angle hysteresis is to increase the slosh frequency, and since contact angle hysteresis is not a function of the ambient acceleration, the frequency change is smaller when gravity is removed. It can be inferred that in space the contact angle hysteresis dominates the restoring force, keeping the frequency relatively high, the damping ratio low and the nonlinear nature present.

Water Coupled Tests. The coupled water experimental results (Figs. 3.23, 3.25 and 3.27) clearly exhibit nonlinear and non-planar dynamics, similar to the behavior observed in the equivalent ground tests (Figs. 3.22, 3.24 and 3.26). As in the uncoupled tests, it can also be concluded that the onset of the swirling motion is more gradual than was observed in ground tests and no sudden response jumps occur. In space, swirl also occurs over a wider frequency range. The softening frequency shift in the spacecraft and slosh modes is present in both the space and ground data.

3.5 Conclusions

The MODE ESM, when used on the ground and shuttle middeck, has demonstrated the ability to determine the dynamic characteristics of contained fluids for a wide range of tanks, fluid slosh natural frequencies and gravity conditions. The orbital results demonstrated the ability of the hardware to resolve slosh forces to as low as 0.1 mN.

The existing linear models predicted the fluid slosh natural frequencies to within 5 to 35%, the damping ratios within a factor of three, and of course did not capture the nonlinear behavior, which becomes apparent for tank motions as little as 1% of the diameter. As a result, their application to micro-gravity fluid modeling is problematic.

When the results of all the MODE flat bottom and spherical bottom tank experiments are compared, no significant difference in the dynamic slosh behavior is evident. At lower fill levels the shape of the tank bottom would have an effect on the dynamic behavior.

Compared to the nonlinear, nonplanar and multiple response slosh behavior observed in the silicone oil ground experiments, the slosh behavior of this fluid is essentially linear in space. This is due to the very high damping ratio of the first slosh mode in space. However, both the space uncoupled and coupled water experiments exhibited nonlinear and non-planar characteristics similar to those observed in the ground experiments. This is due to the relatively high restoring force for water which originates from the contact angle hysteresis.

The MODE on orbit experimental results are being used to update and validate the MIT analytical model for micro-gravity conditions. The MODE results established a database with which researchers can validate their analytical models. This may eventually lead to the reliable design and prediction tools necessary to meet the high performance requirements of future spacecraft.

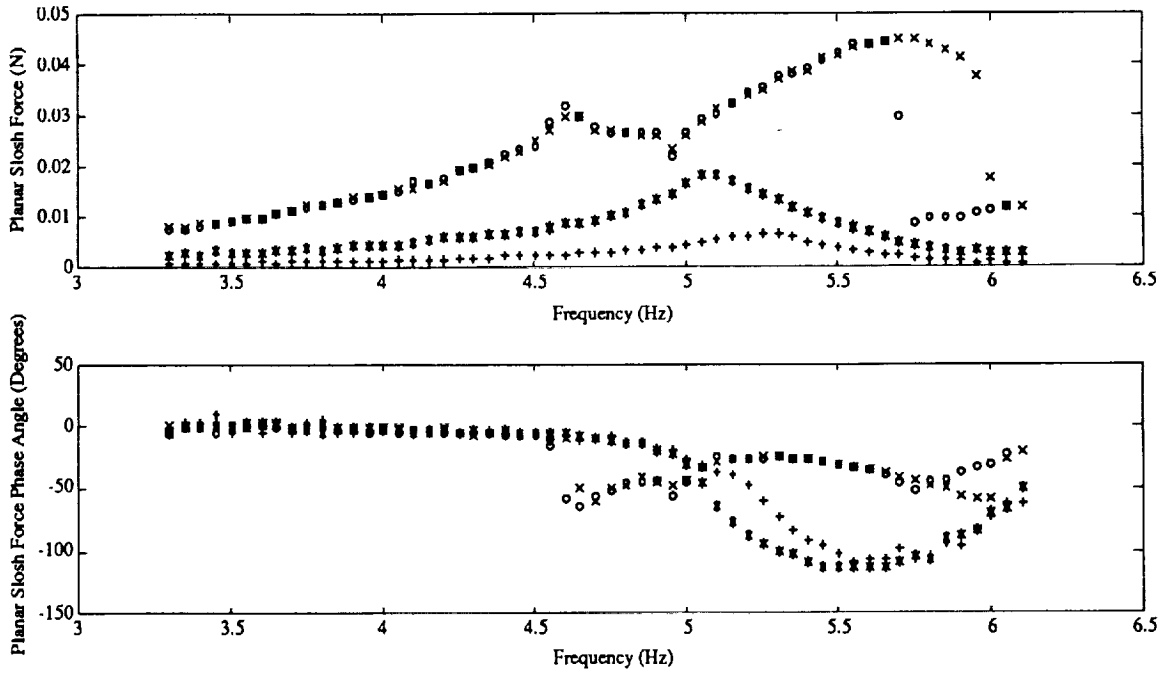

Figure 3.8 Uncoupled test on earth with silicone oil in a flat bottom tank. Planar slosh force and phase angle.

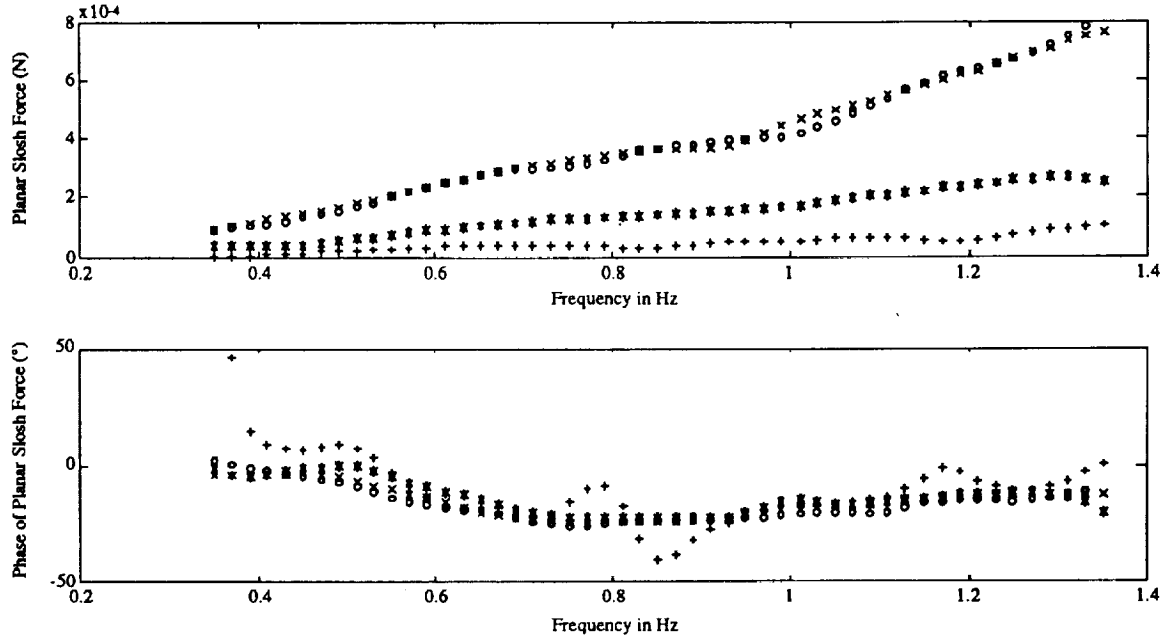

Figure 3.9 Uncoupled test in space with silicone oil in a flat bottom tank. Planar slosh force and phase angle.

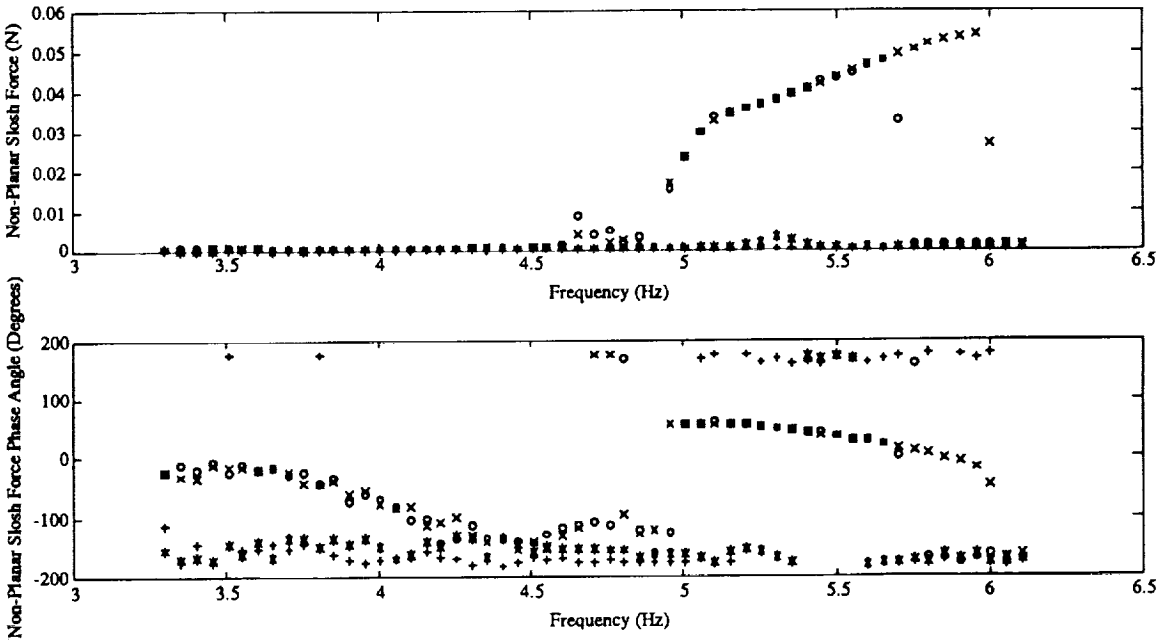

Figure 3.10 Uncoupled test on earth with silicone oil in a flat bottom tank. Non-planar slosh force and phase angle.

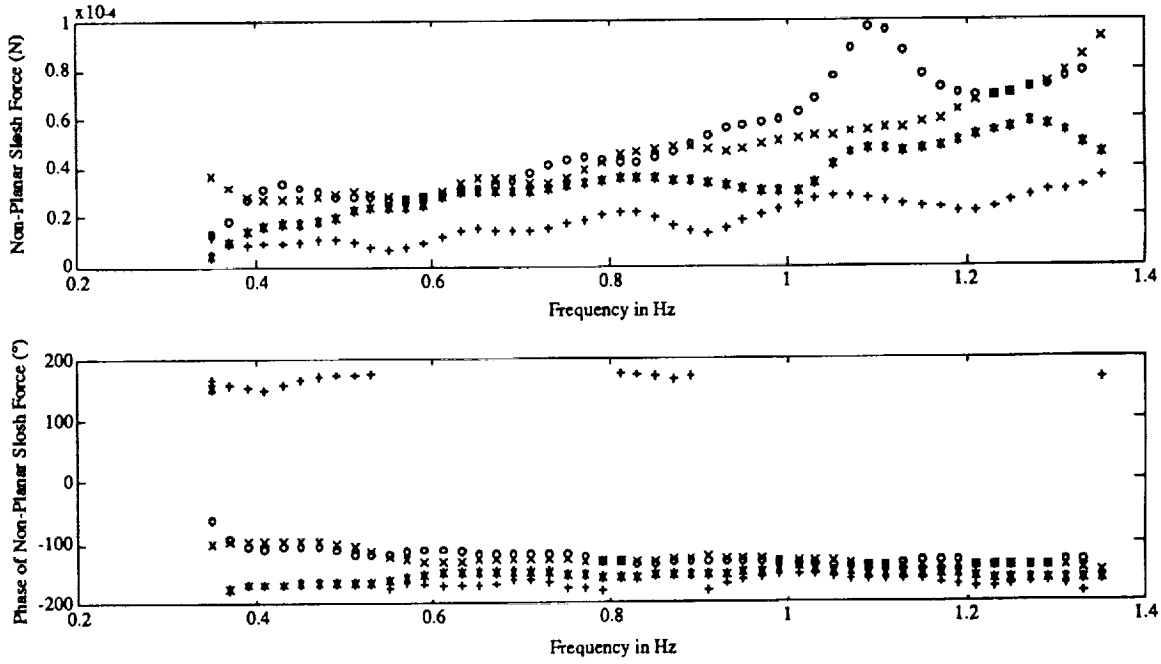

Figure 3.11 Uncoupled test in space with silicone oil in a flat bottom tank. Non-planar slosh force and phase angle.

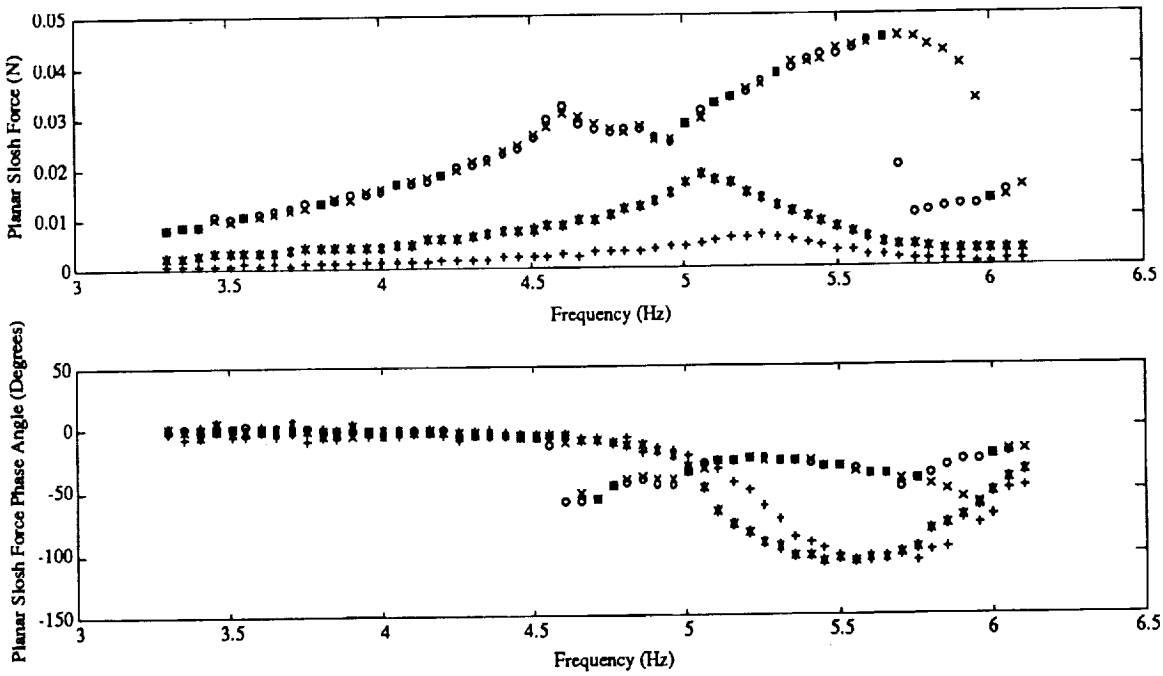

Figure 3.12 Uncoupled test on earth with silicone oil in a spherical bottom tank. Planar slosh force and phase angle.

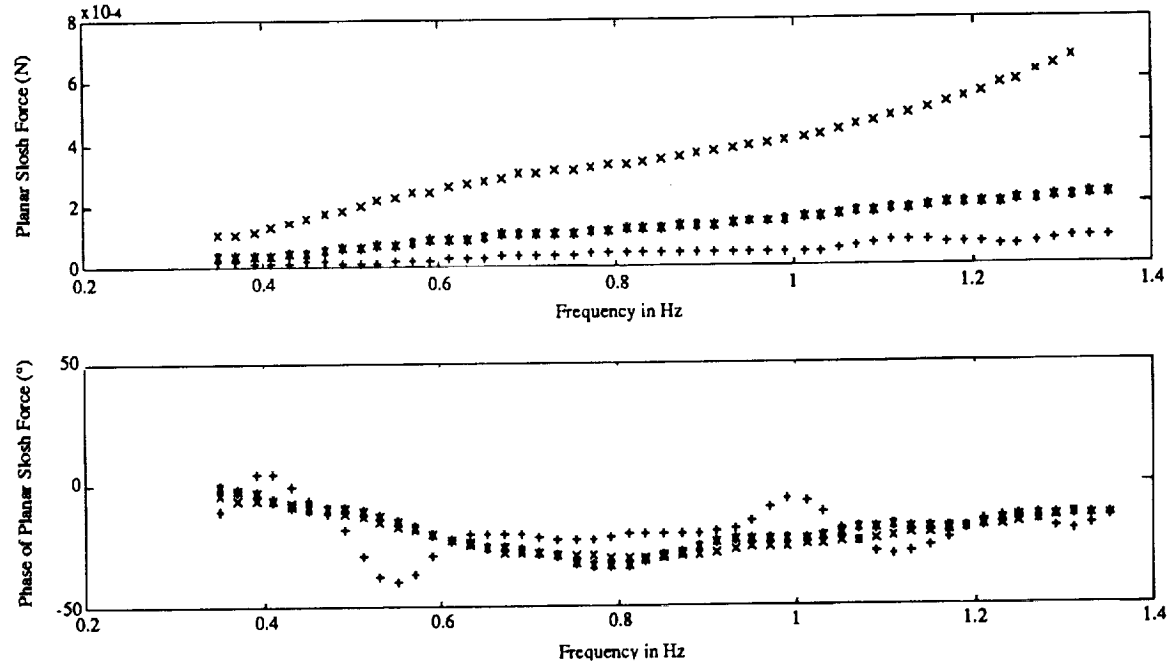

Figure 3.13 Uncoupled test in space with silicone oil in a spherical bottom tank. Planar slosh force and phase angle.

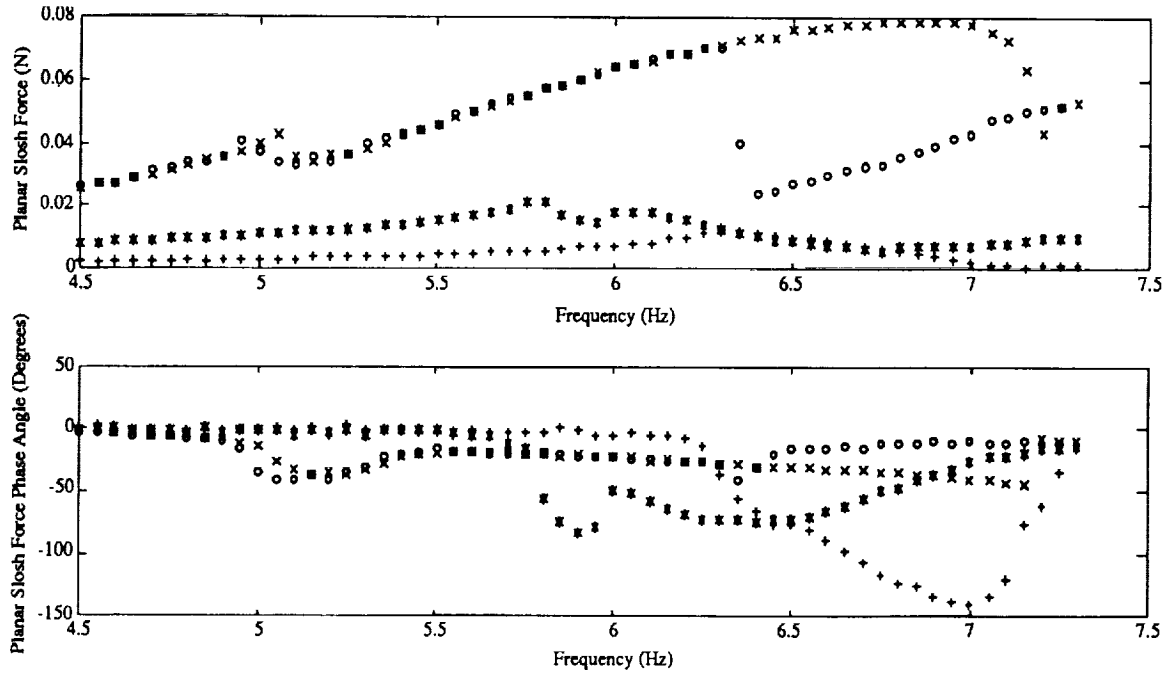

Figure 3.14 Uncoupled test on earth with distilled water in a flat bottom tank. Planar slosh force and phase angle.

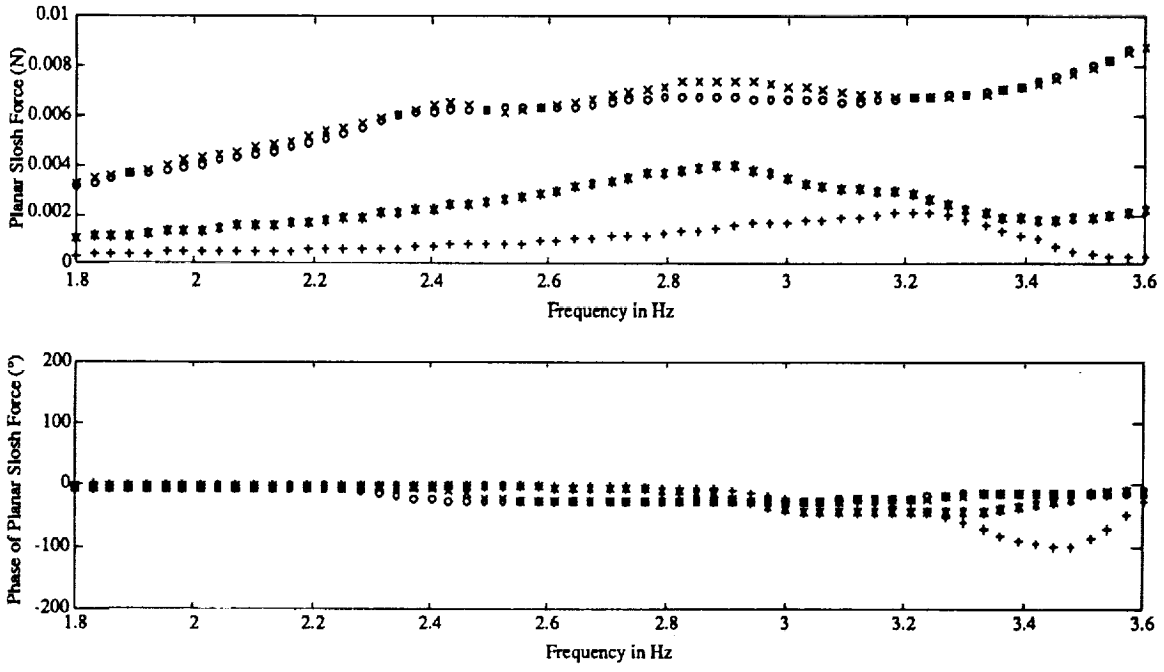

Figure 3.15 Uncoupled test in space with distilled water in a flat bottom tank. Planar slosh force and phase angle.

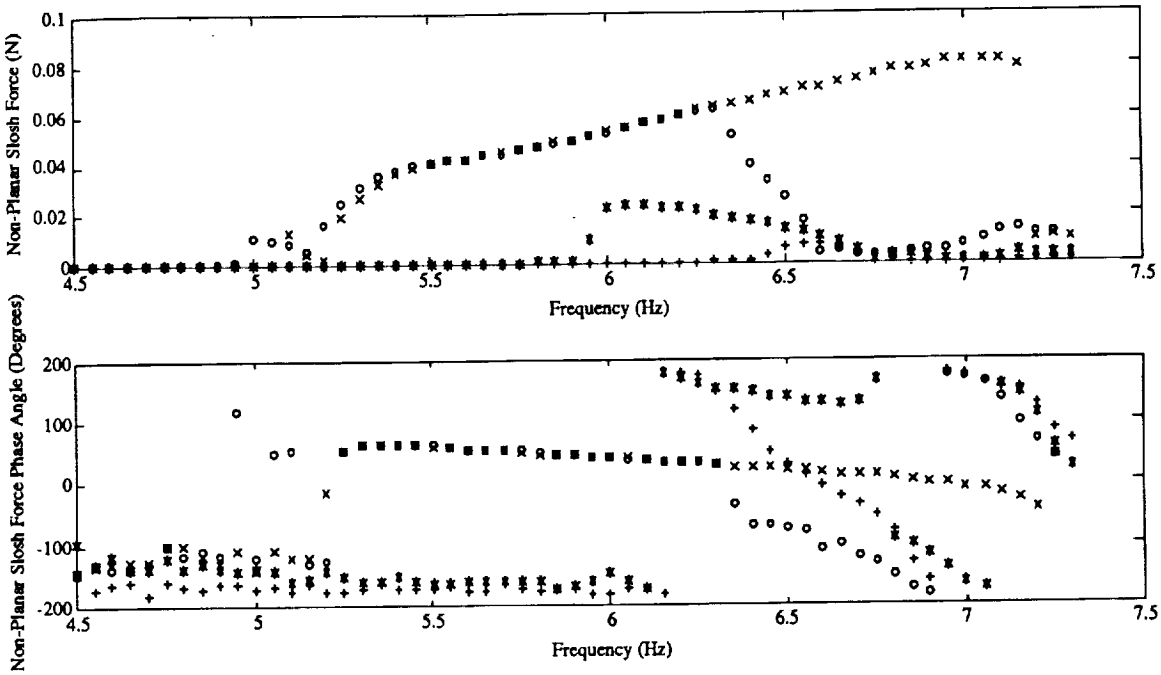

Figure 3.16 Uncoupled test on earth with distilled water in a flat bottom tank. Non-planar slosh force and phase angle.

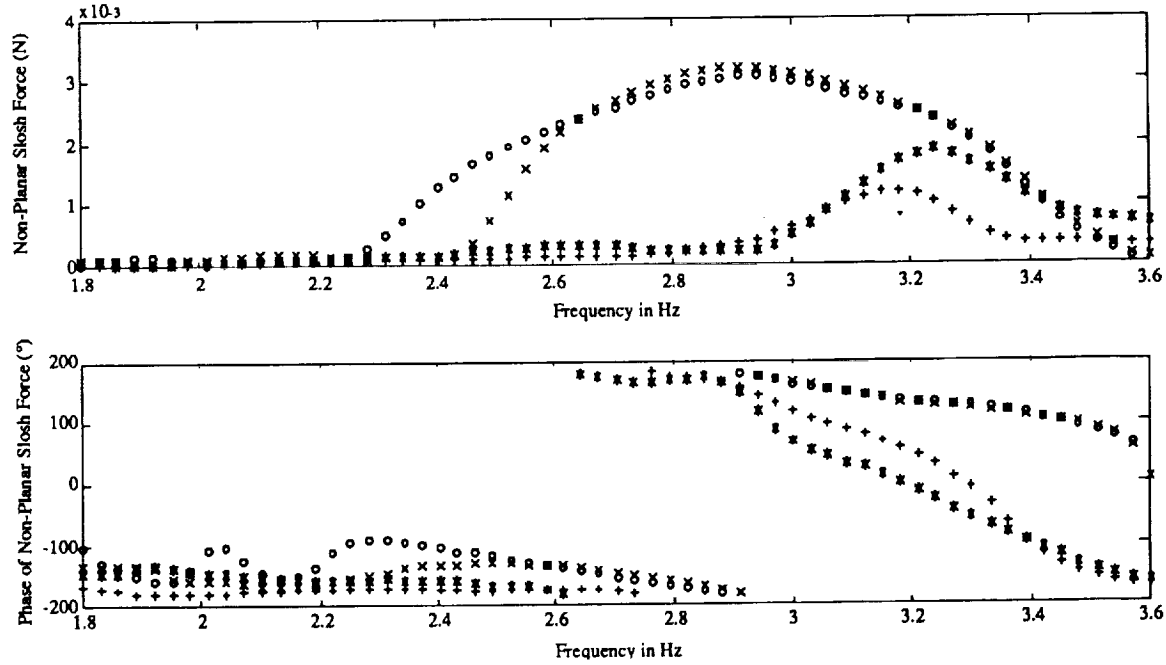

Figure 3.17 Uncoupled test in space with distilled water in a flat bottom tank. Non-planar slosh force and phase angle.

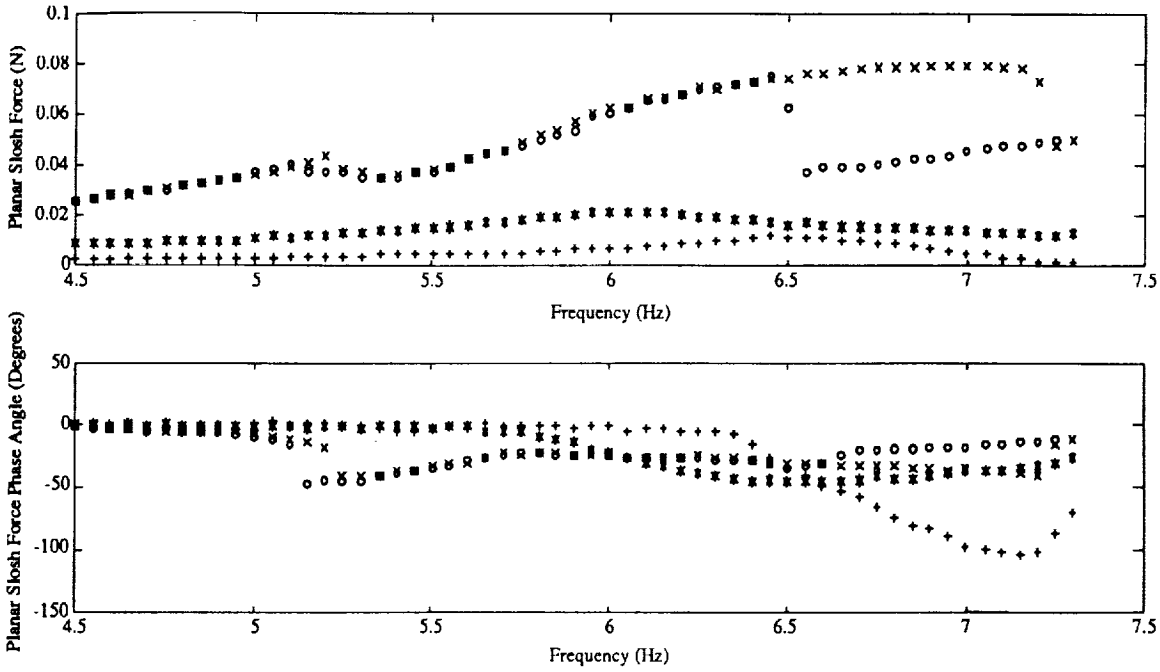

Figure 3.18 Uncoupled test on earth with distilled water in a spherical bottom tank. Planar slosh force and phase angle.

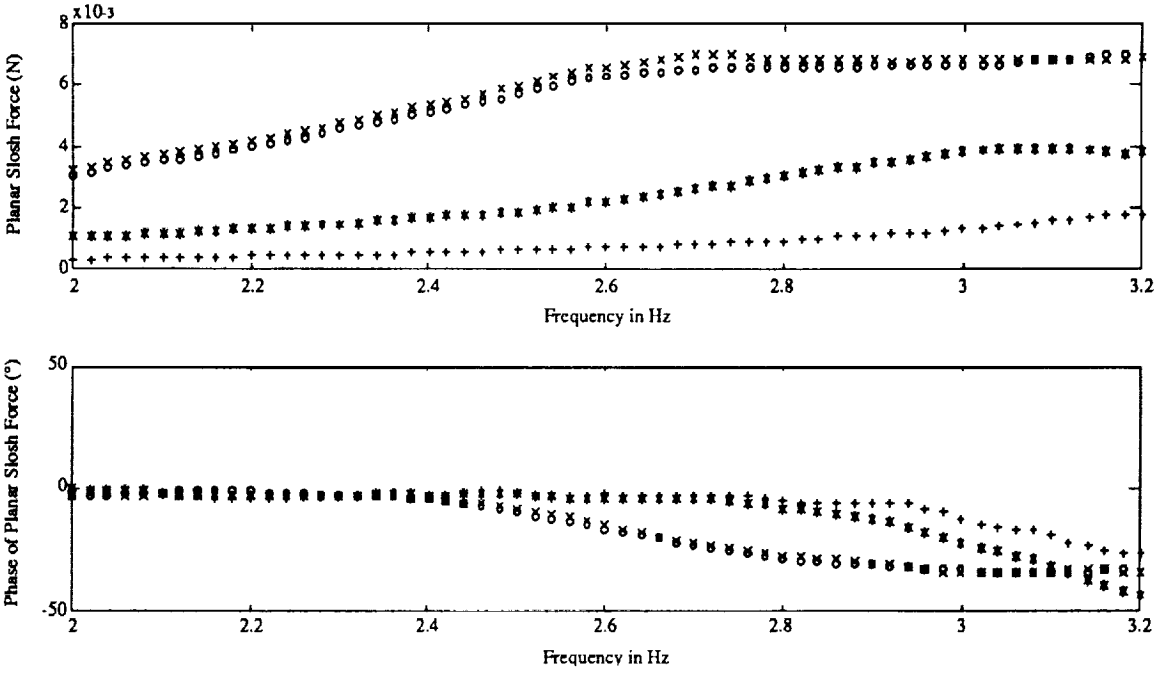

Figure 3.19 Uncoupled test in space with distilled water in a spherical bottom tank. Planar slosh force and phase angle.

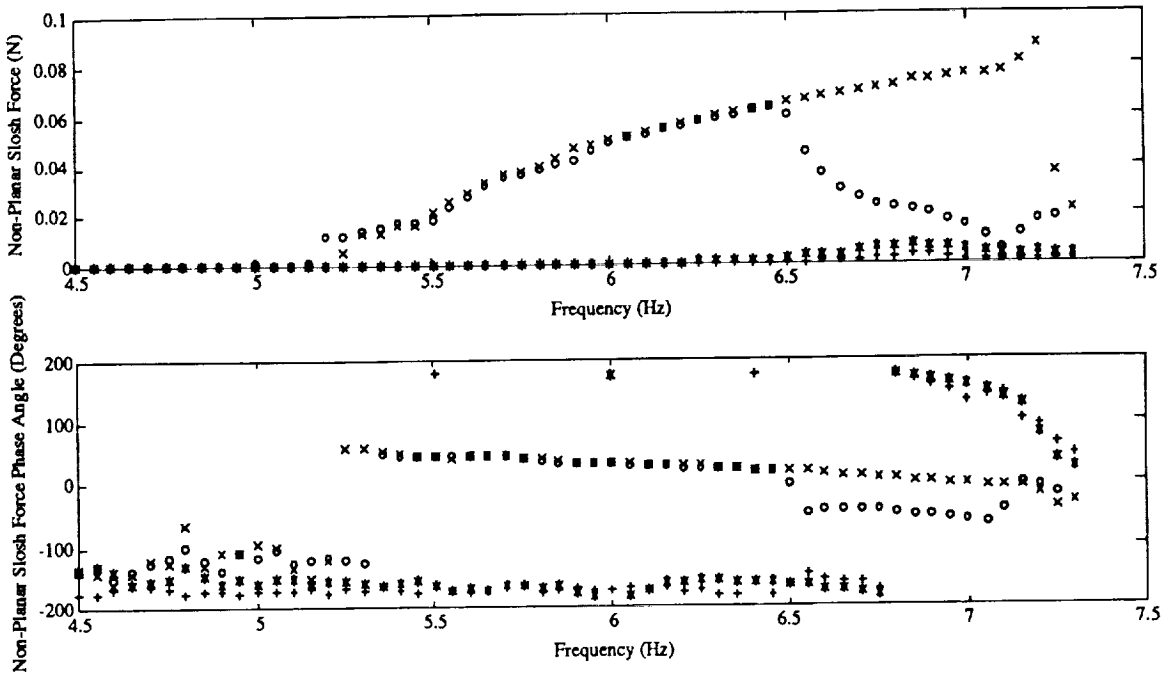

Figure 3.20 Uncoupled test on earth with distilled water in a spherical bottom tank. Non-planar slosh force and phase angle.

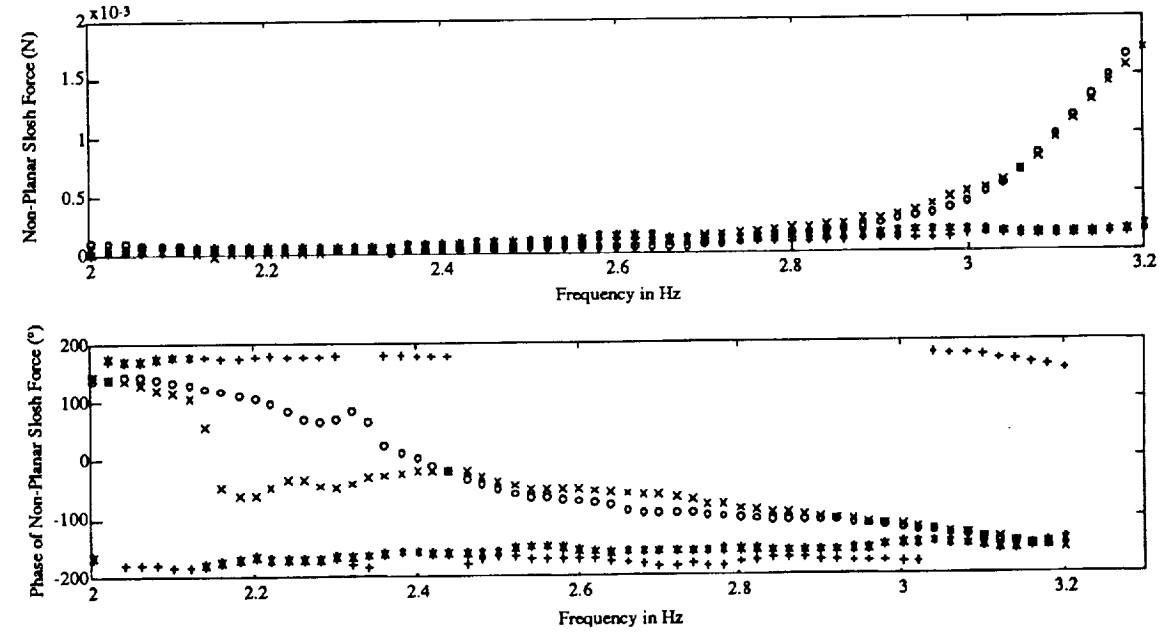

Figure 3.21 Uncoupled test in space with distilled water in a spherical bottom tank. Non-planar slosh force and phase angle.

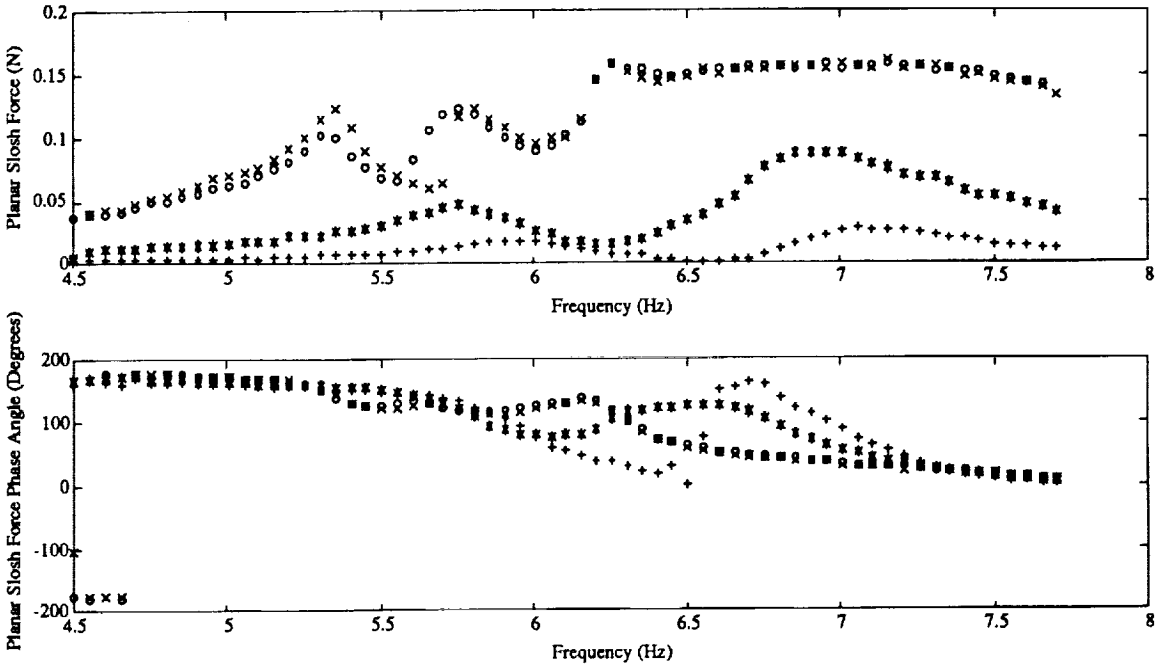

Figure 3.22 Coupled test on earth with distilled water in a flat bottom tank. Planar slosh force. ($\mu = 0.15$, $\zeta = 0.05$, $\nu = 1.04$)

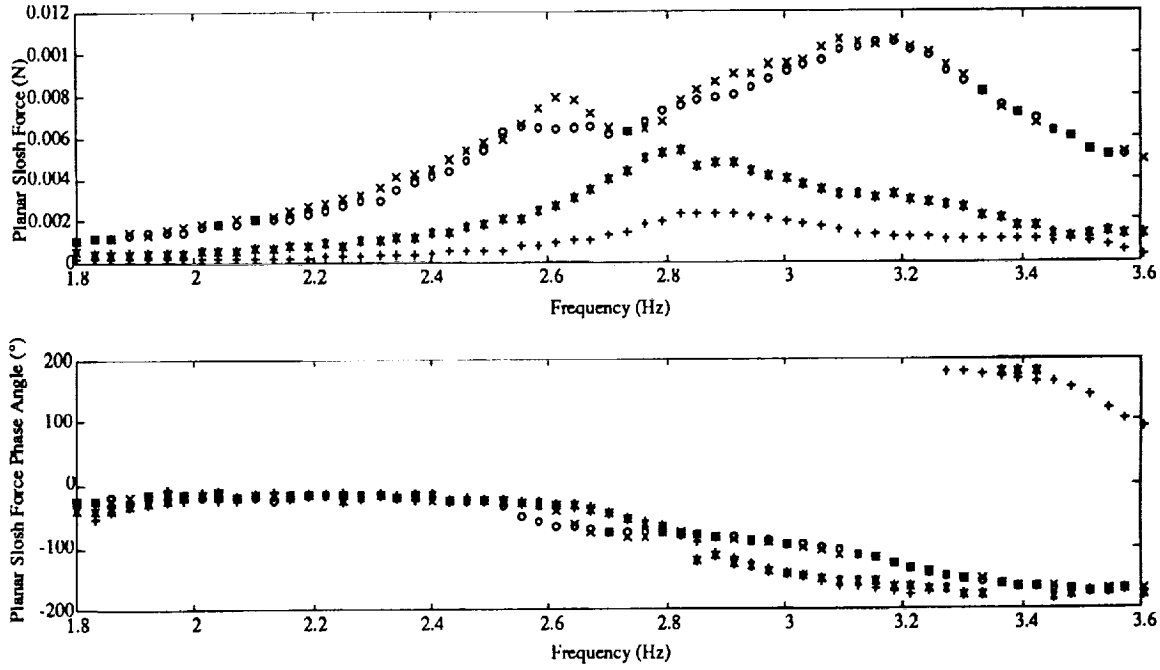

Figure 3.23 Coupled test in space with distilled water in a flat bottom tank. Planar slosh force. ($\mu = 0.15$, $\zeta = 0.05$, $\nu = 1.04$)

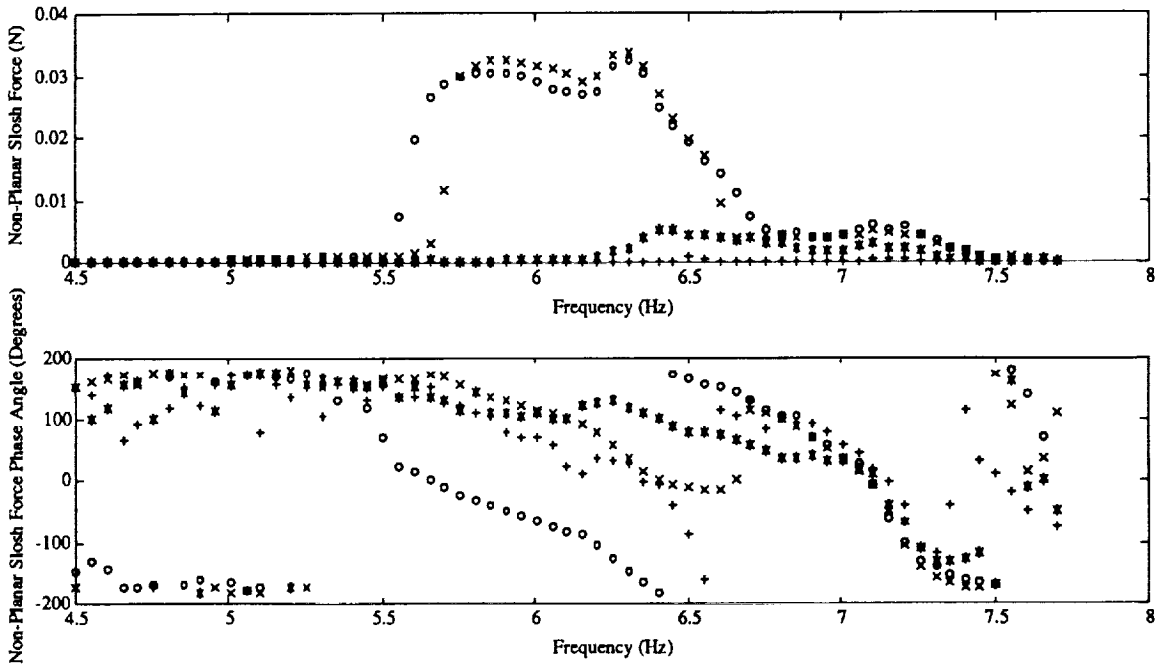

Figure 3.24 Coupled test on earth with distilled water in a flat bottom tank. Non-planar slosh force. (μ = 0.15, ζ = 0.05, ν = 1.04)

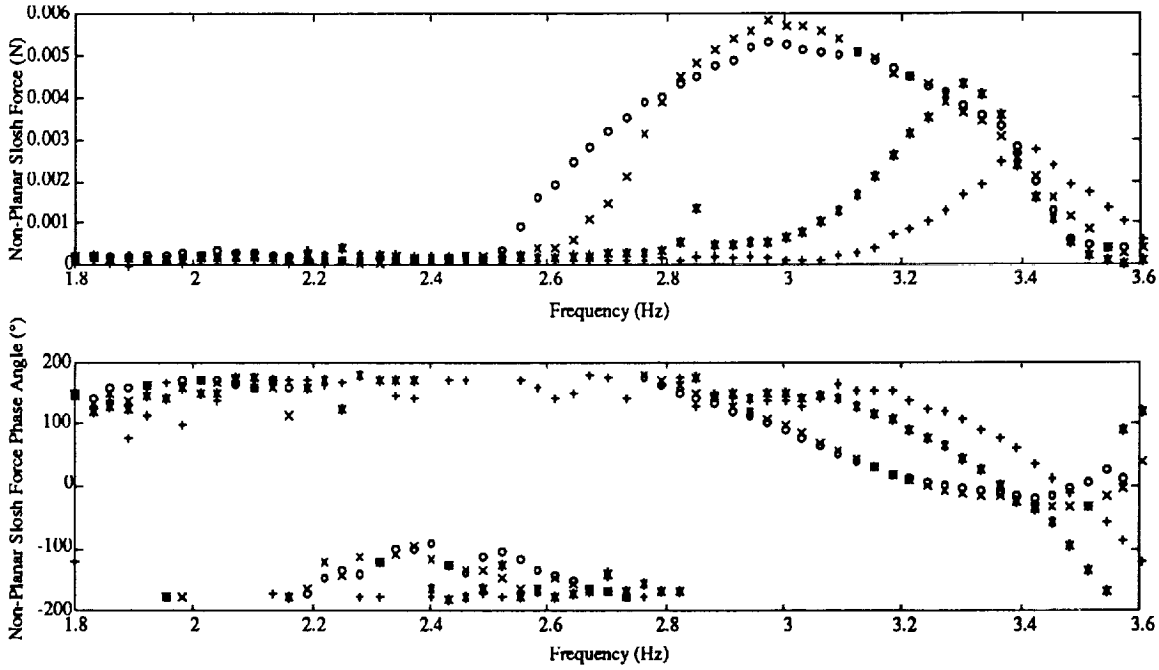

Figure 3.25 Coupled test in space with distilled water in a flat bottom tank. Non-planar slosh force. (μ=0.15, ζ=0.05, ν=1.04)

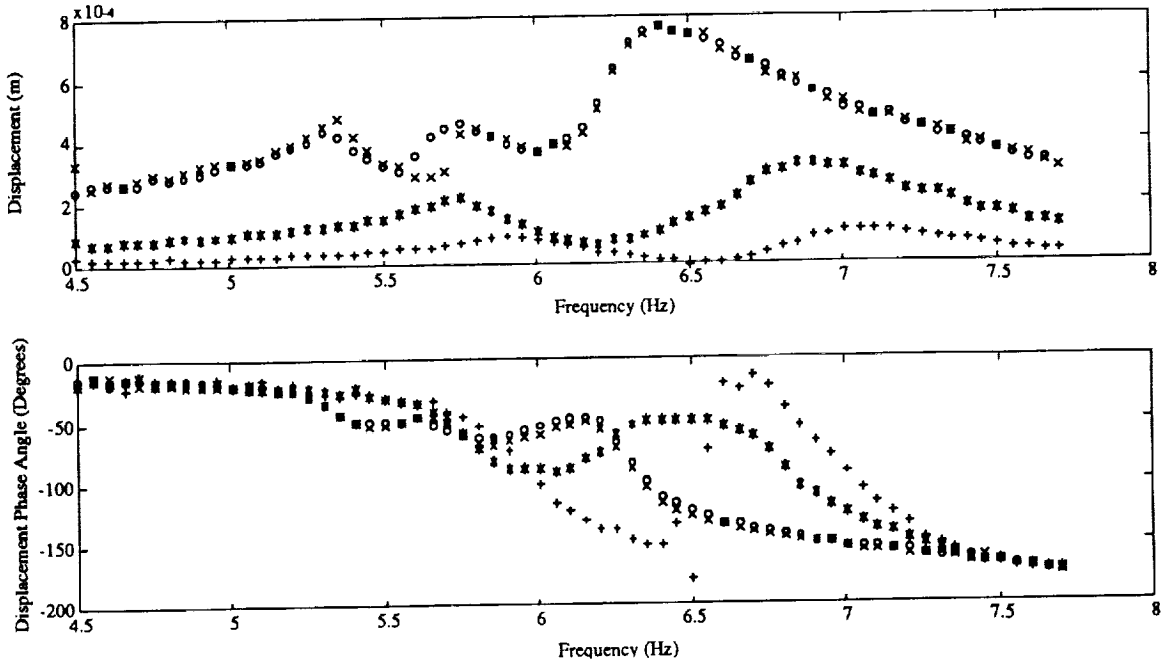

Figure 3.26 Coupled test on earth with distilled water in a flat bottom tank. Tank displacement. (μ=0.15, ζ=0.05, ν=1.04)

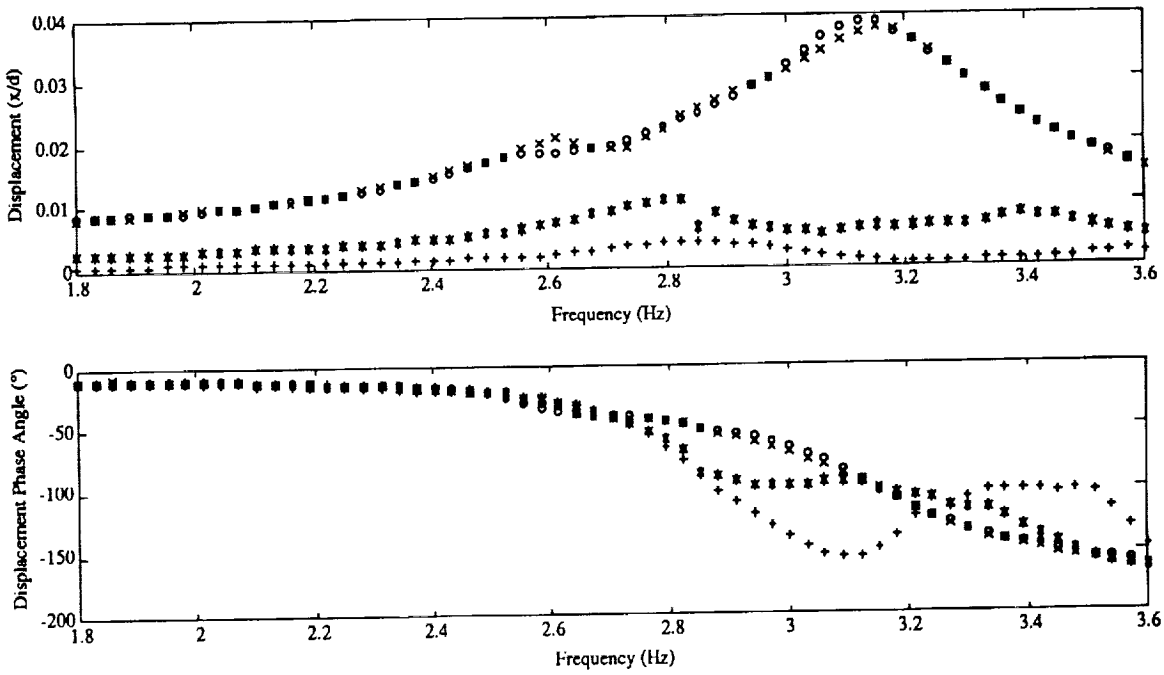

Figure 3.27 Coupled test in space with distilled water in a flat bottom tank. Tank displacement. (μ=0.15, ζ=0.05, ν=1.04)

3.6 References for Chapter 3

Abramson, H.N., ed, "The Dynamic Behavior of Liquids in Moving Containers," NASA SP-106, 1966.

Agrawal, B.N., "An Overview on INTELSAT Activities on Liquid Slosh," Proc. 1st INTELSAT/ESA Symposium on the Dynamic Behavior of Liquids on Spacecraft Attitude Control, Washington, D.C., April 25-26, 1984, pp. 99-120.

Crawley, E.F., Barlow, M.B., van Schoor, M.C. and Bicos, A., "Zero-gravity Measurement of the Modal Parameters of Space Structures," IAF-92-0314, To be presented at the 43rd IAF Conference, Washington, September 1992.

Dodge, F.T. and Garza, L.R., "Experimental and Theoretical Studies of Liquid Sloshing at Simulated Low Gravity," Trans. ASME, J. Applied Mechanics, 34, Sept. 1967, pp. 555-561.

Dodge, F.T, and Garza, L.R., "Simulated Low-gravity Sloshing in Spherical Elipsoidal and Cylindrical Tanks," J. of Spacecraft, 7:3, 1970, pp. 204-206.

Ganiev, R.F., "Nonlinear Resonance Oscillations of Bodies with a Liquid," Soviet Applied Mechanics (translated from Prikladnaya Mekhanika Vol. 13, No. 10, 1977, pp. 23-29).

Komatsu, K., "Non-linear Sloshing Analysis of Liquid in Tanks with Arbitrary Geometries," Int. Journal of Non-linear Mechanics, Vol. 22, No. 3, pp. 193-207, 1987.

Kuttler, J.R., and Sigillito, V.G., "Sloshing of Liquids in Cylindrical Tanks," AIAA Journal, Vol. 22, Feb. 1984, pp. 309-311..

Limarchenko, O. S., "Effect of Capillarity on the Dynamics of a Container–Liquid System," Soviet Applied Mechanics (translated from Prikladnaya Mekhanika vol 17, no 6, pp. 124–128), 1981.

Limarchenko, O. S., "Application of a Variational Method to the Solution of Nonlinear Problems of the Dynamics of Combined Motions of a Tank with Fluid," Soviet Applied Mechanics (translated from Prikladnaya Mekhanika vol 19, no 11, pp. 100–104), 1983.

Luke, J. C., "A Variational Principle for a Fluid with a Free Surface," J.Fluid Mechanics, Vol. 27:2 pp. 395-397, 1967.

Martin, R.E., "Effects of Transient Propellant Dynamics on Deployment of Large Liquid Stages in Zero-gravity with Application to Shuttle/Centaur," IAF-86-119, 1986.

Miles, John W., "Internally Resonant Surface Waves in a Circular Cylinder," J.Fluid Mech., Vol. 149 pp. 1-14, 1984a.

Miles, John W., "Resonantly Forced Surface Waves in a Circular Cylinder," J.Fluid Mech., Vol. 149 pp. 15-31, 1984b.

Reynolds, W.C. and Satterlee, H.M., "Liquid Propellant Behavior at Low and 0-G," in Abramson, 1966.

Salzman, J.A. and Masica, W.J., "An Experimental Investigation of the Frequency and Viscous Damping of Liquids during Weightlessness", NASA TND-5058, 1969.

Satterlee, H.M. and Reynolds, W.C., "The Dynamics of the Free Liquid Surface in Cylindrical Containers Under Strong Capillary and Weak Gravity Conditions," Stanford University TR-LG-2, 1964.

van Schoor, M.C., Crawley, E.F. and Hansman, R.J., "The Coupled Nonlinear Dynamics of Spacecraft with Fluids in Tanks of Arbitrary Geometry," M.I.T., SSL Report #4-89, April 1989.

van Schoor, M.C., Peterson, L.D. and Crawley, E.F., "The Coupled Nonlinear Dynamic Characteristics of Contained Fluids in Zero Gravity," presented at the 31th AIAA/ASME/ASCE/AHS Structures, Structural Dynamics, and Materials Conference, Longbeach, California, April 1990.

Yeh, G.C.K., "Free and Forced Oscillations of a Liquid in an Axi-Symmetric Tank at Low-Gravity Environments," Journal of Applied Mechanics, Vol. 34, No. 1, pp. 23-28, March 1967.

Chapter 4: Flight Systems and Mission Activities

4.1 Introduction

The Middeck 0-gravity Dynamics Experiment (MODE) was an investigation into fluid and structural dynamics in microgravity. The objective of MODE was twofold: to study the gravity-dependent nonlinear sloshing behavior of contained fluids typical of spacecraft fuels, and to investigate the dynamics of space structures. These two separate experiments were combined into a single mission to take advantage of the commonality in the required support electronics. A single Experiment Support Module containing all the power, signal conditioning and data storage capabilities supported both sets of experiments.

A technical description of the hardware and software systems used in MODE is presented in this chapter. MODE consists of three major elements: 1) the Experiment Support Module, a dynamics test bed providing computer experiment control, analog signal conditioning, power conditioning, an operator interface consisting of a keypad and display, experiment electrical and thermal control, and archival data storage; 2) the Fluid Test Article Assembly, used to specifically investigate the dynamics of fluid-structure interaction in zero-gravity; 3) the Structural Test Article for specifically investigating the open-loop dynamics of structures in zero-gravity. The modular nature of the Experiment Support Module subsystems, particularly the experiment control computer, make it readily adaptable as a test facility for other on orbit experiments. This chapter describes the hardware and software elements, their development and certification, and their operation on orbit.

MODE was developed and certified as a standard shuttle middeck experiment. It was stowed in three and a half lockers on the middeck: one for the Experiment Support Module; a second containing the Fluid Test Article assembly and the fluid containers; a third housing the parts of the Structural Test Article; and half of another locker for ancillary equipment such as the NASA supplied video camera.

MODE required active interaction with the Shuttle crew. Crew activities included: experiment power up; test article assembly, disassembly and reconfiguration; the initiation and monitoring of automated test protocols; and the entering and initiation of manual protocols. Most MODE on orbit operations made use of automated test protocols stored in the Experiment Support Module. Modification of experiment operation was possible through the use of manual protocols, allowing near real-time adaptation to on orbit conditions.

4.2 Flight Systems

4.2.1 Development

MODE began as two distinct experiments at the MIT Space Engineering Research Center. At the beginning of the MODE flight program, a ground-based fluid test article apparatus already existed. One of the primary tasks during development was the transformation of this prototype to flight systems that could withstand the rigors of shuttle launch, landing, and space-based operations. The structural test article was designed from scratch, with the primary flight system development task being the reduction of electronics filling several racks in the laboratory to the volume and power levels of a single middeck locker. Several major constraints affected these transformations: budget and schedule, the use of commercial parts, and Shuttle safety.

Budget and Schedule. In order to meet IN-STEP objectives, MODE flight systems were developed on an aggressive 'success oriented' schedule which put launch approximately two years after the Preliminary Design Review. Funding for the experiment was limited. The MODE flight systems were developed for $2.1 million, with approximately half being spent for hardware and software design, manufacture, test, integration, crew training, and mission operations. The remaining funds were spent on experiment design, science development, ground testing, and data reduction.

Use of Commercial Parts. MODE was designed, built and tested to Class D-modified standards. No requirements for 'pedigree' of materials or components were imposed. This allowed significant use of off-the-shelf industrial and commercial grade hardware. MIL-STD-883 parts were used only where cost or lead-time permitted, and if higher reliability was desired.

Documentation and hardware controls were substantially reduced from the levels normally associated with spaceflight hardware. A series of environmental and certification tests were imposed upon the hardware and software as a screen to detect flaws in workmanship or design.

Shuttle Safety. While the relatively less-stringent requirements of Class D allowed the team to accommodate the short schedule and tight budget, MODE hardware nevertheless had to meet all safety and interface requirements imposed by the Space Shuttle Program. The requirement for a high degree of crew interaction demanded thorough evaluation of Orbiter capabilities, standard and non-standard services, and early involvement with the NASA Astronaut Office Science Advisory Board. Supporting this effort were structural and thermal analyses, a careful selection of materials, and a significant amount of interaction with the Program Integration Office at the NASA Johnson Space Center.

Table 4.1 Summary of MODE properties

Stowage Volume	3 & 1/2 Lockers
Middeck Locker #1	Experiment Support Module
Middeck Locker #2	Fluid Test Article Assembly
Middeck Locker #3	Structural Test Article
Middeck Locker #4	Ancillary Equipment (Half)
Weight	
Exp Support Module	26.8 kg [59.0 lbs]
Fluid Test Article Assy	3.7 kg [8.2 lbs]
Structural Test Article	13.5 kg [29.9 lbs]
Power Required	
Fluid Dyn Testing	110 watts
Structural Dyn Testing	104 watts
Activation Process	Assemble Test Article Connect Power Cable Apply Power to Support Module Insert Optical Disk Initiate Automatic Protocol
Crew Time	
Assembly	Approx 15 minutes to Assemble and Activate
Testing	16 hours
Disassembly	Approx 30 minutes to Disassemble and Stow

4.2.2 Functional Elements

Although the phenomena under study in the fluids and structures experiments of MODE were quite distinct, the testing methods were similar enough that large portions of the hardware could be used for both experiments. Both required sinusoidal excitation of the test articles, sensor signal conditioning with on orbit (pre-programmed) control of individual channel gains, data acquisition and storage, interaction with the crew via keypad and display, active cooling of electronics, and computer control of experiment protocols and sequencing.

MODE Flight Systems development was therefore separated into three major hardware elements:

- Experiment Support Module, a dynamics test bed providing computer experiment control, analog signal conditioning, power conditioning, an operator interface, experiment power and thermal control, and archival data storage.
- Fluid Test Article Assembly, a fluid container with associated excitation and measurement systems.
- Structural Test Article, a truss-like jointed structure with both deployable and erectable components.

Figure 4.1 shows in block diagram form the similarities in support electronics for the Fluid and Structural Test Article experiments. The Experiment Support Module provides power and control to, and obtains sensor readings from the test articles through the umbilical which connects to the front of the module. Table 4.1 summarizes the properties of the MODE flight systems.

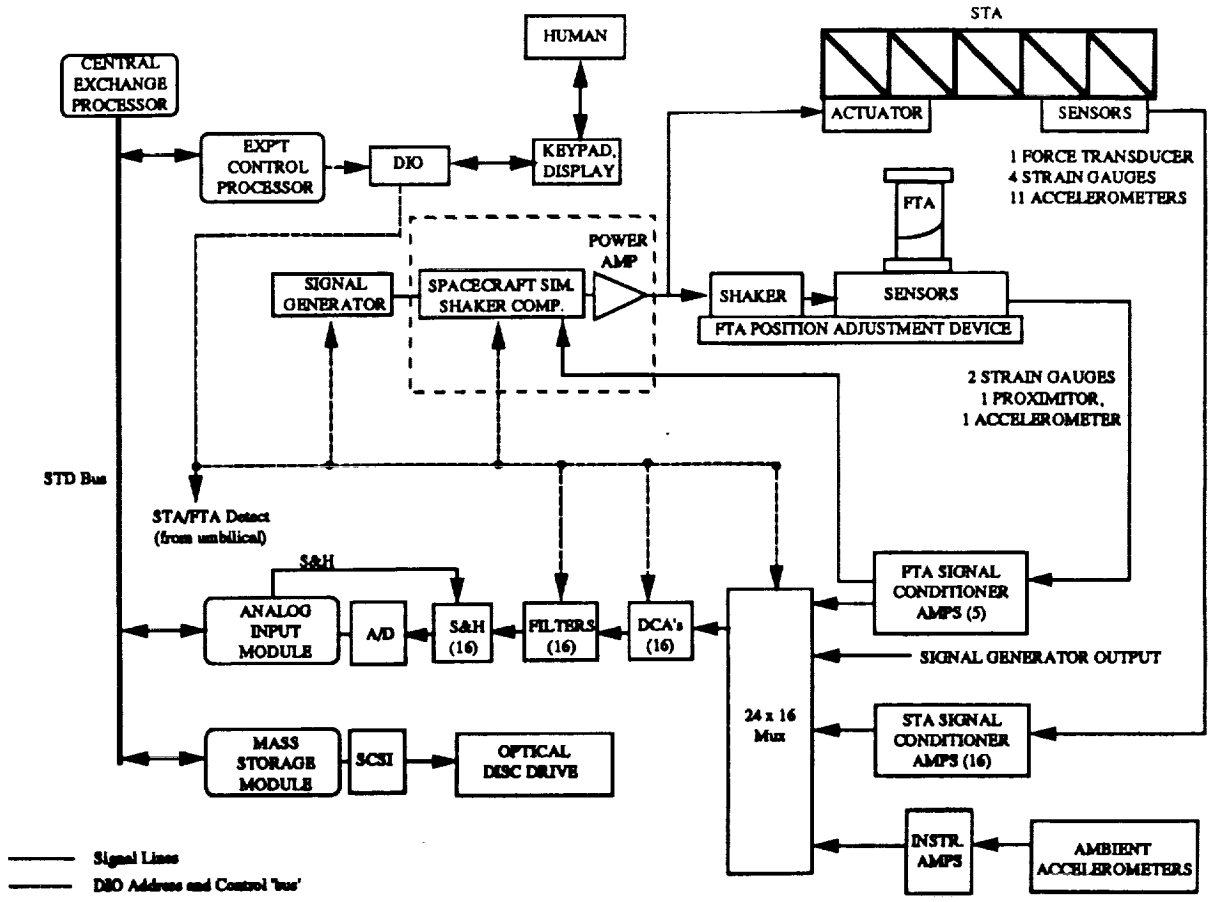

Figure 4.1 MODE block diagram

4.2.3 Fluid Test Assembly

The Fluid Test Article Assembly shown in Figure 4.2 consists of: a fluid test article, a voice-coil actuator, a reaction force balance, an accelerometer, a proximity probe, and a clock display, all mounted on a lockable universal ball joint. The entire unit physically attaches to the front of the Experiment Support Module via a quick-release attachment device; it is electrically connected by an umbilical that provides the power, control, and data interfaces. The universal ball joint allows the test article to be aligned with the residual acceleration vector in the orbiter middeck. This feature stems from concerns that the cumulative effects of residual gravity and aerodynamic drag could reorient the fluid in an undesirable way during testing, thus preventing meaningful slosh measurements.

ORIGINAL PAGE
BLACK AND WHITE PHOTOGRAPH

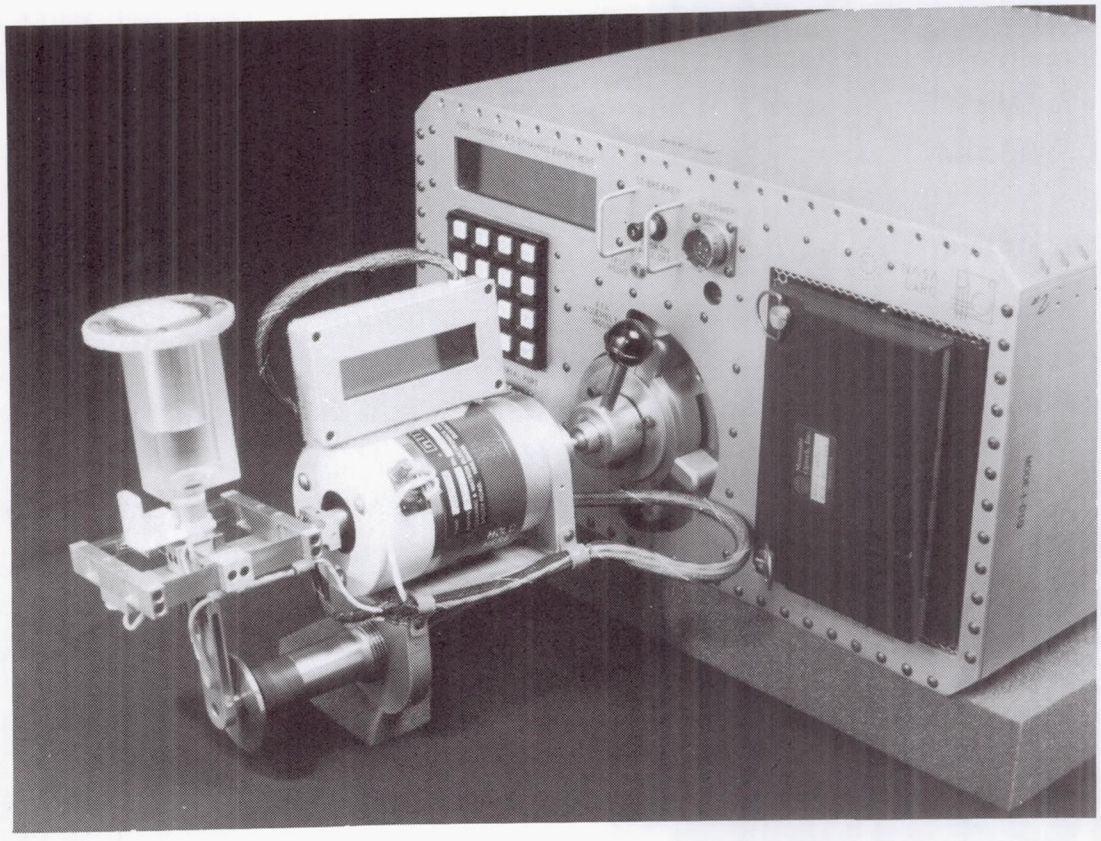

Figure 4.2 Fluid Test Article assembly

The voice-coil actuator excites the test article and force balance sinusoidally along a single axis; the force balance measures the inertial forces due to the mass of the structure and tank, in addition to the fluid slosh forces. The tank and force balance masses can be subtracted from the measurements electronically. During coupled fluid/structures testing, a Spacecraft Simulation Circuit which modifies the actuator response to behave like a single-axis, second-order dynamic system was used. In this way it was possible to study the coupled response of a fluid container attached to a spacecraft. Mass, damping, and frequency ratios of the fluid and spacecraft could be selected through the protocol file or the Experiment Support Module keypad.

Four fluid test articles were flown on STS-48: two cylindrical tanks with flat bottoms, one filled with silicone oil and the other with distilled water; and two cylindrical tanks with spherical bottoms, again one filled with silicone oil and the other with distilled water. Each tank is approximately 7.9 cm (3.1") in height and 3.8 cm (1.5") in diameter, and is made from polycarbonate. The tanks

are sized such that the expected acceleration environment of the middeck would not realign the fluid during testing. Section 4.3 contains a detailed explanation of the rationale for tank sizing, fluid choice and fill ratios. Containment of the fluid is provided by two o-ring seals at the top of the tanks.

4.2.4 Structural Test Article

Elements of the Structural Test Article include: two deployable truss modules, a set of erectable truss components, an articulating/rotary joint module, two rigid appendages with end masses, a flexible appendage, a proof-mass actuator, associated sensors and cabling, and a tether system (described in more detail in Chapter 2). The modular nature of the elements allows different configurations to be studied; two of the flight configurations are shown in Figures 4.3 and 4.4. The basic element used in the trusses is a cylindrical rod of polycarbonate with aluminum end sections; the connecting nodes and the joints are made from aluminum.

ORIGINAL PAGE
BLACK AND WHITE PHOTOGRAPH

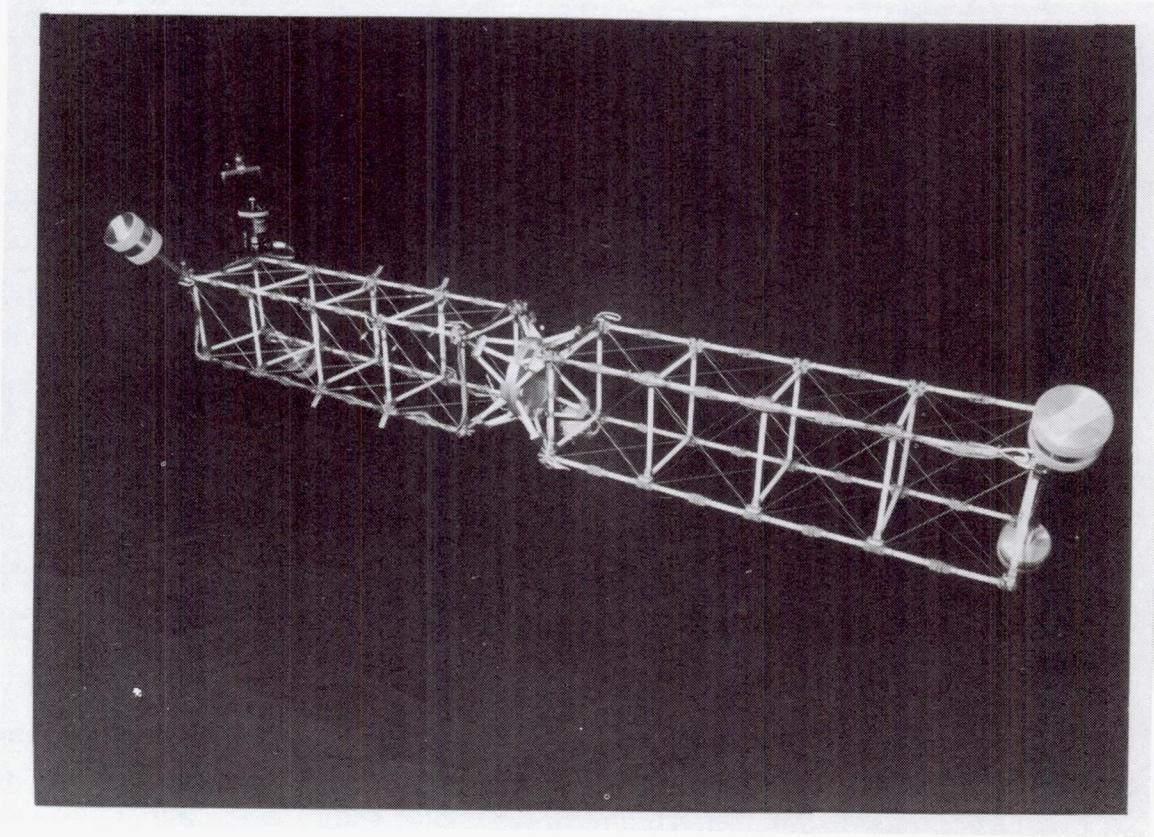

Figure 4.3 Structural Test Article in the alpha configuration

ORIGINAL PAGE
BLACK AND WHITE PHOTOGRAPH

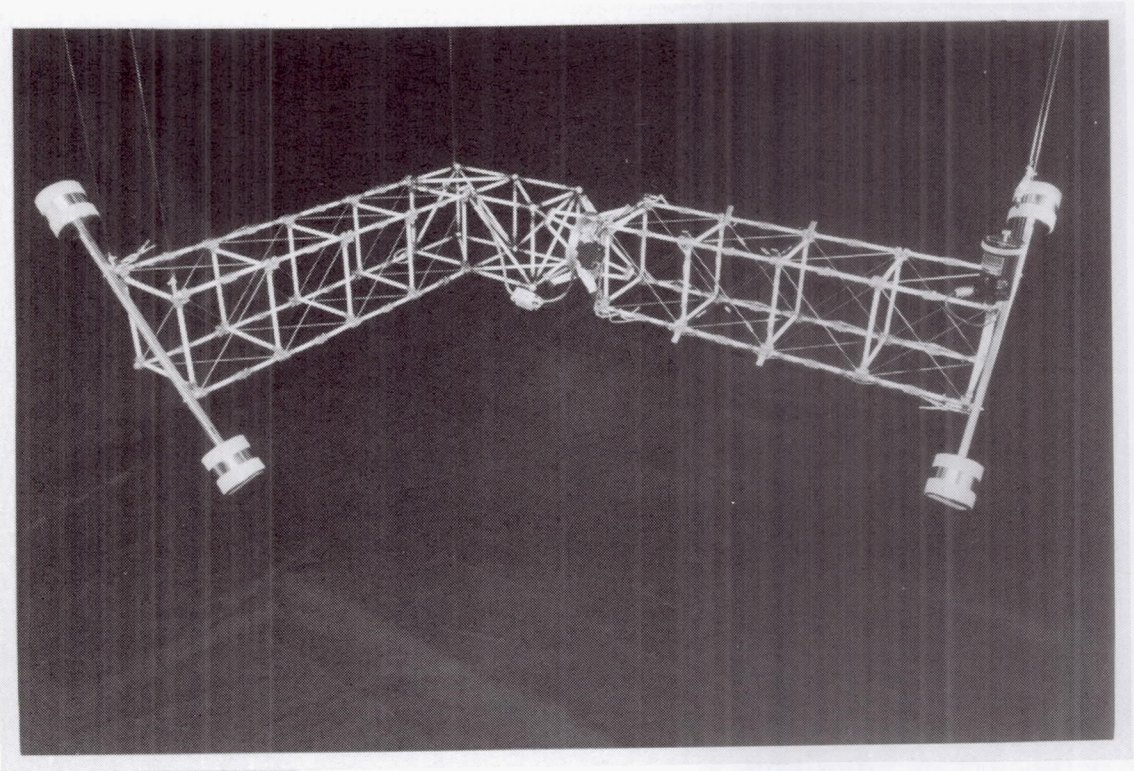

Figure 4.4 Structural Test Article in the L configuration

The test article is excited using a proof-mass actuator, with integral force transducer, attached to a node of one of the deployable truss modules. Sensors distributed along the truss provide eleven acceleration and four strain measurements. A lightweight tether system is used to allow the truss assembly to "free-float" in the center of the middeck while not translating due to air currents. The assembly is electrically connected to the Experiment Support Module by an umbilical that provides the power, control, and data interfaces.

4.2.5 Experiment Support Module

The Experiment Support Module is essentially a compact dynamics laboratory. It requires only +28 VDC nominal orbiter power, and operates in all normal crew compartment pressures and temperatures.

The Experiment Support Module provides:

- DC-to-DC conversion of orbiter +28 volt power
- 20 channels of sensor powering and preamplification

- 16 channels of digitally controlled amplification and filtering (signal conditioning)
- 12-bit analog-to-digital conversion
- Storage of digital data (400 Mbytes per disk)
- Automatic performance of experiment protocols stored in software (100 protocols flown)
- Power amplification of actuation signals
- Safety power switching and inhibits
- Active cooling of electronics
- Control, data, and power interface with test articles via umbilical
- Operator interface through keypad and display for alphanumeric display of experiment status, error messages, and input data.

Major elements of the Experiment Support Module are the SensorNet™ Experiment Computer housed in a 9-slot card cage, the Signal Conditioning System housed in a 14-slot card cage, an optical disk drive, and a power supply. Other elements include a cooling fan and items such as air baffles, circuit breakers, thermostats, air flow sensors, and associated cabling. All of these elements are contained within or secured to the rigid aluminum support frame which completely fills one standard middeck locker. The support frame is designed to provide: structural support for, and containment of the internal components; the containment of EMI emissions by minimizing the number of joints and penetrations; and air distribution via internal air channels. Honeycomb waveguides are used in the air intake and exhaust to reduce EMI emissions, while a dust screen on the air intake provides protection from airborne debris.

Figure 4.5 shows the Experiment Support Module ready for installation, while Figure 4.6 shows its internal configuration.

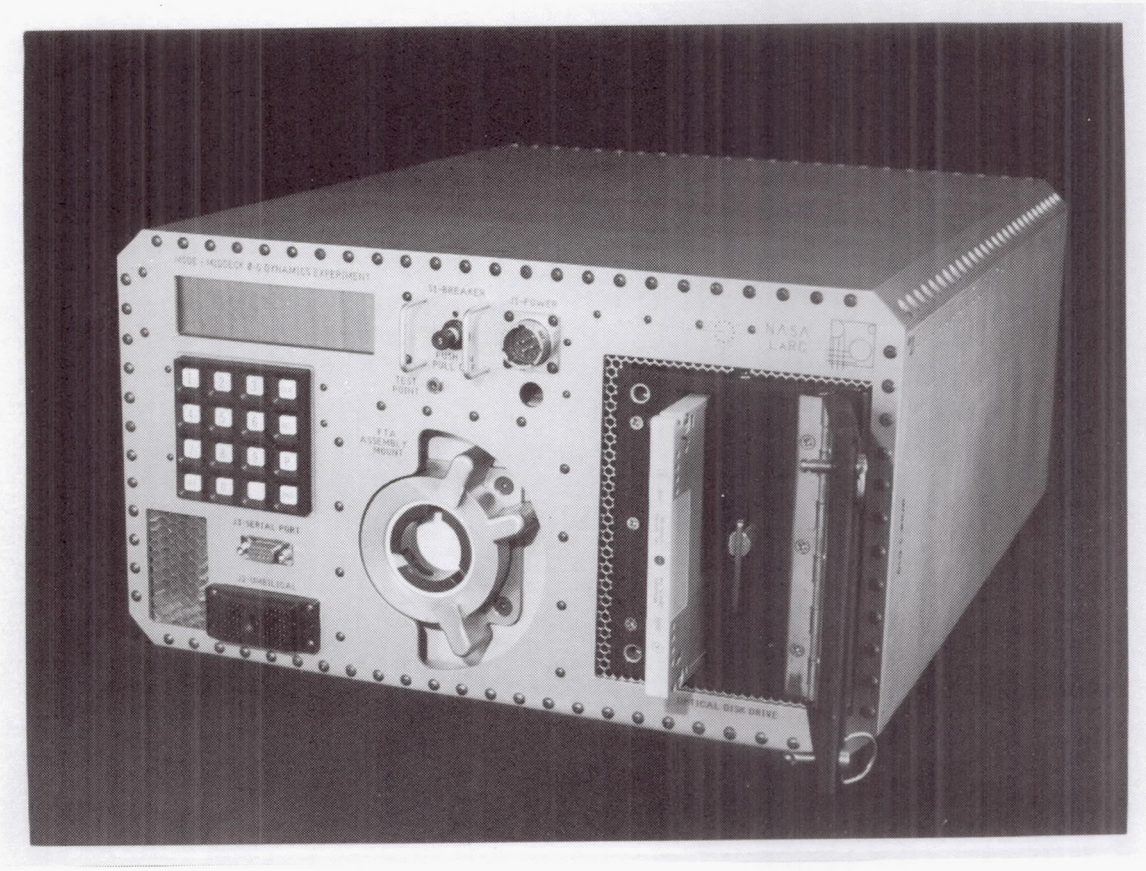

Figure 4.5 Experiment Support Module

ORIGINAL PAGE
BLACK AND WHITE PHOTOGRAPH

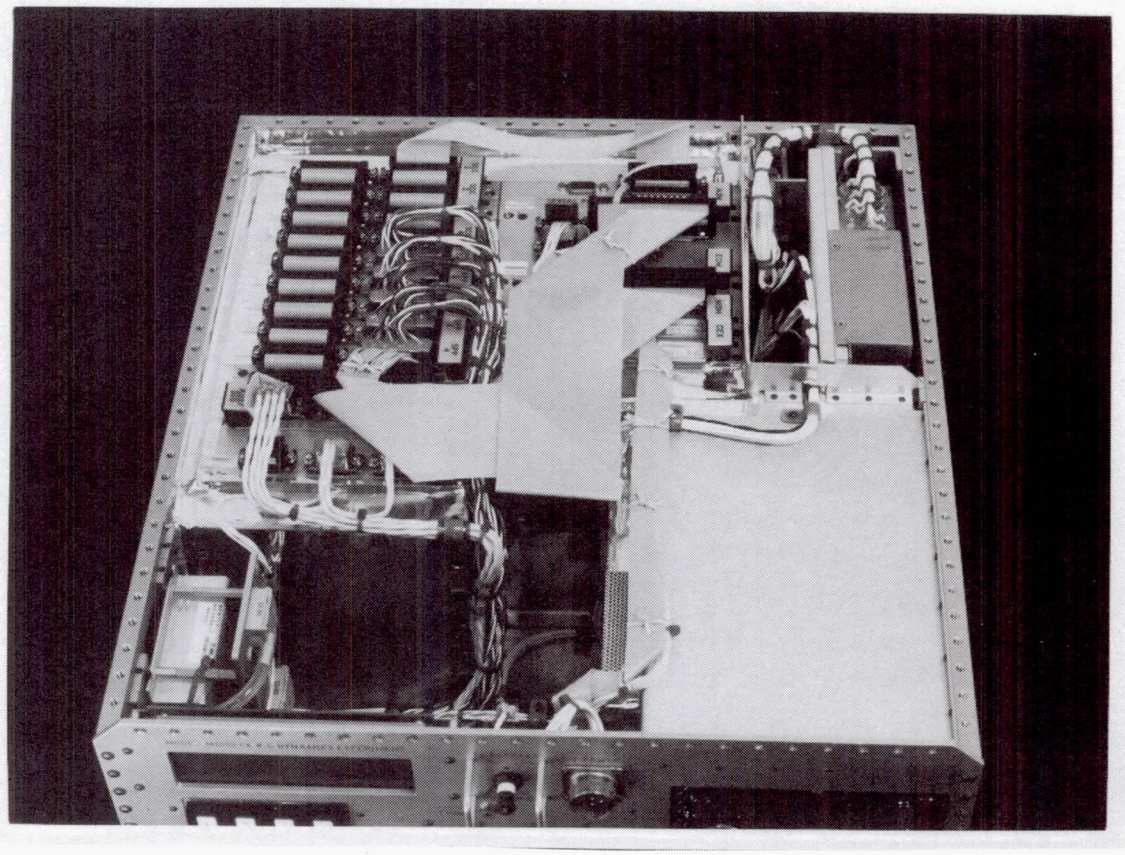

Figure 4.6 Experiment Support Module (with top cover removed)

Experiment Computer. MODE utilized Payload Systems' SensorNet™ Experiment Computer, housed in a rugged 9-slot card cage with removeable card modules (see Figure 4.7). The system used four processor cards and three iSBX function cards which fully implemented the MODE experiment control, data acquisition, and data storage tasks.

ORIGINAL PAGE
BLACK AND WHITE PHOTOGRAPH

ORIGINAL PAGE
BLACK AND WHITE PHOTOGRAPH

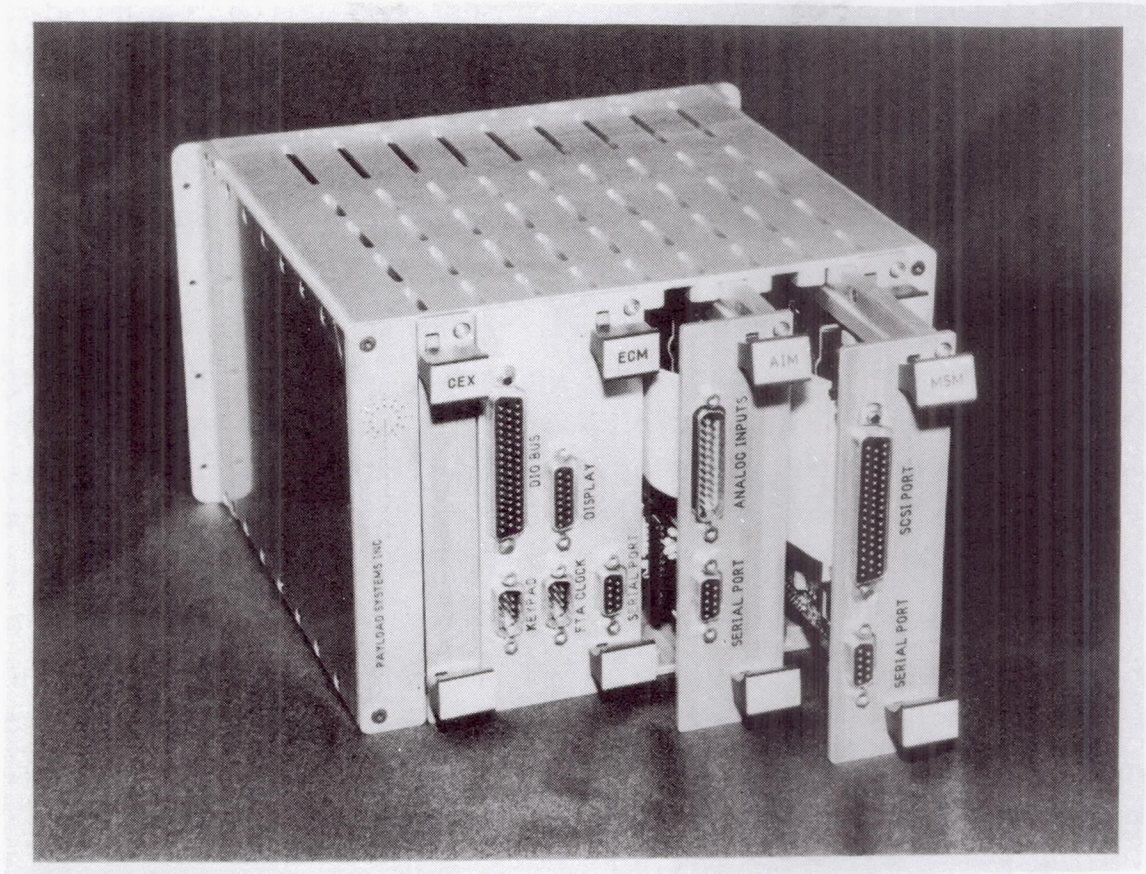

Figure 4.7 SensorNet™ Experiment Computer

The four functional modules of the Experiment Computer are: the Experiment Control Module, for experiment sequencing and digital input and output; the Analog Input Module, for analog-to-digital conversions; the Mass Storage Module, for data transfer and command of the optical disk drive; and the Central Exchange, for inter-processor communications management.

Each computer module contains a dedicated processor card and, except for the Central Exchange, an iSBX daughter-board performing module-specific functions. The processor cards conform to STD bus standards. This architecture allows much greater real-time computing capability than a single board solution, due to the distribution of high-rate tasks to the dedicated processors. All electronics used in the SensorNet™ Experiment Computer are available off the shelf.

The Experiment Control Module controls experiment sequencing by generating commands that instruct the other modules to perform a specific task.

Built-in parallel input/output ports allow operator interaction and real-time data and status information display during operation.

The Analog Input Module handles the analog-to-digitial conversion task. The sampling rate is software-selectable to a maximum of 1000 Hz. The converter section has 12-bit resolution, and is configured for an input range of ±15 volts.

The Mass Storage Module handles the data storage task. The module communicates with the data storage unit over a SCSI bus and can store configuration status such as gain settings, filter settings, time tags, spacecraft simulator settings, signal generator frequency command, experiment status, software version numbers, etc. The throughput rate is greater than 40 kbytes per second.

The Central Exchange handles all inter-processor communication tasks. It uses the V53 processor (80186 instruction set) operating at 16 MHz, and has up to 1 Mbyte of dedicated RAM. As with all of the modules, software is stored onboard with EPROMs. The Central Exchange provides a real-time clock for use in time-stamping data.

The common base for each computer module is a software entity called the Virtual Module. The Virtual Module provides: power-up diagnostics and initialization; interrupt-driven, buffered inter-module communications via a packet transfer manager; management of a module's shared memory; command management; event handling via custom, user-developed event handlers; error management and reporting; and local input/output management. The Virtual Module is implemented in the SensorNet™ Distributed Real-Time Operating System embedded in the Central Exchange.

The Experiment Control Module software is unique among the computer modules because it is used to generate the commands that instruct the other modules to work in concert for a given task. A user development interface is available which allows the user to easily develop experiment-specific codes. The interface utilizes a library of object-oriented software modules.

The Analog Input Module software is responsible for the accurate sampling of the analog-to-digital converters. Sampling is performed by an interrupt service routine of which three command-selectable versions are available for use.

The Mass Storage Module software controls the creating, opening, reading, writing, and closing of files to the data storage unit.

Data Storage Subsystem. Data are stored on a commercially available Write-Once-Read-Many (WORM) optical disk drive. It uses disk cartridges capable of storing 200 Mbytes per side (400 Mbytes total per disk), which are replaceable on orbit. The drive communicates with the SensorNet™ Experiment Computer Mass Storage Module over a SCSI bus.

Archival data storage on a WORM optical disk was used to guarantee data integrity because: once data are written they cannot be erased; files into which data are written, or from which data are read, are opened one at a time; disk status and the location of the next free sector on the disk can be determined; and a list of the files that are on the disk can be obtained.

Signal Conditioning System. The Signal Conditioning System is housed in a rugged card cage identical in construction to the Experiment Computer, except for the larger number of card slots (14). Signal conditioning available consists of Sensor Powering and Preamplification (SPP) cards followed by Signal Conditioning Cards (SCC) which contain digitally controlled gain stages, anti-alias filters, and sample-and-hold amplifiers. Each pair of STD-sized SPP and SCC cards provides four channels of conditioning. MODE flew five SPP cards and four SCC cards.

Each preamplification channel has an instrumentation amplifier front end with gains selectable from 2 to 5000 volts/volt; in addition to hardware gain and offset trim adjustments, they provide for auto-zero of input offsets under software control. The twenty preamplification channels are multiplexed to sixteen outputs, switchable on orbit (via software or hardware) to allow two instrumentation configurations.

The four SCC cards allow sixteen channels of data to be recorded per configuration. Each channel has software-selectable gains of 1, 2, 4, 8, and 16, followed by 8th-order lowpass (anti-alias) Bessel filters. Filter rolloff is controlled by a clock source, whose frequency is switchable under hardware or software control between two values. This permits each instrumentation configuration (e.g., Fluid Test Article or Structural Test Article) to have a unique rolloff frequency, corresponding to the software-selectable sampling frequency used for each experiment. Finally, the SCC cards provide a sample-and-hold

function under computer control to allow simultaneous sampling of all sixteen channels.

Signal Generation/Actuator Drive. Actuator drive signals are generated by a digital frequency synthesizer, which has a range of DC to 3 MHz. The computer can control the output frequency in 10 mHz steps (configureable to 1 mHz minimum). The output phase is continuous between frequency steps, which permitted the very smooth, very low frequency actuation required for MODE.

The power amplifier operates in bridge mode, with a ±20 volt output maximum (no load), and 1.7 amp maximum drive capability with two individually fused output lines. The amplifier is current limited, and the output level is software-selectable. Circuitry is provided which can modify drive signals to simulate a single degree-of-freedom, second-order dynamic system. Mass, damping, and spring constants are software-selectable. A displacement servo circuit is also provided to compensate for actuator response at low frequencies.

A triaxial accelerometer package is located within the Experiment Support Module, along with a set of dedicated preamplification circuits. This package has a ±50 g maximum range, and resolution is set with a load resistor on each axis. The standard configuration is a 50 μg to 0.1 g dynamic range.

Circuit Development. Circuit designs for the Signal Conditioning Circuitry were verified first by breadboard and prototype tests at MIT, followed by flight printed circuit fabrication by Payload Systems. The printed circuit boards were tested upon arrival, then populated with components (as received from the manufacturers) to MIL standards. Each assembled card was tested for functionality, then each flight set was tested together in order to verify proper system operation. The cards were then conformally coated, installed in the flight card modules, and the flight cabling installed. The remaining tests were performed as part of the certification and acceptance tests described below.

Power Supply. A custom power supply was designed to convert Orbiter +28 VDC to +5, ±12, and ±15 VDC needed to power the MODE elements. It uses commercially available DC to DC converters that meet MIL standards for input transient, inrush current, shock and vibration, and radiated and conducted emissions and susceptibility.

The power supply and distribution system provides several safety features: short circuit output protection in the power supply; current limiting to prevent excessive excitation of the test article actuators; and independent inhibits to detect and prevent operation in the event of excessive internal air and/or power supply temperature, or fan failure.

4.2.6 Certification

In compliance with the certification requirements placed on flight experiments by NASA, the MODE hardware successfully passed the following:

- Electromagnetic compatibility testing (conducted and radiated EMI - Shuttle middeck specifications)
- Leak testing (fluid test articles)
- Materials flammability testing (polycarbonate)
- Materials offgas testing
- Materials usage review - flammability
- Materials usage review - toxicity
- Random vibration testing (Experiment Support Module): 7.1 gRMS, 2 mins, 3 axes
- Random vibration testing (test articles): 6.5 gRMS, 2 mins, 3 axes
- Thermal cycle testing (Experiment Support Module only): 0°C to +50°C, 6 cycles.

4.3 Mission Activities

4.3.1 Fluid Dynamics Testing

In order to begin on orbit operations, the Experiment Support Module was connected to Orbiter +28 V power, and to the appropriate test article through the umbilical port on the front panel.

The fluid test articles were filled four days before launch and delivered to the Kennedy Space Center for stowage. Once on orbit, the Fluid Test Article Assembly was removed from its locker by a crew member and attached to the

front of the Experiment Support Module using the attachment device. Prior to the start of testing, the astronaut determined the Shuttle orientation (i.e., residual acceleration direction) and aligned the assembly at a predetermined angle using the universal ball joint. The astronaut then removed a test article from its storage locker and oriented the fluid inside to the bottom of the tank by moving the tank in a conical motion with his hand. After having accomplished fluid alignment, the fluid test article was attached to the reaction force balance. The astronaut then applied power to the Experiment Support Module and inserted an optical disk into the disk drive.

The astronaut began testing by initiating an automatic protocol stored on the optical disk. The Experiment Computer then excited the test article through a sequence of frequency and amplitude sets while collecting and storing data from the test article instrumentation. Periodic monitoring of the fluid surface by the astronaut was needed to detect fluid surface disruption. If the fluid equilibrium free-surface broke during a test run, the astronaut interrupted the experiment, removed the fluid tank, reoriented the fluid to the bottom of the tank, remounted the tank on the force balance, and resumed the test.

After completion of the protocol, the astronaut initiated the next protocol which excited the test article through a different sequence of frequency and amplitude sets. Fluid dynamics testing was conducted in this manner for a total of eight hours on STS-48. Figure 4.8 shows astronaut Jim Buchli during MODE Fluid Test Article operations while Table 4.2 summarizes the testing.

Figure 4.8 MODE Fluid Test Article operations on STS-48

ORIGINAL PAGE
BLACK AND WHITE PHOTOGRAPH

Table 4.2 MODE fluid dynamics testing

	Test Duration (mins)	Frequency Range (Hz)	Amplitude Range
Silicone Oil			
Flat Btm Uncoupled	110	.35-1.35	Lo/Mid/Hi
Sph Btm Uncoupled	110	.35-.75	Lo/Mid/Hi
Distilled Water			
Flat Btm Uncoupled	110	1.80-3.60	Lo/Mid/Hi
Coupled	110	1.80-3.60	Lo/Mid/Hi
Sph Btm Uncoupled	110	2.00-3.20	Lo/Mid/Hi
Coupled	110	2.10-3.30	Lo/Mid/Hi

4.3.2 Structural Dynamics Testing

Structural dynamics testing began with the removal of the elements of the Structural Test Article from their stowage locker, and their assembly into the baseline configuration by the crew. The test article was then lightly tethered to several velcro locations on the Shuttle middeck, with only the umbilical cable providing a connection to the Experiment Support Module. Test operations started in the same manner as for fluid dynamics testing: by initiating an automated protocol stored on an optical disk.

After completion of the protocol, the astronaut initiated the next protocol which excited the test article through a different sequence of frequency and amplitude sets. When testing was completed on the baseline configuration, the modules were partially disassembled, and reassembled to form the alpha configuration. The appropriate protocols were then run. This pattern continued until all four configurations were tested. Ten hours of structural dynamics testing were conducted on STS-48. Figure 4.9 shows astronaut Mark Brown at the completion of MODE Structural Test Article operations; Table 4.3 summarizes the testing.

Table 4.3 MODE structural dynamics testing

	Test Duration (mins)	Frequency Range (Hz)	Amplitude Range Lo/Mid/Hi
Straight			
Preload 1	60	7.5-29.7	Lo/Mid/Hi
Preload 2	60	7.5-29.7	Lo/Mid/Hi
Preload 3	34	7.5-29.7	Mid/Hi
Straight With Alpha Joint			
Tight Joint	51	7.2-10.8	Lo/Mid/Hi
Loose Joint	51	6.7-10.6	Lo/Mid/Hi
L Shape With Alpha Joint			
Preload 1	44	7.5-32.4	Lo/Mid/Hi
Preload 2	44	7.4-32.5	Lo/Mid/Hi
L Shape With Alpha Joint & Flexible Appendage	12	.40-1.00	Lo

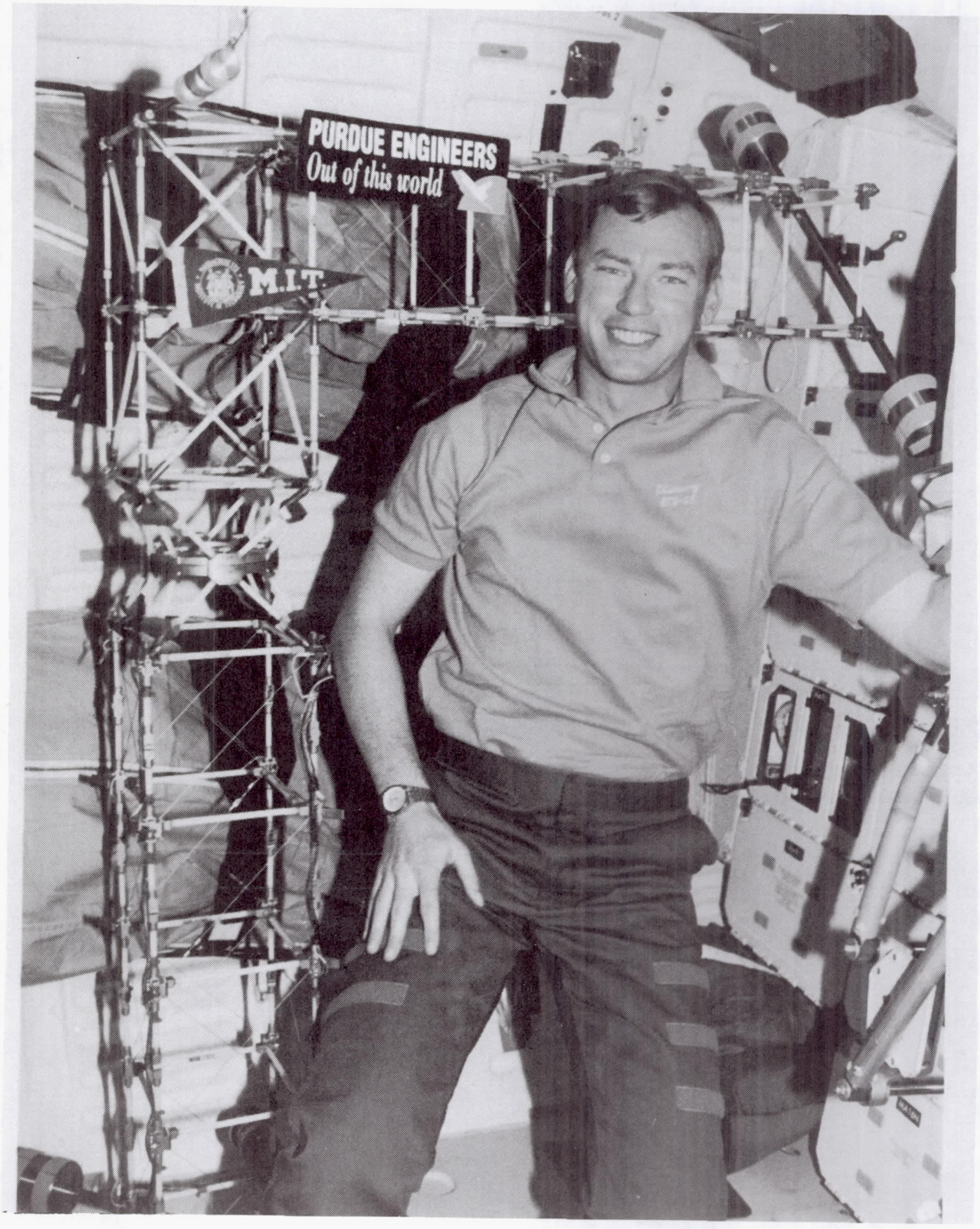

Figure 4.9 MODE Structural Test Article operations on STS-48

ORIGINAL PAGE
BLACK AND WHITE PHOTOGRAPH

4.4 Summary

The MODE hardware was designed, built and tested in two and one half years, and was certified to shuttle standards for a Class D modified payload. The flight systems successfully completed eighteen hours of on orbit operation during STS-48 (*Discovery*) in September, 1991. Initial activation of the MODE hardware occurred on September 13, with subsequent operational periods on September 15 and 16. During on orbit operations, MODE recorded over 600 Mbytes of data on the nonlinear behavior of fluids and truss structures in the microgravity environment of the shuttle middeck. On orbit operation of the MODE hardware and software was flawless.

REPORT DOCUMENTATION PAGE

Form Approved
OMB No. 0704-0188

Public reporting burden for this collection of information is estimated to average 1 hour per response, including the time for reviewing instructions, searching existing data sources, gathering and maintaining the data needed, and completing and reviewing the collection of information. Send comments regarding this burden estimate or any other aspect of this collection of information, including suggestions for reducing this burden, to Washington Headquarters Services, Directorate for Information Operations and Reports, 1215 Jefferson Davis Highway, Suite 1204, Arlington, VA 22202-4302, and to the Office of Management and Budget, Paperwork Reduction Project (0704-0188), Washington, DC 20503.

1. AGENCY USE ONLY (Leave blank)	2. REPORT DATE	3. REPORT TYPE AND DATES COVERED
	March 1993	Contractor Report

4. TITLE AND SUBTITLE
The Middeck 0-Gravity Dynamics Experiment - Summary Report

5. FUNDING NUMBERS
C NAS1-18690
WU 589-01-21-01

6. AUTHOR(S)
Edward F. Crawley, Marthinus C. Van Schoor, and Edward B. Bokhour

7. PERFORMING ORGANIZATION NAME(S) AND ADDRESS(ES)
MIT Space Engineering Research Center
Massachusetts Institute of Technology
Cambridge, Massachusetts 02139

8. PERFORMING ORGANIZATION REPORT NUMBER
SERC #16-92-R

9. SPONSORING/MONITORING AGENCY NAME(S) AND ADDRESS(ES)
National Aeronautics and Space Administration
Langley Research Center
Hampton, VA 23681-0001

10. SPONSORING/MONITORING AGENCY REPORT NUMBER
NASA CR-4500

11. SUPPLEMENTARY NOTES
Langley Technical Monitor: Sherwin M. Beck
Subject Category 18

12a. DISTRIBUTION/AVAILABILITY STATEMENT
Unclassified - Unlimited

12b. DISTRIBUTION CODE

13. ABSTRACT *(Maximum 200 words)*

The Middeck 0-Gravity Dynamics Experiment (MODE), flown on board the Shuttle STS-48 Mission, consists of three major elements: the Experiment Support Module, a dynamics test bed providing computer experiment control, analog signal conditioning, power conditioning, an operator interface consisting of a keypad and display, experiment electrical and thermal control, and archival data storage; the Fluid Test Article assembly, used to investigate the dynamics of fluid-structure interaction in zero-gravity; and the Structural Test Article for investigating the open-loop dynamics of structures in zero-gravity.

Deployable, erectable, and rotary modules were assembled to form three one- and two-dimensional structures, in which variations in bracing wire and rotary joint preload could be introduced. Change in linear modal parameters as well as the change in non-linear nature of the response is examined. Trends in modal parameters are presented as a function of force amplitude, joint preload, and ambient gravity. An experimental study of in the lateral slosh behavior of contained fluids is also presented. A comparison of the measured earth and space results identifies and highlights the effects of gravity on the linear and nonlinear slosh behavior of these fluids.

14. SUBJECT TERMS	15. NUMBER OF PAGES
Fluids, Space Structures, Dynamics, Shuttle Middeck, Nonlinear Phenomena, Space Testing	108
	16. PRICE CODE: A06

17. SECURITY CLASSIFICATION OF REPORT	18. SECURITY CLASSIFICATION OF THIS PAGE	19. SECURITY CLASSIFICATION OF ABSTRACT	20. LIMITATION OF ABSTRACT
unclassified	unclassified	unclassified	UL